

2010

Analysis of LiDAR point data and derived elevation models for mapping and characterizing bouldery landforms

Aaron Edward Maxwell
West Virginia University

Follow this and additional works at: <https://researchrepository.wvu.edu/etd>

Recommended Citation

Maxwell, Aaron Edward, "Analysis of LiDAR point data and derived elevation models for mapping and characterizing bouldery landforms" (2010). *Graduate Theses, Dissertations, and Problem Reports*. 3048. <https://researchrepository.wvu.edu/etd/3048>

This Thesis is protected by copyright and/or related rights. It has been brought to you by the The Research Repository @ WVU with permission from the rights-holder(s). You are free to use this Thesis in any way that is permitted by the copyright and related rights legislation that applies to your use. For other uses you must obtain permission from the rights-holder(s) directly, unless additional rights are indicated by a Creative Commons license in the record and/ or on the work itself. This Thesis has been accepted for inclusion in WVU Graduate Theses, Dissertations, and Problem Reports collection by an authorized administrator of The Research Repository @ WVU. For more information, please contact researchrepository@mail.wvu.edu.

Analysis of LiDAR Point Data and Derived Elevation Models for
Mapping and Characterizing Boulderly Landforms

Aaron Edward Maxwell

Thesis Submitted to the Eberly College of Arts
And Sciences at West Virginia University
In Partial Fulfillment of the Requirements for
the Degree of

Master of Science in Geology

J. Steven Kite, Ph.D., Chair
Gregory Elmes, Ph.D.
Timothy Warner, Ph.D.

Department of Geology and Geography

Morgantown, West Virginia
2010

Keywords: LiDAR, surficial mapping,
geomorphology, remote sensing,
global information science

Abstract

Analysis of LiDAR Point Data and Derived Elevation Models for Mapping and Characterizing Bouldery Landforms

Aaron Edward Maxwell

This thesis assessed the viability of using LiDAR-derived elevation data in accurately mapping and characterizing bouldery geomorphic features in a study area in the Allegheny Mountains. This study showed that the ground returns classification process conducted by the Canaan Valley Institute (CVI) for their property using the TerraScan software generally removed 5 to 10 m scale local topographic variability and bouldery landforms in creating the CVI classified ground returns data. In open areas, last returns elevation and intensity data were successfully used in this study to map bouldery landforms in the study area. Identifying and describing boulders under a tree canopy required a relatively reliable ground classification of LiDAR points. This study's classifications conducted within Prologic LiDAR Explorer provided a more useful representation than the CVI classified ground data for mapping bouldery landforms and generalized rugged topography. Index overlay for likelihood of presence of bouldery landforms using supervised classified aerial imagery and LiDAR-derived parameters in a raster environment was explored as an alternative means of detecting bouldery landforms because hillshade imagery derived from CVI classified ground data were inadequate for mapping bouldery landforms.

Acknowledgements

I would like to thank the Canaan Valley Institute (CVI) for their generosity in providing the LiDAR data used in this study. Specifically, I would like to thank Janette McNeer for providing relevant background data, Paul Kinder for allowing access to the data, and Adam Riley for helping transfer the data and answering technical questions. Without the assistance of Adam Riley this research would not have been possible. He went above and beyond to provide assistance.

I would like to thank my committee. Dr. Steve Kite advised me throughout this research and helped keep the work geomorphically relevant. Dr. Gregory Elmes instructed on the best GIS techniques to answer the questions posed. Dr. Timothy Warner explained the technical aspects of LiDAR data collection and provided assistance with interpretations. I would also like to thank Kevin Kuhn and Dr. Jaime Toro for assisting with GPS and ArcPad.

I would like to thank my father, Jaybob Maxwell, and wife, Julie Maxwell, for assisting in fieldwork. Most importantly, I would like to thank my parents, Jaybob and Debbie Maxwell. Without their support and sacrifices my education would not have been possible.

Table of Contents

Abstract.....ii

Acknowledgements.....iii

Table of Contents.....iv

List of Figures.....vi

List of Tables.....xi

Introduction.....1

Purpose.....3

Study Area and Data.....4

Defining Geomorphic Features of Interest.....10

Previous Works with LiDAR.....12

Goal and Objectives.....18

Methods.....19

 Preparation.....19

 Bedrock Geology Maps.....20

 Supervised Classifications.....21

 CVI Classified Ground Returns Processing.....22

 Last Returns and CVI Classified Ground Returns
 Comparison.....23

Return Density and Distribution.....24

*Elevation Comparison of LiDAR Last Returns and CVI
 Classified Ground Returns Data*.....25

Intensity of LiDAR Last Returns Data.....26

Return Number of LiDAR Last Returns Data.....27

 Prologic LiDAR Explorer Ground Classifications.....27

Index Overlay for Likelihood of Presence of Bouldery Landforms Analysis.....	28
Results and Discussion.....	34
Bedrock Geology Maps.....	34
Supervised Classifications.....	36
CVI Classified Ground Returns Processing.....	41
Last Returns and CVI Classified Ground Returns Comparison.....	44
<i>Return Density and Distribution</i>	44
<i>Elevation Comparison of LiDAR Last Returns and CVI Classified Ground Returns Data</i>	60
<i>Intensity of LiDAR Last Returns Data</i>	75
<i>Return Number of LiDAR Last Returns Data</i>	80
Prologic LiDAR Explorer Ground Classifications.....	83
Index Overlay for Likelihood of Presence of Bouldery Landforms Analysis.....	103
Conclusions.....	119
References Cited.....	123
Appendix.....	125
Field Data.....	125
<i>Site 1</i>	126
<i>Site 2</i>	128
<i>Site 3</i>	130
<i>Site 4</i>	133
<i>Site 5</i>	134

List of Figures

Figure 1: Comparison of the visual effects of DEM resolution.....2

Figure 2: Figure 2: County map of West Virginia: study area in Tucker County, West Virginia.....5

Figure 3: LiDAR coverage of CVI property.....8

Figure 4: Bedrock geology map of Canaan Valley study area.....9

Figure 5: Photographs of bouldery features of interest.....11

Figure 6: The Five study sites.....19

Figure 7: Subset of CVI property used in index overlay analysis.....20

Figure 8: CVI property bedrock geology map from Matchen *et al.* (1999) Data.....35

Figure 9: SAMB Natural color supervised classification using Erdas Imagine.....38

Figure 10: CIR NAIP supervised classification using Erdas Imagine.....39

Figure 11: Comparison of last returns and CVI classified ground returns over 0.6 m pixel natural color imagery at Site 1.....46

Figure 12: Comparison of last returns and CVI classified ground returns over 0.6 m pixel natural color imagery imagery at Sites 2 and 4.....47

Figure 13: 3D point distribution at Sites 1 and 4.....48

Figure 14: CVI classified ground returns compared to hillshade imagery in power line clearing.....50

Figure 15: CVI classified ground returns compared to hillshade imagery at bouldery features in forest.....51

Figure 16: CVI classified ground returns compared to hillshade imagery at site classified as ground.....53

Figure 17: Examples of data density reduction over bouldery landforms in power line clearing 1.....	56
Figure 18: Examples of data density reduction over bouldery landforms in power line clearing 2.....	57
Figure 19: Examples of data density reduction over bouldery landforms at bouldery features in forest.....	57
Figure 20: Examples of bouldery landforms included in ground model.....	58
Figure 21: Examples of data density reduction in area with coniferous canopy.....	58
Figure 22: Data density reduction over bouldery features at Sites 1 and 4.....	59
Figure 23: Elevation difference between last returns and CVI classified ground returns raster grid.....	61
Figure 24: Elevation difference between last returns and CVI classified ground returns at Site 1.....	62
Figure 25: Elevation difference between last returns and CVI classified ground returns at Site 4.....	63
Figure 26: Elevation difference between last returns and CVI classified ground returns at Site 2.....	64
Figure 27: Elevation difference between last returns and CVI classified ground returns at Site 5.....	65
Figure 28: Elevation difference between last returns and CVI classified ground returns and natural color supervised classification comparison.....	67
Figure 29: Topographic profile at Site 1a.....	71
Figure 30: Topographic profile at Site 1b.....	72
Figure 31: Topographic profile at Site 4.....	73
Figure 32: Topographic Profile at Site 2.....	74
Figure 33: Last returns intensity raster grid.....	77

Figure 34: Intensity value within 0.69 m raster grids at selected study sites.....	78
Figure 35: Intensity comparison in power line clearing.....	79
Figure 36: Return number of last returns.....	81
Figure 37: Last returns intensity box and whisker plots.....	82
Figure 38: Prologic LiDAR Explorer ground classifications at Site 1a.....	85
Figure 39: 3D point distribution of last returns at Site 1a.....	86
Figure 40: 3D point distribution of CVI classified ground returns at Site 1a.....	86
Figure 41: 3D point distribution of Prologic LiDAR Explorer classification Kernel Size = 5 and Z Tolerance = 0 at Site 1a.....	87
Figure 42: 3D point distribution of Prologic LiDAR Explorer classification Kernel Size = 5 and Z Tolerance = 1 at Site 1a.....	87
Figure 43: 3D point distribution of Prologic LiDAR Explorer classification Kernel Size = 5 and Z Tolerance = 2 at Site 1a.....	87
Figure 44: Prologic LiDAR Explorer ground classifications at Site 1b.....	88
Figure 45: Prologic LiDAR Explorer ground classifications at Site 4.....	89
Figure 46: 3D point distribution of last returns at Site 4.....	90
Figure 47: 3D point distribution of CVI classified ground returns at Site 4.....	90
Figure 48: 3D point distribution of Prologic LiDAR Explorer classification Kernel Size = 5 and Z Tolerance = 1 at Site 4.....	91
Figure 49: 3D point distribution of Prologic LiDAR Explorer classification Kernel Size = 5 and Z Tolerance = 2 at Site 4.....	91

Figure 50: 3D point distribution of Prologic LiDAR Explorer classification Kernel Size = 5 and Z Tolerance = 5 at Site 4.....	92
Figure 51: Prologic LiDAR Explorer ground classifications at Site 2.....	93
Figure 52: 3D point distribution of last returns at Site 2.....	94
Figure 53: 3D point distribution of CVI classified ground returns at Site 2.....	94
Figure 54: 3D point distribution of Prologic LiDAR Explorer classification Kernel Size = 5 and Z Tolerance = 0 at Site 2.....	95
Figure 55: 3D point distribution of Prologic LiDAR Explorer classification Kernel Size = 5 and Z Tolerance = 2 at Site 2.....	95
Figure 56: 3D point distribution of Prologic LiDAR Explorer classification Kernel Size = 5 and Z Tolerance = 5 at Site 2.....	96
Figure 57: Prologic LiDAR Explorer ground classifications at site 3.....	97
Figure 58: Prologic LiDAR Explorer ground classifications hillshade comparison at Site 3.....	100
Figure 59: Prologic LiDAR Explorer ground classifications hillshade comparison at Site 2.....	101
Figure 60: Hillshade comparison of last returns and CVI classified ground returns at large bouldery feature in power line clearing.....	102
Figure 61: Averaged index overlay for likelihood of presence of bouldery landforms.....	106
Figure 62: Index overlay for likelihood of presence of bouldery landforms at power line clearing (Site 1).....	108
Figure 63: Figure 63: Index overlay for likelihood of presence of bouldery landforms at boulder feature in power line clearing.....	109

Figure 64: Index overlay for likelihood of presence of bouldery landforms at bouldery feature in forest.....110

Figure 65: Index overlay for likelihood of presence of bouldery landforms at bouldery feature included in CVI classified ground model.....111

Figure 66: Index overlay for likelihood of presence of bouldery landforms in forest (Site 3).....112

List of Tables

Table 1: Metadata for CVI property LiDAR data collection 2008 flight.....6

Table 2: Boulder and block classifications.....10

Table 3: Natural color supervised classification training areas.....21

Table 4: CIR supervised classification training areas.....22

Table 5: Prologic LiDAR Explorer ground classification parameters.....28

Table 6: Statistics for elevation difference between last returns and CVI classified ground returns raster grids and last returns intensity collected by zonal statistics with ArcGIS30

Table 7: Reclassification scores for criteria.....32

Table 8: Likelihood of presence of bouldery landforms ranges for averaged index overlay model.....32

Table 9: Summary of supervised classifications of the study area37

Table 10: SAMB natural color supervised classification error matrix (accuracy estimated as +/- 7.2).....40

Table 11: Table 11: NAIP CIR supervised classification error matrix (accuracy estimated as +/- 7.2%).....41

Table 12: First ground classification parameters, provided by CVI.....42

Table 13: Second ground classification parameters, provided by CVI.....42

Table 14: Mean distance between nearest last returns and ground returns comparison for thirteen samples.....55

Table 15: Ordinary least squares regression results.....68

Table 16: Percentage of study area classified as likely to be bouldery landforms.....105

Table 17: Index overlay for likelihood of presence of bouldery landforms polygon ranking using spatial compromise programming results.....115

Table 18: Comparison of index overlay and supervised classification results116

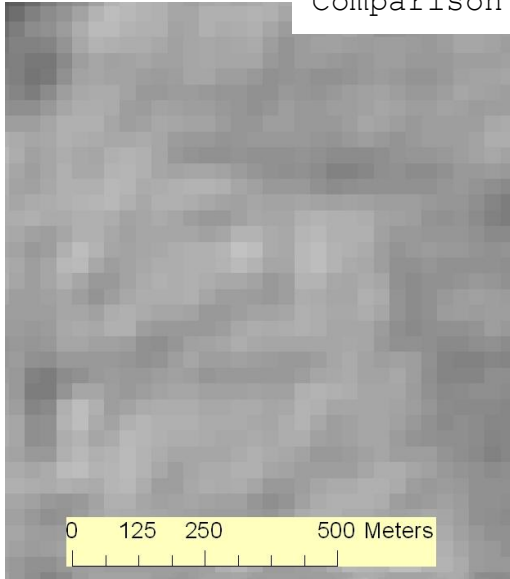
Table 19: Index overlay for likelihood of presence of bouldery landforms error matrix (accuracy estimated as +/- 7.2%).....118

Introduction

Digital elevation models (DEMs) have applications in many fields including geomorphology. In the past, elevation models were created by interpolation of digitized contour lines from topographic maps, which traditionally were created from aerial photographs. DEMs at a spatial resolution of 10 to 90 m were commonly produced; however, greater resolution is required for research investigating finer-scale features and stream morphology. Light detection and ranging (LiDAR) instruments can provide an effective resolution of 0.5 m or finer. The advances in DEM resolution provided by LiDAR (Figure 1) are transforming researchers' ability to quantify and visualize landscapes and the processes that shape them (Snyder, 2009).

This thesis is an investigation of how LiDAR point data and products derived from these data can be used to study bouldery terrains in a study area in the Allegheny Mountains and how rough topography influences the production of bare-earth surface models derived from such data. This thesis utilizes LiDAR-derived elevation point data for geomorphological research and explores issues associated with DEM production. Analyzing the ability to map bouldery geomorphic units with LiDAR is a means of understanding the uses and limitations of LiDAR for surficial mapping and characterization of complex landscapes.

Comparison of DEM Resolutions



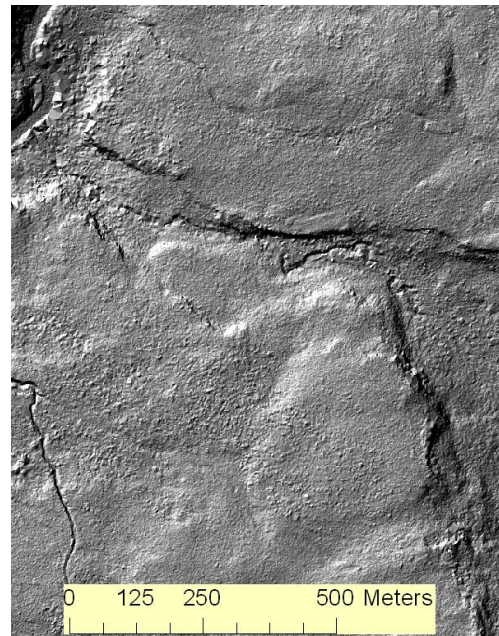
Hillshade from 30 m photogrammetrically-derived DEM



Hillshade from 10 m photogrammetrically-derived DEM



Hillshade from 3 m photogrammetrically-derived DEM



Hillshade from 0.69 m LiDAR-derived DEM

Figure 1: Comparison of the visual effects of DEM resolution. Elevation data sets were provided by the West Virginia GIS Technical Center and the Canaan Valley Institute. Note that LiDAR usually provides much higher spatial resolution elevation data in comparison to traditional techniques.

Purpose

The purpose of this thesis is to assess the viability of using LiDAR-derived elevation data for mapping and characterizing bouldery geomorphic features, such as block talus, boulder fields, and other very coarse-textured landforms, features that are considered 9th order scale or medium scale geomorphic process units in Bloom's (2004) classification system of terrestrial geomorphic features. Other 9th order features include pools and riffles, river bars, and solution pits (Bloom, 2004). It is hypothesized that ground returns classification algorithms utilized by the Canaan Valley Institute (CVI) to create the CVI classified ground data utilized in this research removed local topographic variability due to rugged topography and that ground data classified by CVI are insufficient for the purpose of mapping bouldery landforms.

Study Area and Data

The study area is located in Tucker County, West Virginia (Figure 2), where the rugged topography and forest-dominated land cover provides an optimal location to study bouldery landforms. CVI provided LiDAR data collected in 2008 covering their property near Davis, West Virginia, and the metadata are summarized in Table 1. The following data were obtained for use in this project:

1. All returns data for CVI property 2008 (From CVI as LAS (binary) files)
2. Ground returns data classified by CVI using the TerraScan software for CVI Property 2008 (from CVI as LAS (binary) files)
3. Metadata for 2008 CVI property data (from CVI as a text file)
4. Hillshade raster grid of CVI property created from LiDAR data collected in 2003 (from CVI as an ESRI GRID file)
5. A 2 ft (0.6 m) pixel 2003 Statewide Addressing and Mapping Board (SAMB) red-green-blue (natural color) aerial photograph mosaic of the study area (MrSID compressed file)
6. A 1 m pixel 2007 National Agriculture Imagery Program (NAIP) color infrared (CIR) photograph mosaic of the study area (MrSID compressed file)
7. Canaan Valley bedrock maps at 1:24,000 scale (retrieved from the West Virginia GIS Technical Center and original data by Matchen *et al.* (1999))
8. West Virginia geology shapefile at 1:250,000 scale (retrieved from the West Virginia GIS Technical Center and original data by Cardwell *et al.* (1968))



Figure 2: County map of West Virginia: study area in Tucker County, West Virginia (Source data: West Virginia GIS Technical Center).

Metadata for CVI Property LiDAR Data Collection 2008 Flight

Data Source	Canaan Valley Institute
LiDAR Collection Date	July 28, 2008
Aircraft	Piper Navajo Twin Engine Aircraft
Approximate Collection Height	2500 feet Above Ground Level (AGL) (760 m AGL)
Average Speed	135 Knots
Sensor	ALTM 3100
Pulse Rate/Beam Divergence	100 kHz/0.26 mrad
Scan Frequency	35 Hz
Scan Angle	20° (Half)
Number of Recorded Returns from One Pulse	Up to 4
Estimated Vertical Accuracy	15 cm
Average Ground Sample Distance	0.69 m
Horizontal Datum and Vertical Datum	Horizontal: North American Datum of 1983 Ellipsoid: Geodetic Reference System 80 Vertical: North American Vertical Datum of 1988
Extent	Zone 17 Top: 4334884.75N Bottom: 4329669.56N Left: 633233.22E Right: 637762.59E

Table 1: Metadata for CVI property LiDAR data collection 2008 flight. These data were provided by CVI.

The LiDAR point cloud coverage for the CVI property near Davis, West Virginia, is outlined in Figure 3. The bedrock geology of the Canaan Valley area (Matchen *et al.*, 1999) is shown in Figure 4. Within the property, the Pottsville Group is exposed on the northwestern limb of the plunging Blackwater anticline (Matchen *et al.*, 1999). Anderson and Kite (2007) and Anderson (2008) have shown that large Pottsville boulders are abundant in isolated locations in this landscape.

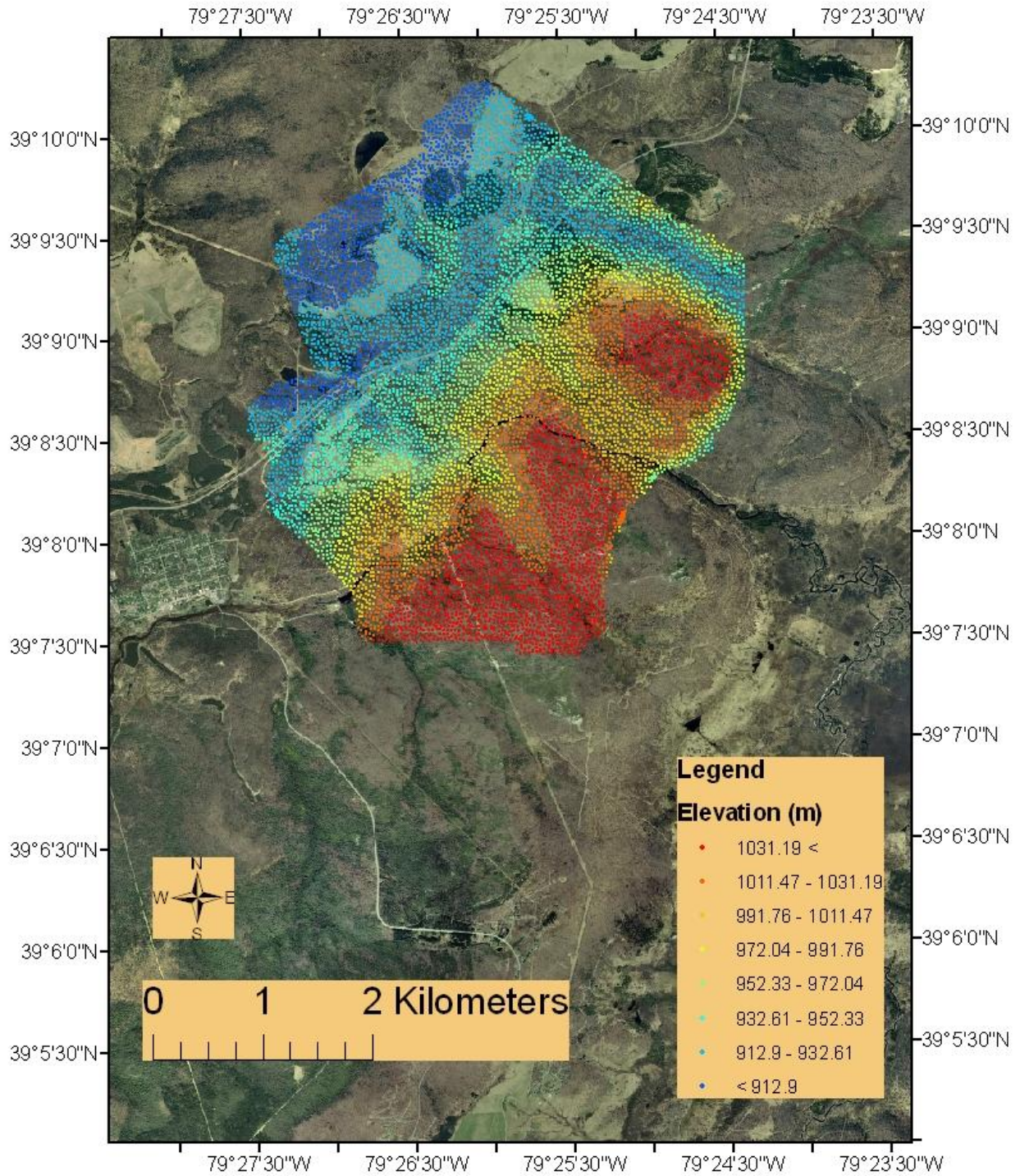


Figure 3: LiDAR coverage of CVI property. Base image is the 2003 SAMB imagery.

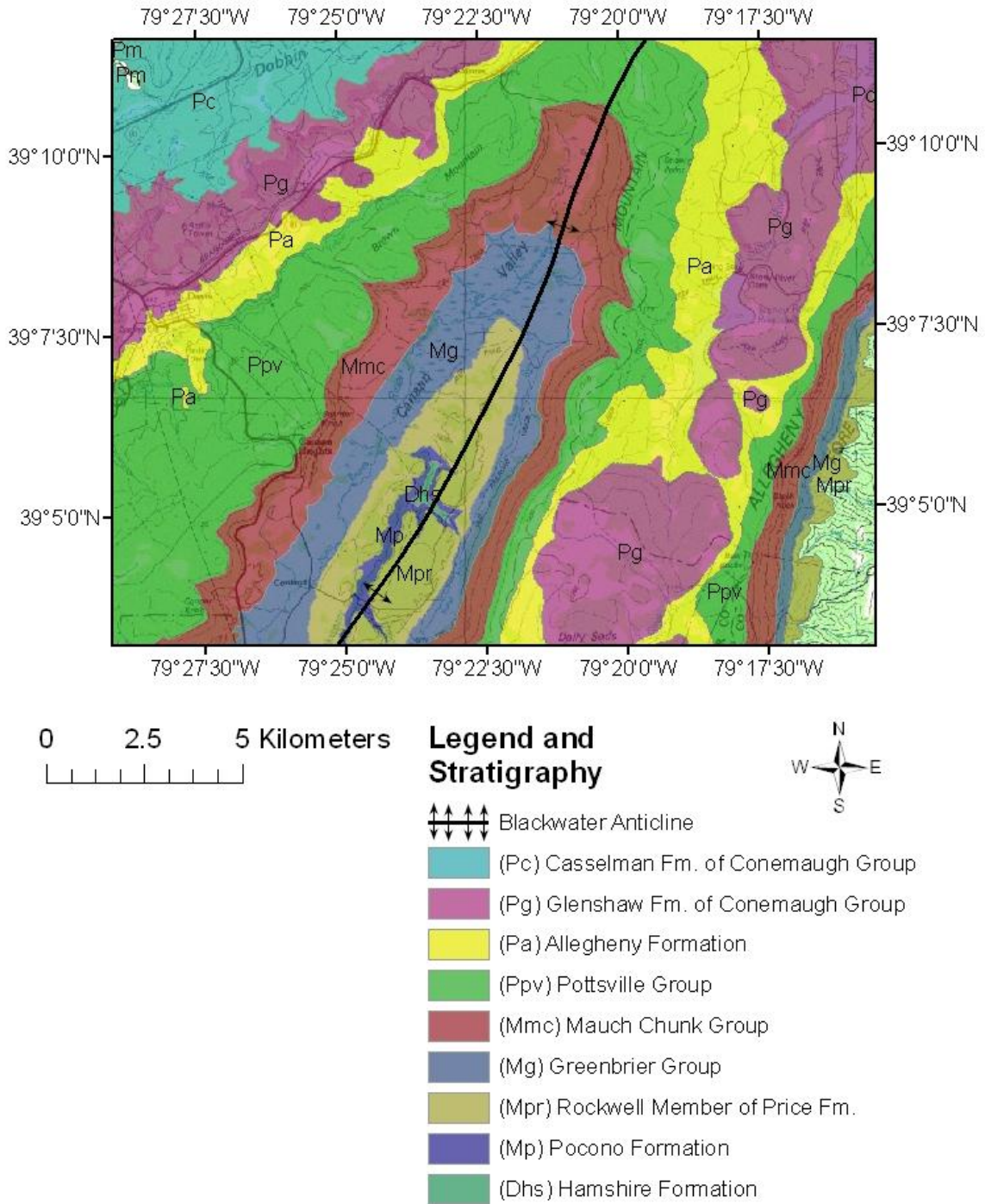


Figure 4: Bedrock geology map of Canaan Valley study area. Bedrock geology layer provided by the West Virginia GIS Technical Center from original geologic mapping by Matchen *et al.* (1999). Base image is a United States Geologic Survey 1:100,000 scale topography map.

Defining Geomorphic Features of Interest

The sizes of large particles on the surface of the geomorphic landscape were classified using the Blair and McPherson (1949) adaption of the Udden-Wentworth grain-size scale (Table 2). The researcher measured exposed intermediate axial length in the field to classify the bouldery landforms.

Boulder and Block Classifications

<u>Boulder</u>
Fine: 0.25 m to 0.5 m
Medium: 0.5 m to 1 m
Coarse: 1 m to 2 m
Very Coarse: 2 m to 4.1 m
<u>Block</u>
Fine: 4.1 m to 8.2 m
Medium: 8.2 m to 16.4 m
Coarse: 16.4 m to 32.8 m
Very Coarse: 32.8 m to 65.5 m

Table 2: Boulder and block classifications.

Geomorphic features examined in the field range from coarse boulders to medium blocks based on a physical measure of exposed intermediate axial length performed in the field (Figure 5).



Figure 5a: Fine Block



Figure 5b: Fine Block



Figure 5c: Fine Block



Figure 5d: Fine Block

Figure 5: Photographs of bouldery features of interest. Photographs taken by researcher on March 20, 2010.

Previous Works on LiDAR

Geodesy is the science of measuring physical attributes of the Earth, such as elevation. Very accurate elevation and location data are collected using global positioning systems (GPS). Differential and kinematic GPS offer vertical accuracies of 4 to 8 cm, while being even more accurate horizontally (Carter *et al.*, 2007). However, collecting a large number of measurements with such a method is time consuming. As a result, laser scanning instruments, such as LiDAR, offer alternative means of collecting highly accurate x, y, z data when a large number of measurements are required (Carter *et al.*, 2007).

Aerial LiDAR collection systems have three major components: laser rangefinder, inertial measurement unit (IMU), and GPS. First, a laser capable of pulsing provides the energy source. As a result, LiDAR is an active, as opposed to passive, remote sensing technique. The laser operates at a specific frequency in the infrared range. Normally, the laser wavelength is between 0.8 and 1.6 μm at a high pulse rate, up to 250 or higher kHz (Liu *et al.*, 2007a). Second, an IMU is used to correct the point data with respect to the motion of the aircraft. Third, an extremely accurate GPS device records the location of the return. Additional devices include a clock, additional computer hardware, digital storage devices, and,

potentially, a digital camera to record images that are of use when the data are later processed (Lillesand *et al.*, 2008).

Once a laser pulse has been transmitted, after it strikes an object, it is potentially reflected back to the sensor. The time required for the signal to return is directly related to the two-way travel distance from the sensor to the surface. An elevation measurement is calculated by combining this information with the directional orientation of the sensor (Liu *et al.*, 2007a). The ground x , y , z coordinates of the laser strike are derived from the ground coordinate system, inertial measurement unit body frame coordinates, laser unit coordinate system, and laser beam coordinate system. Appropriate rotation values also must be applied. The coordinates are achieved through vector, geometric relationships (Habib *et al.*, 2008).

Most modern LiDAR systems are capable of recording multiple returns for each pulse, and this capability allows characterization of multiple features or surfaces. For example, the top of a vegetation canopy can be mapped and also the ground surface. The intensity of the returned pulse may also be recorded. Different surfaces will absorb or reflect the laser differently, resulting in differences in return strength. This variation in reflectance allows better understanding of the surface feature (Lillesand *et al.*, 2008); however, intensity is influenced by many variables including footprint size, scan

angle, and range distance. It is difficult to use intensity quantitatively (Lin and Mills, 2010).

Not all raw LiDAR points represent ground returns, or data points that represent the ground surface, so extensive post-processing of the data is required. Data processing time greatly exceeds collection time (Liu *et al.*, 2007a). Computer algorithms are applied to make ground returns classifications of the points. Identifying ground points is a complex process, especially in areas containing vegetation and variable terrain. In geomorphology, ground data are normally required. Raw ASCII (text) or LAS (binary) point data can be used in research. LAS data provide smaller files than ASCII. Digital elevation models (DEMs) can be produced by converting the point data to a raster format. The finest effective resolution of the derived DEM depends on the density of the point data; as a result, the attainable resolution varies with the LiDAR systems used, vegetation density, and terrain characteristics of the study area (Liu *et al.*, 2007b). Triangular Irregular Networks (TINs) can also be created from the raw point data within ArcGIS using the 3D Analyst Extension. DEMs can be created from TIN files to convert the data to a raster format (Hinke and Wittkop, 2007).

There is a wide range of algorithms for ground returns classification (Sithole and Vosselman, 2004). Some algorithms process raw returns data while others require points to be

resampled into an image grid. Some algorithms are iterative while others are a single step process. Returns are processed point-to-point, point-to-points, or points-to-points. Point-to-point classification is a comparison of two points at a time, in which one point will be considered ground and the other an object if the elevation difference is above a defined threshold. Point-to-points classification classifies one point at a time using elevation relationships to multiple neighboring points. Points-to-points classification classifies multiple points at once. All of these processes use discriminate functions and classify the points based on some measure of discontinuity. The filtering concept can be slope-based, block-minimum, surface-based, or cluster/segmentation. Each model makes certain assumptions about the bare-earth surface. For example, clustering/segmentation algorithms assume that a cluster of points must represent an object if they are above neighboring points, while slope-based algorithms assume that the slope between two neighboring ground points cannot exceed a defined threshold. Block-minimum algorithms compare points to a horizontal plane, and, in order for a point to be included in the ground surface, it must be within a defined vertical distance from the plane. Surface-based algorithms are similar to block-minimum algorithms; however, a parabolic surface is used instead of a flat, horizontal surface. Advanced algorithms take

into account return number and intensity of returns (Sithole and Vosselman, 2004).

Two types of ground-returns classification error exist. Type I error is a rejection of ground returns while Type II error is the inclusion of object returns, or data points that are not ground surface, in the category of ground returns. Most filters are designed to minimize Type II error, or reduce the number of object points classified as ground. Steep slopes, discontinuities, vegetation, low ground return density, and terrain complexity can induce error in the classification of ground returns (Sithole and Vosselman, 2004).

Adequate surface representation requires accurate algorithms; if ground data points cannot be selected from other returns, adequate DEMs and bare-earth surface models cannot be created. Representing natural systems with abrupt and variable elevation changes can be complex. Ground classification algorithms are known to induce error (Weed *et al.*, 2002). Reusser and Bierman (2007) studied strath terraces in Holtwood Gorge and found that bedrock outcrop points were not included in the DEM, and areas with dense vegetation and variability were not accurately modeled. Webster (2005) found that ground classification algorithms inappropriately flatten cliff faces. Some non-ground points, such as rooftops, were included in the

ground surface. Webster (2005) stresses validation if LiDAR data are intended for research purposes.

Previous West Virginia University (WVU) Geology and Geography students have analyzed LiDAR data in geomorphology research. Konsoer (2008) used a 0.5 m DEM of the Horseshoe Run Watershed of Preston and Tucker counties, West Virginia, derived from LiDAR data collected in 2006 to create a surficial geologic map of the area and a landslide inventory. Konsoer performed statistical analysis and created a landslide susceptibility map. The influence of slope failure on channel instability and colluvium availability within the watershed was analyzed. Downing (2008) used the same data to investigate fluvial geomorphology in the watershed. Cross-sectional and longitudinal profiles were created for Maxwell and Drift runs. The variables were then compared to ground survey data, and the results showed a systematic underestimation of channel depth and overestimation of channel width. Anderson and Kite (2008) used a hillshade image of the CVI property created from LiDAR data collected in 2003 to create a surficial geologic map, including areas of boulder accumulation that were not previously mapped by Kite *et al.* (2004).

Goal and Objectives

The goal of this thesis is to assess the viability of using LiDAR-derived elevation data in accurately mapping and characterizing bouldery geomorphic features in a study area in the Allegheny Mountains. The following objectives are intended to fulfill this goal:

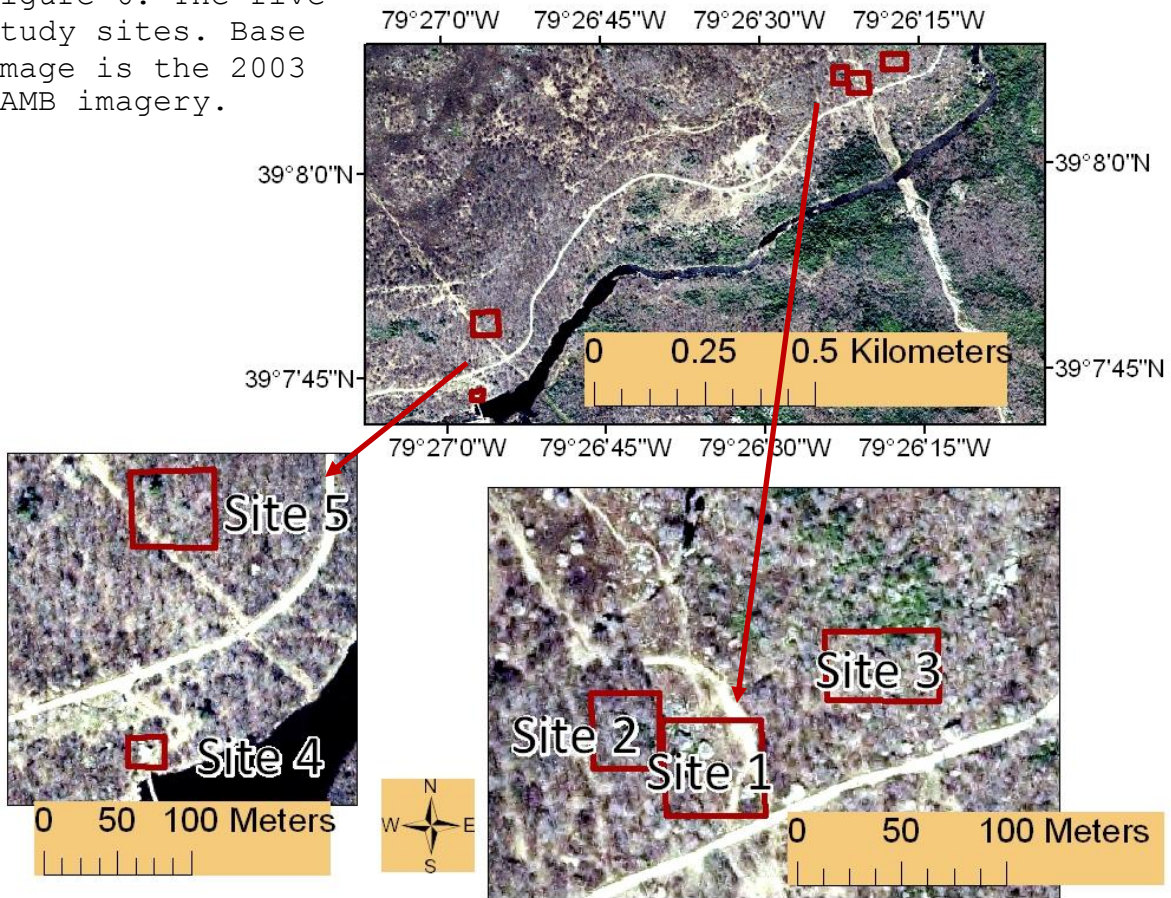
1. To create bedrock geology maps of the study area using the Matchen *et al.* (1999) and Cardwell *et al.* (1968) data.
2. To create a supervised classification of the study area that represents bouldery landforms using a 0.6 m (2 ft.) pixel natural color aerial image.
3. To describe how CVI classified ground returns and what algorithms they used.
4. To visually and statistically compare last returns data to ground returns data classified by CVI for usefulness in mapping and characterizing bouldery landforms.
5. To reclassify the LiDAR returns and create DEMs that more accurately characterize bouldery landforms in comparison to the CVI classified ground data.
6. To develop an approach to detect boulders remotely using index overlay for likelihood of presence of bouldery landforms, LiDAR-derived parameters, and aerial imagery.

Methods

Preparation:

Five sites within the CVI property (Figure 6) were purposefully selected for a detailed analysis. Sites containing boulders and blocks of varying size were selected under the tree canopy, in open areas, and under a partial canopy. These features are described in the Appendix. Additionally, eight LiDAR data tiles, a 5.4 km² subset of the property (Figure 7), were used in an index overlay analysis.

Figure 6: The five study sites. Base image is the 2003 SAMB imagery.



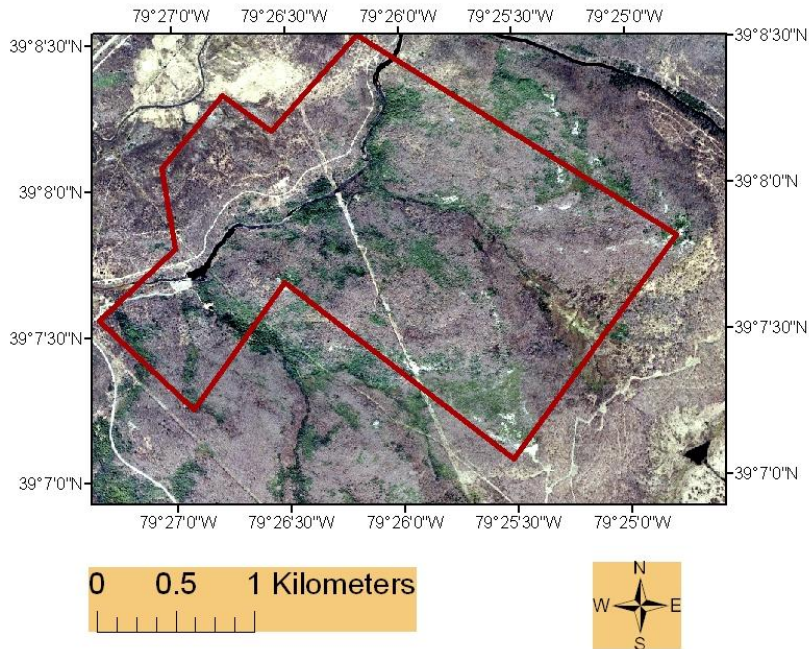


Figure 7: Subset of CVI property used in index overlay analysis. Base image is the 2003 SAMB imagery.

Within each of the five study sites, bouldery landforms were described. Features were measured and classified, differentially post-processed GPS data were collected using a Magellan Mobilemapper 6 unit with ArcPad, and photographs were obtained. Polygons were produced outlining the features using the field data and aerial photograph interpretation.

Bedrock Geology Maps:

A bedrock geology map was produced from Matchen *et al.* (1999) data and a 2003 SAMB base image. The Canaan Valley bedrock geology shapefile was downloaded from the West Virginia GIS Technical center and clipped to extract the rock units of interest. The geologic map was produced within ArcMap 9.3. A geologic map was also created from the coarser scale Cardwell *et al.* (1968) data for comparison.

Supervised Classifications:

The Erdas Imagine software was used to conduct a supervised classification of the 0.6 m pixel 2003 SAMB image using maximum likelihood classification. The imagery was collected during leaf-off conditions. An attempt was made to highlight bouldery landforms based on the image digital numbers (DNs). This technique was investigated so that results could be compared to the LiDAR-based analysis. Bouldery landforms in this study area could be identified in the imagery, so grid cells that represented bouldery landforms were selected as training pixels and used for the classification. The classification was used in the index overlay for likelihood of presence of bouldery landforms analysis. Table 3 describes the type and number of training areas digitized.

Bouldery Landforms	16 Training Areas
Forest	8 Training Areas
Field	6 Training Areas
Water	9 Training Areas
Road	8 Training Areas

Table 3: Natural color supervised classification training areas. Data were collected using aerial photograph interpretation.

A NAIP 1 m pixel CIR aerial image collected during leaf-on conditions in 2007 by the United States Department of Agriculture was also classified for comparison using the same

process. Table 4 describes the type and number of training areas digitized.

Bouldery Landforms	10 Training Areas
Forest	6 Training Areas
Field	4 Training Areas
Water	4 Training Areas
Road	5 Training Areas

Table 4: CIR supervised classification training areas. Data were collected using aerial photograph interpretation.

The accuracy of each classification was evaluated by comparison to one hundred ground reference data points. An error matrix was produced. Based on Jensen (2005), sampling one hundred points from a binomial distribution with a confidence of 85% will have an expected 7.2% error in the accuracy estimation. The data points were randomly sampled in an accessible area of the property. Using the natural color classification results, fifty bouldery and fifty non-bouldery points were sampled. HawthTools was used to create the random points. A Magellan Mobilemapper 6 GPS unit was used to find and document the reference ground points. It should be noted that GPS error was a problem in the ground sampling method due to the size of grid cells being sampled.

CVI Classified Ground Returns Processing:

The procedure used by CVI to classify LiDAR returns as ground data was provided and explained by employees at CVI. The

TerraScan software manual was referenced to understand how ground returns classification is conducted within this software package.

Last Returns and CVI Classified Ground Returns Comparison:

CVI classified ground returns data were compared to the last returns data, and how these different data represent bouldery landforms were investigated. Last returns were used for comparison to this classified ground data instead of all returns because bouldery landforms were of interest, and such landforms would usually be the lowest surface that could return a laser pulse (Lillesand *et al.*, 2008). As a result, only first-and-only or last-of-many returns were regarded as being potentially from bouldery landforms. Prologix LiDAR Explorer Data Management Edition (DME) software was used to extract the last returns data and export those points as a separate file. Comparison of last returns and CVI classified ground returns was achieved through visual and statistical GIS-based analysis of multiple variables including the following:

1. Return Density and Distribution
2. Elevation Comparison of LiDAR Last Returns and CVI Classified Ground Returns Data
3. LiDAR Last Returns Intensity
4. Return Number of Last Returns

Return Density and Distribution:

The shapefiles of LiDAR returns were displayed over the 2003 SAMB base imagery. Polygons that showed bouldery landforms of interest were digitized by interpretation of aerial photography so that distribution of LiDAR returns over such features could be visualized. Where this was not possible due to canopy cover in forested areas, polygons were digitized in the field using a Magellan Mobilemapper 6 GPS unit with differential post-processing correction. Due to the size of the features of interest, it was difficult to outline bouldery features accurately. Polygons were meant for visual identification and not quantitative measures. Polygons provided a visual representation of how the LiDAR point distribution relates to the terrain. The point distribution was also compared to hillshade raster grids created from the CVI classified point data using the 3D Analyst Extension in ArcMap 9.3. An attempt was made to relate the point density to rough hillshade texture.

ArcScene was used to create 3D models of LiDAR point data distribution using the CVI classified ground returns point data, last returns point data, and a TIN vector model of the CVI classified ground point data. This 3D visualization provided an illustration of how returns were distributed and how last returns related to the CVI classified ground returns.

Mean distance from one return to its nearest neighbor, calculated by averaging the distance from one point to its nearest neighbor within thirteen sample areas, was calculated using the "Distance between Points within Layer" command within HawthTools, an extension for ArcMap 9.3. Mean distance between nearest neighbors was estimated to evaluate the average point spacing value provided by CVI.

A raster point count process within ArcToolbox was used to create a raster grid displaying number of returns in a given area using the "Point to Raster" command and using "Count" as the cell assignment. A 1.0 m cell size was used for the analysis because, after experimentation with different cell sizes, that resolution provided an appropriate representation of point density for this research. This process provided an illustration of how the CVI classified ground returns were clustered and where data were absent. Also, the point count process provided a description of changes in data density in comparison to last returns and CVI classified ground returns. Comparisons of the mean point spacing and the point count 1.0 m rasters were performed.

Elevation Comparison of LiDAR Last Returns and CVI Classified Ground Returns Data:

Raster grids at 0.69 m cell size were created because CVI reported this distance to be the average ground sample distance

(Table 1). The LAS files were converted to shapefiles using GeoCue LAS Reader. The shapefiles were then converted to TINs using the 3D Analyst Extension. Raster grids were produced from the TIN surfaces.

The following raster math was performed:

[0.69 m Raster Grid of Elevation Data from Last Returns - 0.69 m
Raster Grid of Elevation Data from CVI Classified Ground
Returns]

This process created a raster grid of elevation difference between the last returns and CVI classified ground returns that was used for visual and statistical comparison of the data sets. Areas containing a greater elevation difference indicated locations where last returns were not classified as ground.

Elevation profiles were created using the profiling tool within the 3D Analyst Extension, which provided a comparison of the last returns data and CVI classified ground data. Data were exported to Microsoft Excel to construct graphs. In order to use such tools, the point data were converted to TINs and elevation raster grids using the 3D Analyst Extension.

Intensity of LiDAR Last Returns Data:

The LiDAR data available also provided a return intensity measurement for each data point. Raster grids were created from the last returns intensity values using the 3D Analyst Extension, and statistics were collected. Changes in intensity

values were compared between the last returns and CVI classified ground returns data. This intensity information and elevation difference information were used in the index overlay for likelihood of presence of bouldery landforms analysis.

Return Number of LiDAR Last Returns Data:

Return number for the last returns data were displayed, and return number was related to the intensity values. Box and whisker plots were produced at two sample locations under the forest canopy to compare how intensity varies with return number.

Prologic LiDAR Explorer Classifications:

Ground classifications of the available LiDAR data were attempted in this study that serve a geomorphic analysis purpose without inducing considerable error, such as incorporating vegetation in the ground elevation data. Prologic LiDAR Explorer Feature Class Edition (FCE) allows reclassification of points as ground using a raster trend-surface analysis in which points are compared to a raster grid surface created from minimum elevation values within a defined kernel size. This function allows the user to adjust the size of the kernel and the elevation (Z) tolerance (Prologic, 2008). This function was used to classify points from the last returns data as ground in an attempt to create classifications that captured bouldery landforms and the variable terrain. Table 5 describes the parameters used. The

resulting classifications using different parameters were compared using topographic profiles, 3D surfaces, and hillshade imagery.

Test Number	Kernel Size	Z Tolerance
1	3x3	0
2	3x3	1
3	3x3	2
4	3x3	5
5	5x5	0
6	5x5	1
7	5x5	2
8	5x5	5

Table 5: Prologic LiDAR Explorer ground classification parameters.

Index Overlay for Likelihood of Presence of Bouldery Landforms

Analysis:

Multiple criteria as raster data layers were used to classify bouldery landforms including the following: natural color aerial imagery, elevation difference between last returns and CVI classified ground returns elevation raster grids, point count of CVI classified ground returns, and LiDAR last returns intensity. An index overlay analysis was conducted in ArcMap. The natural color supervised classified raster grid produced previously was used here. The elevation difference, point count, and intensity raster grids were also used. Polygons were digitized at known bouldery areas, non-bouldery forested areas,

and non-bouldery open areas to extract desired grid cells, and zonal statistical data (Table 6) were collected within ArcGIS to determine an adequate elevation difference range and last returns intensity range for bouldery landforms. Bouldery landforms had a higher mean elevation difference value than non-bouldery open areas, 3.67 m compared to 0.05 m. Also, mean intensity values were lower for bouldery landforms than non-bouldery areas, 77.4 as compared to 134.2. Separating bouldery landforms and non-bouldery forest areas based on these two variables was complex due to a wide range of values in forested areas. The standard deviation for non-bouldery forest areas was larger in comparison to the other classifications for elevation difference, 3.78 m, and last returns intensity, 32.3. Also, the mean values were similar to those for bouldery landforms. Lower values for the CVI classified ground point count raster grid were considered preferable for bouldery landforms based on previous research results. Road and water classification were weighted higher than field and forest because, based on visual interpretation of the classification results, bouldery areas would more likely be misclassified into one of these groups.

Table 6a: Bouldery Landforms		
Statistics	Elevation Difference between last returns and CVI Classified Ground Returns (m)	Last Returns Intensity
Minimum	0.12	20.2
Maximum	6.61	117.5
Range	6.49	97.3
Mean	3.67	77.4
Standard Deviation	1.38	21.7
Table 6b: Non-Bouldery Forest		
Statistics	Elevation Difference between last returns and CVI Classified Ground Returns (m)	Last Returns Intensity
Minimum	-0.05	1.9
Maximum	17.4	154.2
Range	17.45	152.4
Mean	6.68	70.1
Standard Deviation	3.78	32.3
Table 6c: Non-bouldery Open		
Statistics	Elevation Difference between last returns and CVI Classified Ground Returns (m)	Last Returns Intensity
Minimum	-0.11	60.4
Maximum	0.61	179.1
Range	0.72	118.7
Mean	0.05	134.2
Standard Deviation	0.06	12.6

Table 6: Statistics for elevation difference between last returns and CVI classified ground returns raster grids and last returns intensity collected by zonal statistics with ArcGIS. These data were used to determine likelihood of presence of bouldery landforms reclassifications for the index overlay analysis.

Reclassifications were performed, and new raster grids were produced using an index overlay for likelihood of presence of bouldery landforms procedure within ArcGIS. Three models were produced, and the varying parameters used are outlined in Table 7. The scores ranged from zero to five with five indicating most likely and zero indicating not likely to be bouldery landforms. Scoring allowed for likelihood of presence of bouldery landforms ranges to be produced. The three models were averaged to produce a final likelihood of presence model using the raster calculator:

$$([\text{Model 1}] + [\text{Model 2}] + \text{Model 3})/3 = \text{Averaged Model}$$

Larger values indicated increased likelihood of presence of bouldery landforms. Cells were classified as does not meet criteria, least likely, moderately likely, and most likely based on parameters described in Table 8. The ranges were decided upon based on natural breaks in the data.

Reclassification Scores for Criteria
(Model 1, Model 2, Model 3)

Table 7a: Elevation Difference Ranges	Reclassification Score (Model 1, Model 2, Model 3)
< 0.1 m	0,0,0
0.1 m - 0.12 m	1,1,2
0.12 m - 0.5 m	3,3,4
0.5 m - 6.0 m	5,5,5
6.0 m- 6.5 m	3,3,4
6.5 m - 7. 0 m	1,1,2
> 7.0 m	0,0,0

Table 7b: Intensity Ranges	Reclassification Score (Model 1, Model 2, Model 3)
< 15	0,4,4
15 - 20	1,4,4
20 - 34	3,4,4
34 - 115	5,5,5
115 -118	3,3,3
118 - 120	2,2,2
> 120	0,0,0

Table 7c: CVI Ground Point Count	Reclassification Score (Model 1, Model 2, Model 3)
0	5,5,5
1	3,3,3
2	1,1,1
> 2	0,0,0

Table 7d: Natural Color Classification	Reclassification Score (Model 1, Model 2, Model 3)
Bouldery Landform	5,5,5
Road	3,3,3
Water	3,3,3
Forest	0,2,2
Field	0,2,2

Table 7: Reclassification scores for criteria. Three different models were produced.

Likelihood of Presence of Bouldery Landforms Ranges

Likelihood	Raster Values
Does Not Meet Criteria	0-48
Least Likely	48-138
Moderately Likely	138-318
Most Likely	318-625

Table 8: Likelihood of presence of bouldery landforms ranges for averaged index overlay model. Likelihood of presence ranges were selected based on natural breaks in the data set.

The results of the three models were tested using a spatial compromise programming statistical analysis in which test areas, as polygons, were compared. Test data were obtained from the following contexts:

1. Bouldery landforms in open areas identified by aerial imagery interpretation (9 test areas)
2. Bouldery landforms under tree canopy identified from field-based differential GPS data (6 test areas)
3. Non-bouldery forested areas identified from field-based differential GPS data (10 test areas)
4. Non-bouldery open areas identified by aerial imagery interpretation (10 test areas)

Polygons in bouldery areas should meet the criteria and be ranked higher than the non-bouldery field and forested areas if the models are adequate. The results were also compared to the natural color supervised classification. The one hundred randomly sampled ground reference locations were compared to the model, an error matrix was produced, and accuracy was assessed.

Results and Discussion

Bedrock Geology Maps:

Bedrock geology maps were produced from the 1:24,000 scale Matchen *et al.* (1999) data (Figure 8) and the 1:250,000 scale Cardwell *et al.* (1968) data. The larger-scale data are more appropriate for describing the geology of a study area of this extent. Contacts are better defined based on topography, and the rule of Vs is observed. Based on these geologic data, sandstone of the Pottsville Group underlies this study area and forms the bouldery landforms of interest (Matchen *et al.*, 1999).

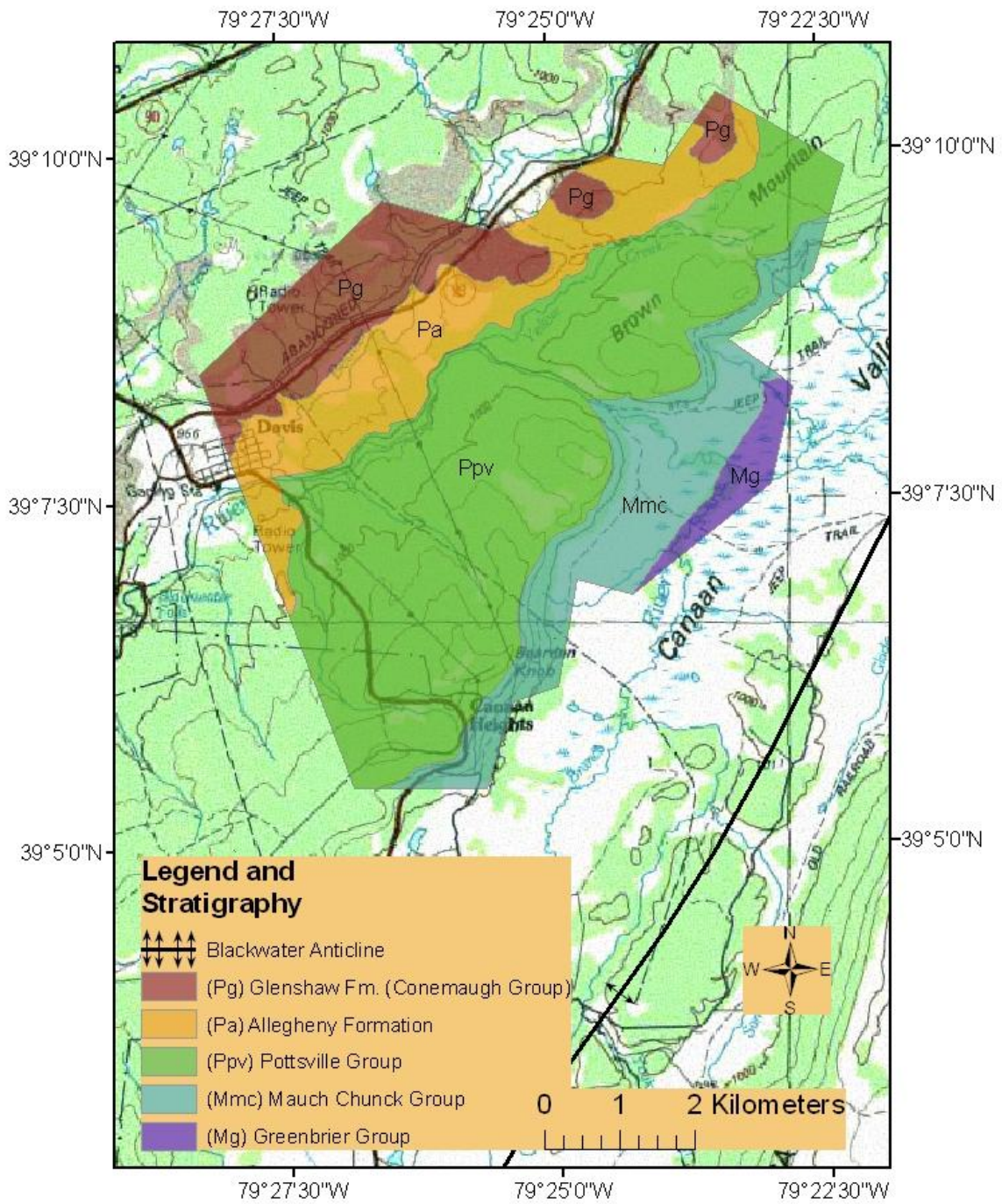


Figure 8: CVI property bedrock geology map from Matchen *et al.* (1999) data. Base image is a United States Geologic Survey 1:100,000 scale topography map.

Supervised Classifications:

The 0.6 m pixel natural color SAMB supervised classification identified 10.9% of the 5.4 km² area as bouldery landforms. The 1 m pixel CIR NAIP supervised classification identified 3.1% of the area as bouldery landform (Table 9). Figure 9 demonstrates that the natural color classification detects bouldery landforms throughout the area; Figure 10 demonstrates that the CIR classification detects bouldery landforms primarily in open areas and locations where bouldery features disrupt the tree canopy. This pattern is a result of data collection when a vegetated canopy was present. Accurate detection of bouldery landforms using this technique requires leaf-off data, such as the natural color data, because features under the tree canopy are of interest. However, leaf-off conditions induce variability in the classification because forest structure influences the DN values. Areas with canopy cover are not easily classified due the irregularity of their DN values; as a result, detecting bouldery landforms under a tree canopy was inadequate. Areas on slopes are often classified as water due to shadowing; also, features under conifers are not detected due to the year-round canopy cover. It is difficult to separate road or gravel surfaces from bouldery landforms based on natural color DN values alone. Overall, the leaf-off, natural color imagery provides a better classification for detecting

bouldery landforms throughout the study area, but bouldery features are not separated from road surfaces and detection in forested areas is hindered due to reflectivity variability. Supervised classification of natural color imagery for bouldery landform detection is effective in open areas.

Natural Color 0.6 m Imagery (Figure 9)	
Bouldery Landform	10.9%
Forest	60.6%
Field	11.6%
Water	11.7%
Road	5.3%
CIR 1 m Imagery (Figure 10)	
Bouldery Landform	3.1%
Forest	69.0%
Field	26.5%
Water	0.9%
Road	0.5%

Table 9: Summary of supervised classifications of the study area. These values were collected within the 5.4 km² area using zonal statistics within ArcMap's Spatial Analyst Extension.

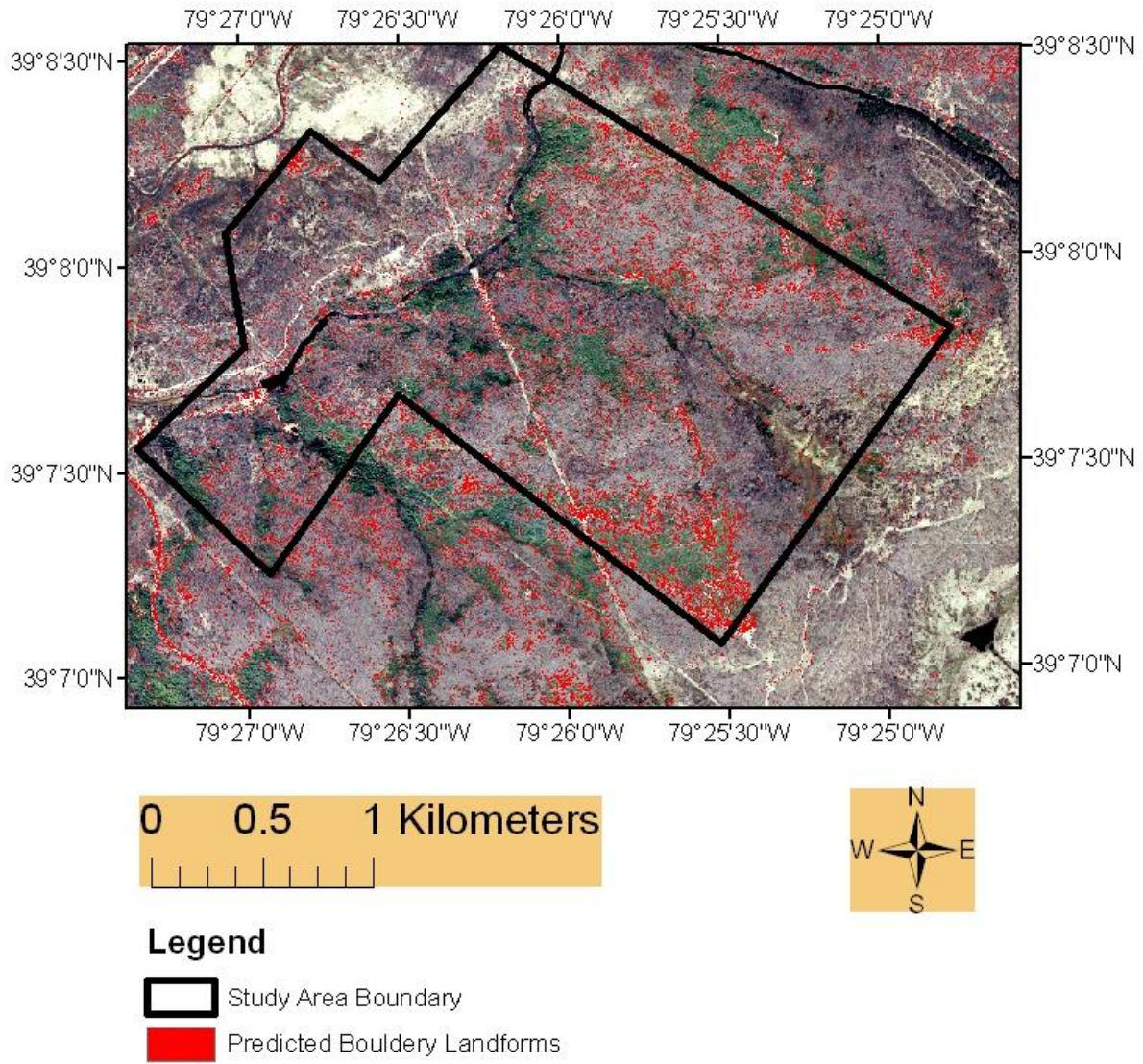


Figure 9: SAMB natural color supervised classification using Erdas Imagine.

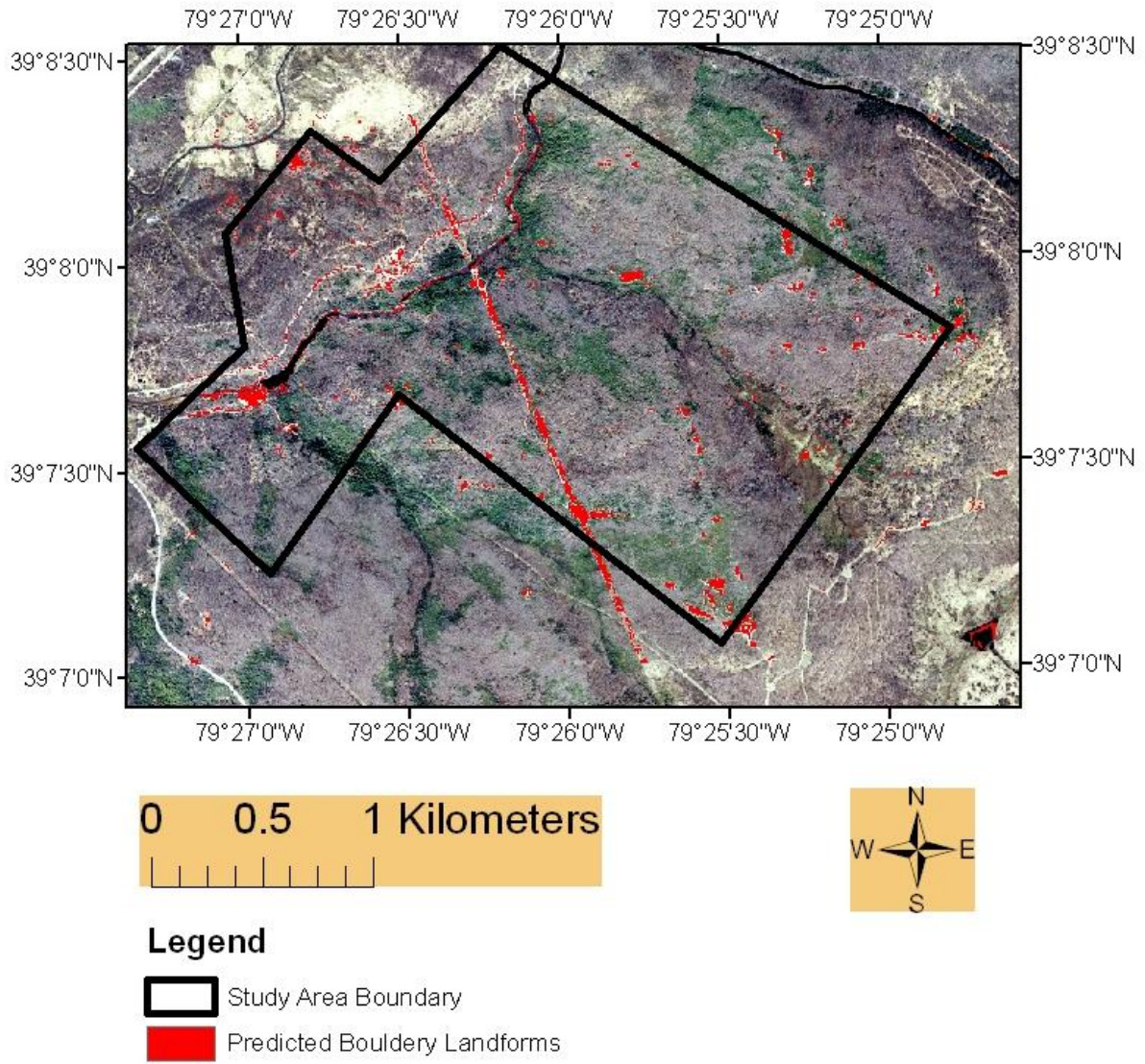


Figure 10: CIR NAIP supervised classification using Erdas Imagine.

Tables 10 and 11 summarize the accuracy of the classifications based on the ground reference data. The natural color classification is more accurate because bouldery landforms under a tree canopy are more often correctly identified in the model. These features are generally not correctly identified in the CIR classification due to the canopy cover at the time of acquisition. It should be noted the GPS error was a problem in the ground sampling method because grid cells were only 0.6 m in size in the natural color model. Identifying the true location of the pixel in the field was difficult. The researcher attempted to collect the best ground data that were obtainable with the equipment available. Due to the number of ground reference points used to conduct the analysis, the accuracy estimate is estimated to +/- 7.2%. The natural color supervised classification overall accuracy was estimated as 82%.

		Ground Reference Data		User's Accuracy
		Bouldery	Non-Bouldery	
Natural Color Supervised Classification Data	Bouldery	39	11	78%
	Non-bouldery	7	43	86%
Producer's Accuracy		85%	77%	
Overall Accuracy		82%		

Table 10: SAMB natural color supervised classification error matrix (accuracy estimated as +/- 7.2%).

		Ground Reference Data		User's Accuracy
		Bouldery	Non-Bouldery	
CIR Supervised Classification Data	Bouldery	3	42	7%
	Non-bouldery	2	53	11%
Producer's Accuracy		60%	44%	
Overall Accuracy		56%		

Table 11: NAIP CIR supervised classification error matrix (accuracy estimated as +/- 7.2%).

CVI Classified Ground Returns Processing:

The processes used to create the CVI classified ground returns data made available for this project were explored by speaking with CVI employees. CVI utilized POSpac, a LiDAR processing tool, to convert the raw data to LiDAR data as LAS files. Pospac allows for GPS, IMU, and LiDAR rangefinding data to be processed to x, y, z points as LAS files (J. McNeer, Personal Communication, December 11, 2009). CVI processed the LAS all returns data to classified ground returns using the ground classification tool within the TerraScan software, an extension for Microstation. First, CVI removed points that were farther than 5 m from any other return in x, y, z space as outliers. They performed an initial ground classification on all remaining returns using parameters described in Table 12. CVI processed the classified ground returns a second time using parameters described in Table 13, and this processing created

the CVI classified ground returns used in this research (A. Riley, Personal Communication, January 28, 2010).

First Ground Classification

Parameter	Value
Maximum Building Size	60.0 m
Terrain Angle	88.00°
Iteration Angle	10.00°
Iteration Distance	1.00 m

Table 12: First ground classification parameters, provided by CVI.

Second Ground Classification

Parameter	Value
Maximum Building Size	60.0 m
Terrain Angle	88.00°
Iteration Angle	5.00°
Iteration Distance	1.00 m

Table 13: Second ground classification parameters, provided by CVI.

The ground classification routine within TerraScan classifies points by iteratively building a triangulated surface model. The maximum building size, initially set at 60.0 m, determines the initial point selection. The algorithm assumes that at least one return within the maximum building size area is ground and that the lowest point is a ground return. The routine builds an initial model from these selected points. The process adds points iteratively to model the ground surface. Iteration parameters determine how close a point has to be to a triangular plane so that the point is accepted to the model. The iteration angle is the maximum allowed angle in the elevation (z) direction between a point and the triangulated surface that

is iteratively created. The iteration distance controls the size of triangulated surfaces. Fewer points are added to the ground model when the angle is smaller; a smaller angle, such as 4.0° , is commonly used in flat terrain, and a larger angle, such as 10° , is commonly used in hilly terrain. An additional parameter, the terrain angle, specifies the steepest allowed slope on the ground. The value for this parameter depends on the terrain characteristics of the landscape being modeled (Terrasolid, 1998).

The spot size is the average diameter that a LiDAR pulse has when it reaches the ground. The LiDAR footprint size was calculated from the beam divergence and flight height using the following equation (Kukko and Hyyppa, 2007):

$$D = 2z \tan(\Delta\theta/2)$$

Where

D = Spot Size or Diameter in meters

Z = Height of Plane (AGL) = 760 m

($\Delta\theta$) = Beam Divergence = 0.26 mrad = $1.49E-2^\circ$

Based on the parameters provided in the metadata (Table 1), the spot size for this flight was approximately 0.20 m (20 cm).

This background information shows that the ground returns classification process conducted by CVI within TerraScan was designed to reduce Type II error, or the inclusion of object returns in the ground model because two classification routines

were performed to remove topographic variability. First, ground points were classified from all returns, then a second processing was performed on the ground-labeled points from the 1st iteration with a smaller iteration angle. Ground returns classification within Terrascan is a slope-based, point-to-points process in which one point is compared to multiple, additional returns (Sithole and Vosselman, 2004). How this classification influences the modeling of local topographic variability was explored by comparison of the last returns data and CVI classified ground returns data.

Last Returns and Classified Ground Returns Data Comparison:

Return Density and Distribution:

Comparison of the last returns and CVI classified ground returns to 0.6 m pixel SAMB imagery allows for a representation of return distribution over bouldery features. Generally, returns from bouldery landforms were not classified as ground in the CVI ground classification. Even bouldery features not under a tree canopy, such as the two fine blocks at Site 1 (Figures 11a, 11b, 11c, and 11d), were commonly excluded from the ground surface. At Site 4 (Figures 12a and 12b), a fine block partially under a tree canopy, returns were also not classified as ground. Under a tree canopy, such as Site 2 (Figures 12c and 12d), there is a general reduction in ground return density due to

vegetation, and bouldery classification and detection are further hindered.

Models created in three dimensions (Figure 13) using ArcScene further demonstrate that LiDAR returns from bouldery landforms were not classified as ground returns. Two fine blocks at Site 1 (Figure 13a) were not included in the ground surface TIN produced from the CVI classified ground data. The model at Site 4 (figure 13b) shows that detecting boulders under a partial canopy is very complex due to the variability in return elevation. Detecting a boulder as an object at such a location is difficult.

These data support the conclusion that CVI classified ground data provide a smoothed surface model; local topographic variability induced by bouldery landforms is commonly lost. Ground point classification algorithms within TerraScan removed these measurements from the CVI ground model.

Figure 11a: Site 1a
Last Returns

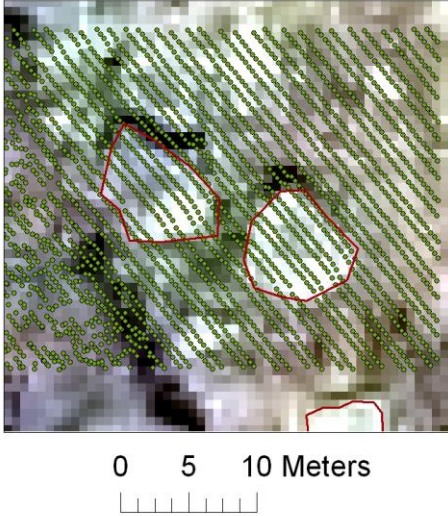


Figure 11b: Site 1a CVI
Classified Ground
Returns

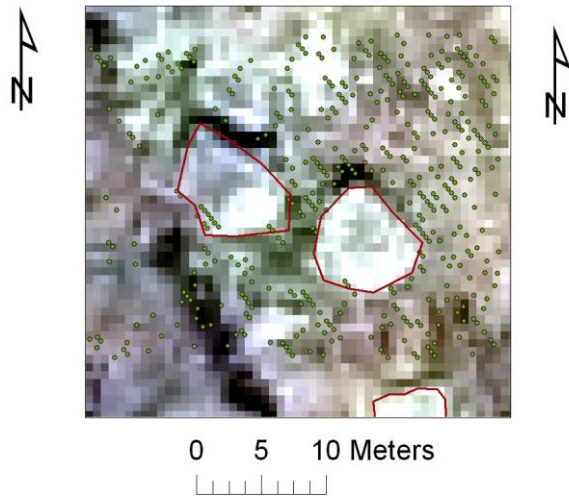


Figure 11c: Site 1b
Last Returns

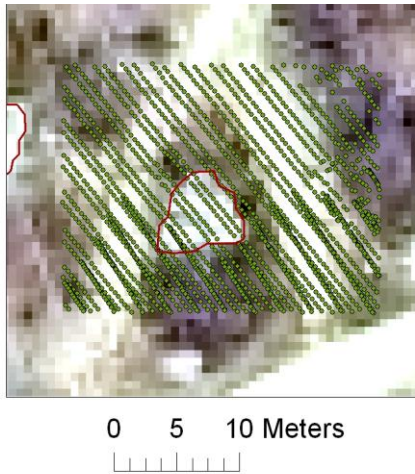
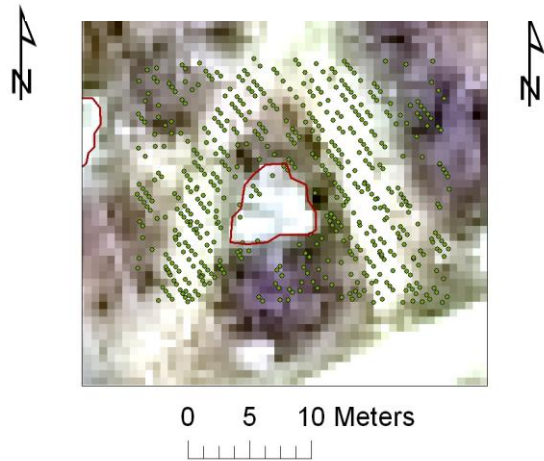


Figure 11d: Site 1b CVI
Classified Ground
Returns




 Bouldery Features

Figure 11: Comparison of last returns and CVI classified ground returns over 0.6 m pixel natural color imagery at Site 1. The base image is the 2003 SAMB imagery. Note how bouldery landforms are commonly associated with gaps in the CVI classified ground returns data.

Figure 12a: Site 4

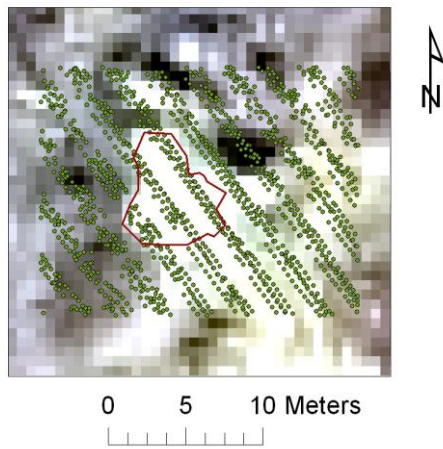


Figure 12b: Site 4 CVI Classified Ground Returns

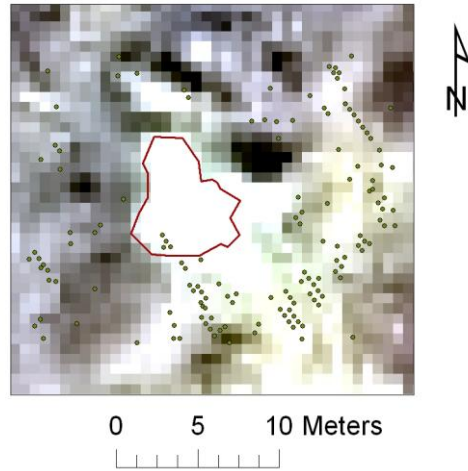


Figure 12c: Site 2 Last Returns

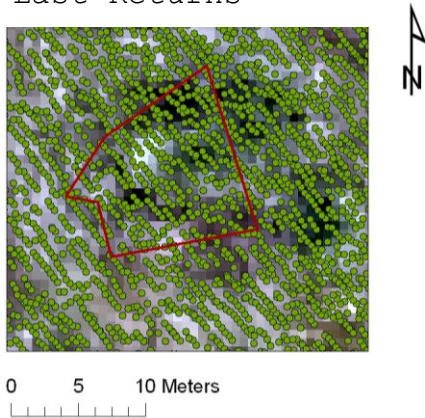
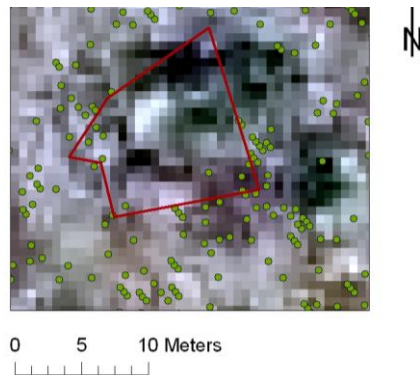


Figure 12d: Site 2 CVI Classified Ground Returns




 Bouldery Features

Figure 12: Comparison of last returns and CVI classified ground returns over 0.6 m pixel natural color imagery at Sites 2 and 4. The base image is the 2003 SAMB imagery. Note how bouldery landforms are commonly associated with gaps in the CVI classified ground returns data.

Figure 13a: Site 1

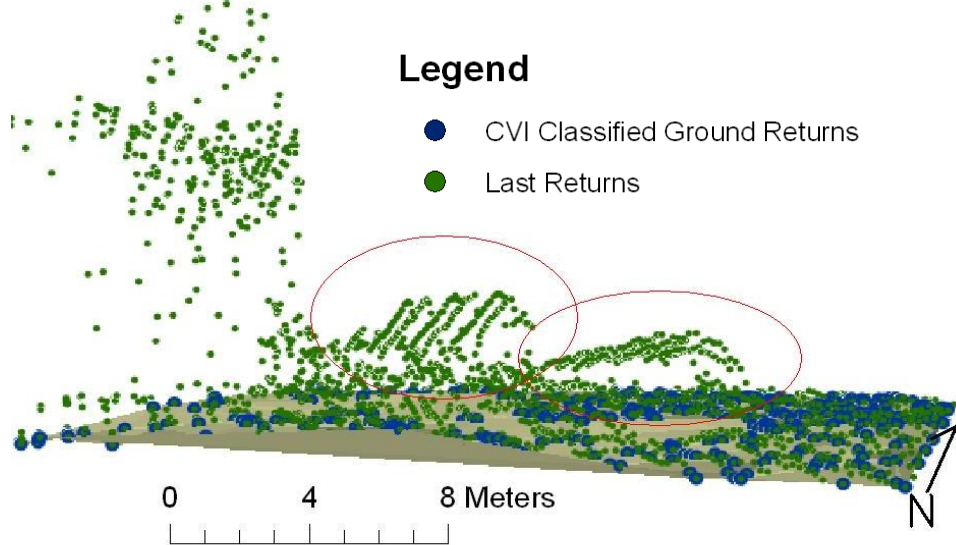


Figure 13b: Site 4

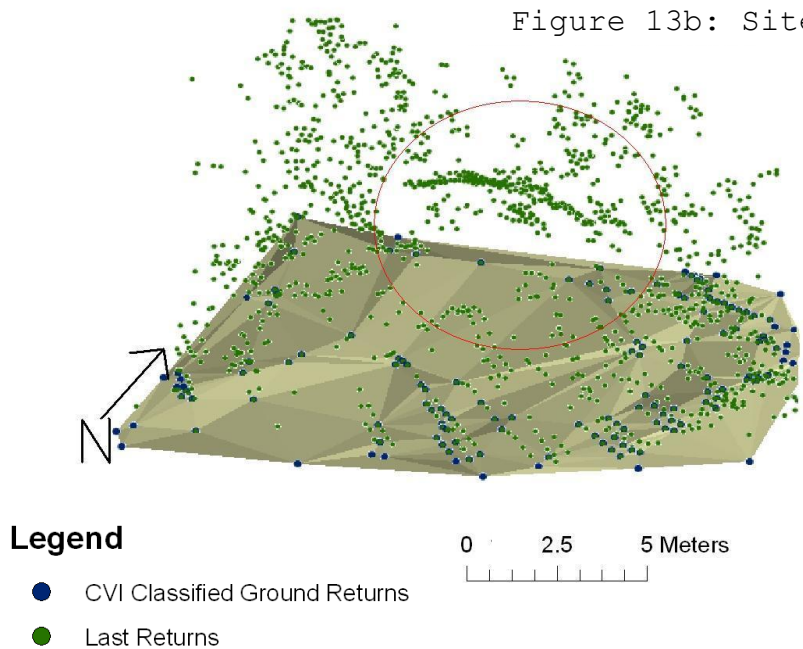


Figure 13: 3D point distribution at Sites 1 and 4. Note that bouldery landforms are positive topographic features up to 6 m above the CVI classified ground data TIN surface.

Comparison of the CVI classified ground returns density and distribution to the hillshade imagery shows that lack of data can give the misleading appearance of a rough ground texture in hillshade imagery. Figure 14 demonstrates a large bouldery feature in an area of rough texture; however, this texture is induced by a lack of point elevation data, not rough topography. Although rough topography may cause a reduction in ground returns density, the resulting rough texture must be interpreted cautiously. As a result, rough texture in hillshade imagery should not be interpreted automatically to mean rough topography. Figure 15 demonstrates an additional large bouldery feature in an area of rough texture, and this texture is induced by a lack of ground returns data.

Figure 14a

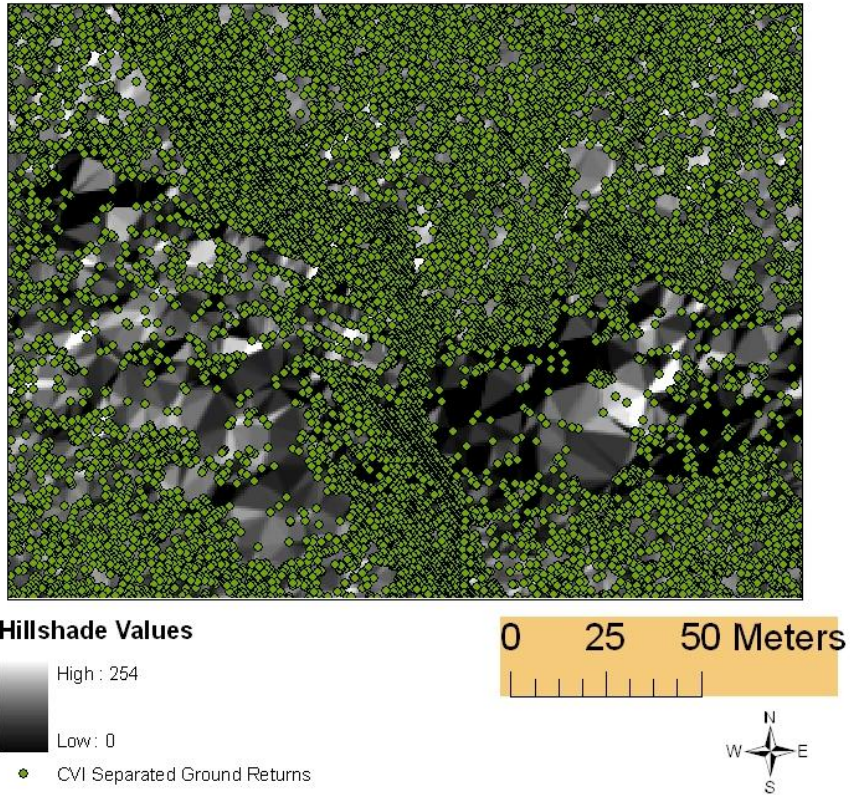


Figure 14b

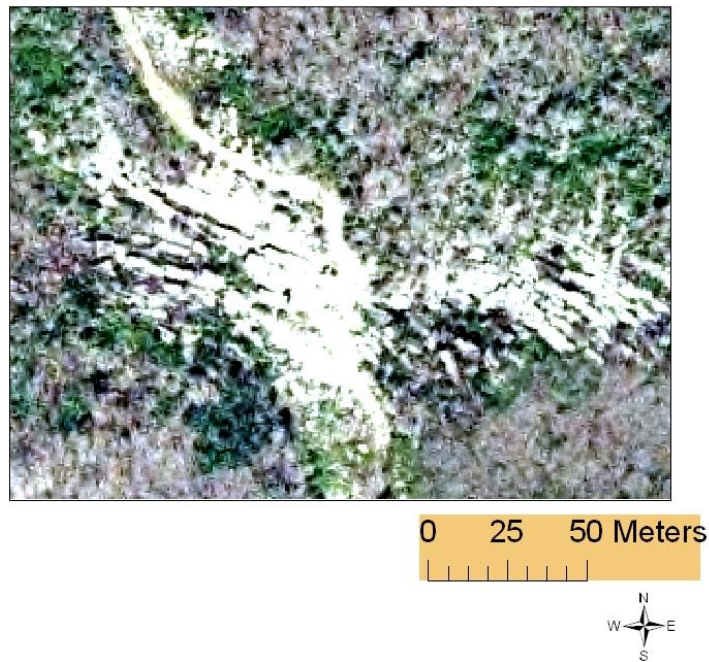


Figure 14: CVI classified ground returns compared to hillshade imagery in power line clearing. The base image is the 2003 SAMB imagery. Note that rough texture in hillshade imagery is caused by a reduction of ground data due to removal during processing. Rugged, bouldery areas are difficult to map based on hillshade texture.

Figure 15a

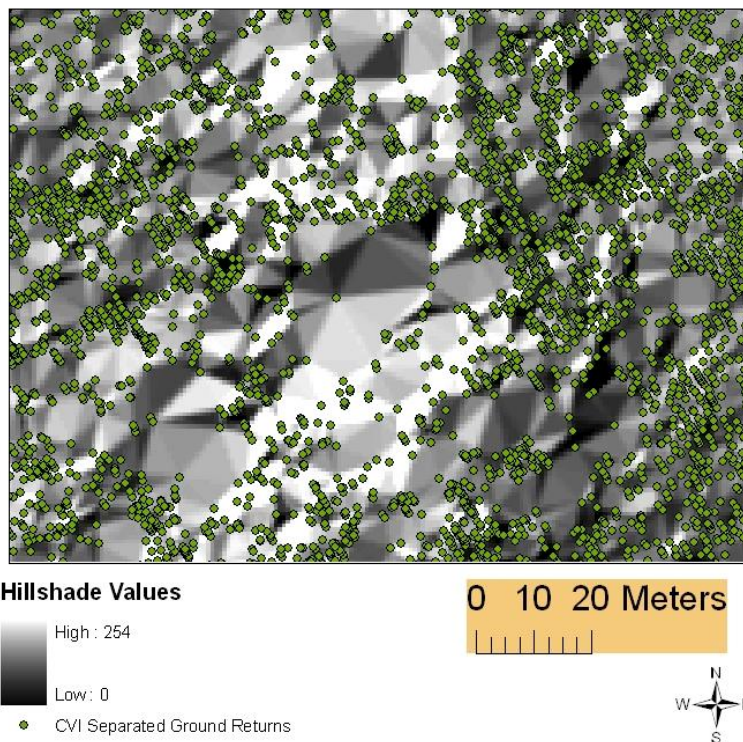


Figure 15b

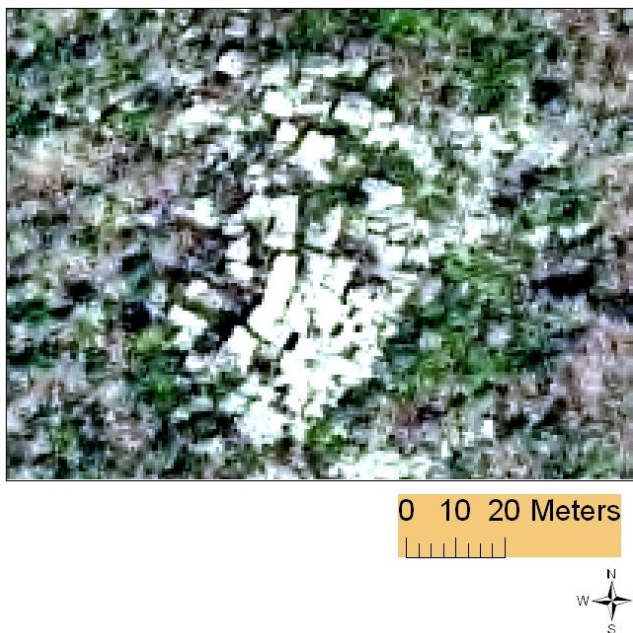


Figure 15: CVI classified ground returns compared to hillshade imagery of bouldery features in forest. The base image is the 2003 SAMB imagery. Note that rough texture in hillshade imagery is caused by a reduction of ground data due to removal during processing. The rock city is difficult to map based on hillshade texture.

Although bouldery features commonly were not classified as ground in the CVI ground returns data set, some features were included as ground classified points, such as the bouldery area in Figure 16. A coniferous canopy may have caused this area to be classified as ground due to a lack of ground returns for comparison to the surrounding area. The morphology of the feature may also have had an influence. A more continuous surface may be classified as ground, whereas disconnected boulders and blocks may not be classified as ground.

Figure 16a

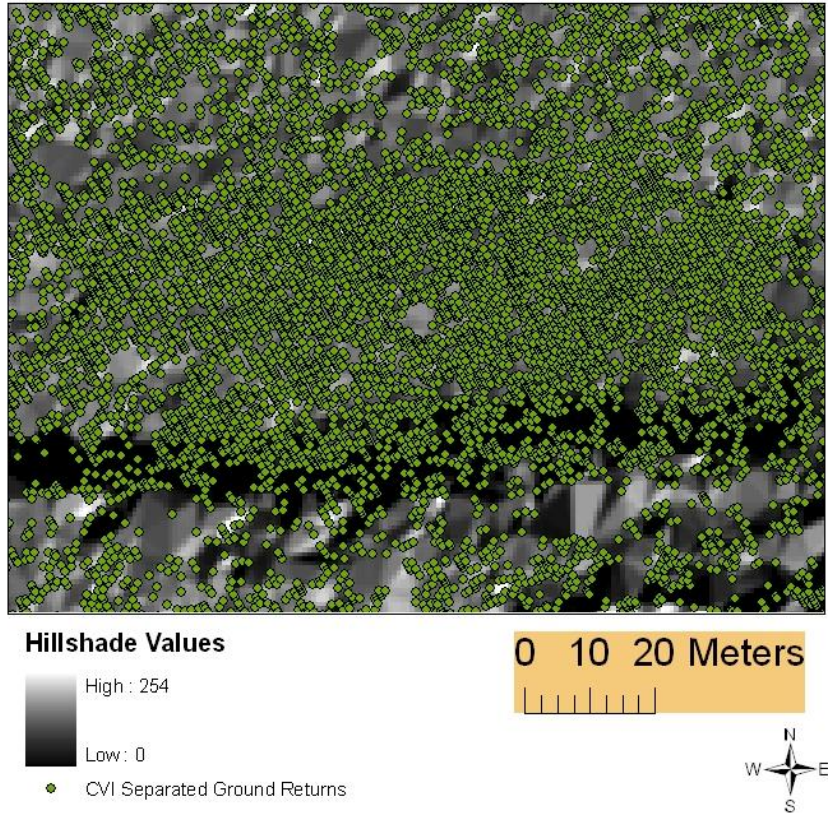


Figure 16b

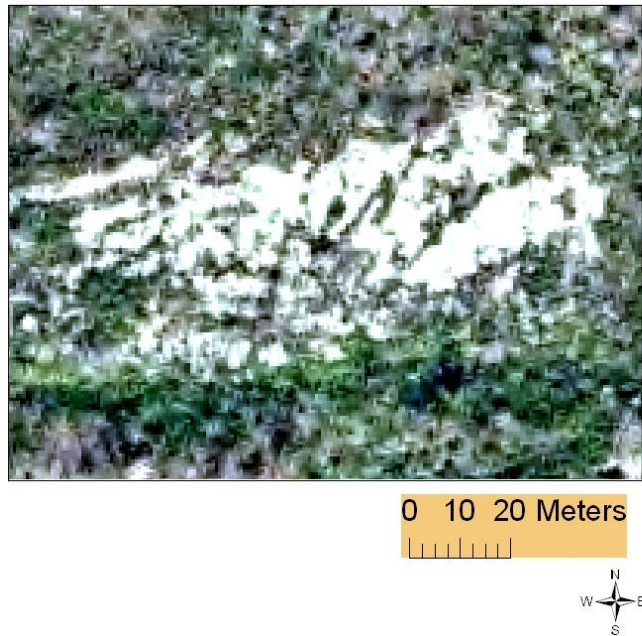


Figure 16: CVI classified ground returns compared to hillshade imagery at site classified as ground. The base image is the 2003 SAMB imagery. Note that not all bouldery landforms were removed from the ground model. The relatively intact boulder and block field is included in the CVI ground classification.

Mean distance from one point to its nearest neighbor, calculated using HawthTools, is summarized in Table 11. As reported in Table 1, CVI stated 0.69 m to be the average ground sampling distance, and Table 14 shows a higher CVI classified ground point density calculated here than reported by CVI. The mean CVI classified ground sampling distance within thirteen sample sites, selected throughout the 5.4 km² study area in areas of varying canopy cover, is 0.62 m with a standard deviation of 0.39 m. The mean last returns sampling distance is 0.30 m with a standard deviation of 0.12 m. As suggested by the standard deviation, there is more variability in point spacing for the CVI classified ground returns than the last returns. The last returns are more evenly spaced because of the uniform LiDAR sensor scanning pattern. This uniform pattern is less evident after the ground point classification process.

	Last Returns Mean	Last Returns Standard Deviation	CVI Classified Ground Returns Mean	CVI Classified Ground Returns Standard Deviation
Sample 1	0.38 m	0.06 m	0.65 m	0.31 m
Sample 2	0.28 m	0.15 m	0.50 m	0.23 m
Sample 3	0.35 m	0.12 m	0.57 m	0.24 m
Sample 4	0.23 m	0.12 m	0.67 m	0.49 m
Sample 5	0.39 m	0.10 m	0.76 m	0.51 m
Sample 6	0.40 m	0.10 m	0.78 m	0.44 m
Sample 7	0.34 m	0.12 m	0.83 m	0.48 m
Sample 8	0.36 m	0.11 m	0.78 m	0.45 m
Sample 9	0.26 m	0.11 m	0.48 m	0.24 m
Sample 10	0.21 m	0.21 m	0.38 m	0.53 m
Sample 11	0.35 m	0.12 m	0.68 m	0.41 m
Sample 12	0.23 m	0.11 m	0.73 m	0.49 m
Sample 13	0.12 m	0.19 m	0.21 m	0.30 m
Mean	0.30 m	0.12 m	0.62 m	0.39 m

Table 14: Mean distance between nearest last returns and ground returns comparison for thirteen samples. These data show a higher ground point density of 0.62 m than reported by CVI, 0.69 m.

Although the CVI classified ground data are shown to have a density higher than that reported by CVI, this density is not evenly distributed. There are large gaps and clusters within the data, and bouldery landforms often exist within the data gaps. Figures 17, 18, and 19 provide examples of areas where bouldery landforms are associated with data gaps in the classified ground data. As a result, the data density is much lower in these areas. Figure 20 demonstrates an area where returns from bouldery landforms were classified as ground by CVI, the same location as Figure 16, made evident by a higher return density over these features than other bouldery landforms. Figure 21

represents a conifer area where data density is reduced compared to open areas. As a result, there are many reasons for lack of data density besides bouldery landforms. Figure 22 provides a comparison of last returns and classified ground returns point density at Sites 1 and 4. Bouldery features occur in data gaps.

This raster-based point count procedure provides a visualization of clustering and dispersion relating to bouldery features. This technique shows that 57.2% of the 1 m grid cells in the 5.4 km² area have no returns within them classified as ground by CVI. Generally, bouldery landforms exist in data gaps, supporting the conclusion that returns over bouldery landforms were not included in the CVI classified ground data.

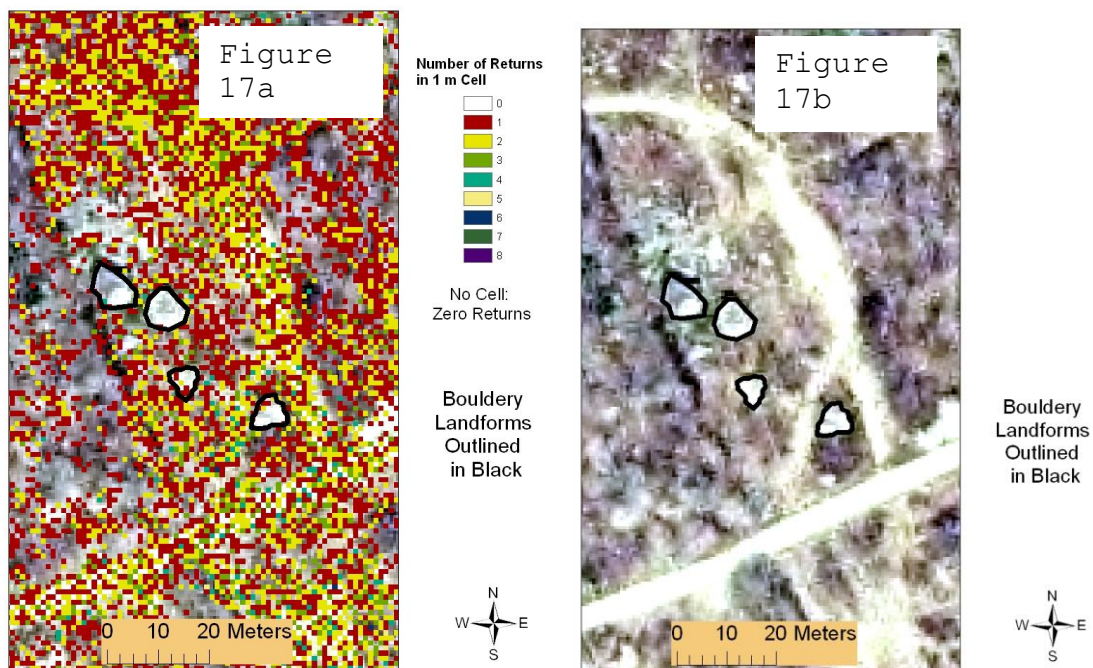


Figure 17: Examples of LiDAR data density reduction over bouldery landforms in power line clearing 1. Base image is the 2003 SAMB imagery.

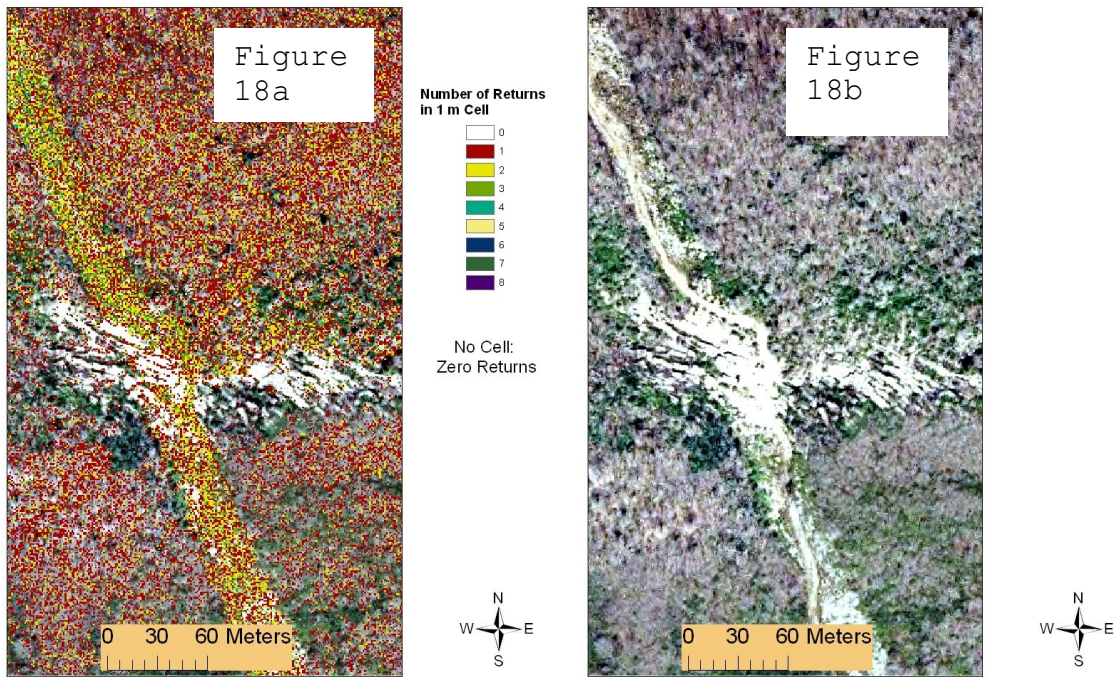


Figure 18: Examples of LiDAR data density reduction over bouldery landforms in power line clearing 2. Base image is the 2003 SAMB imagery.

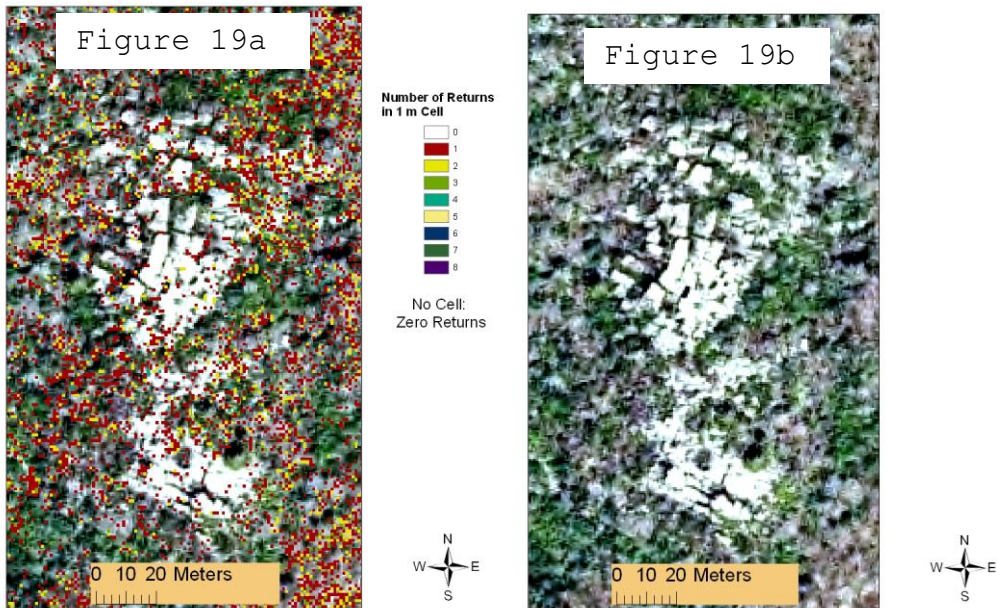


Figure 19: Examples of LiDAR data density reduction over bouldery features in forest. Base image is the 2003 SAMB imagery.

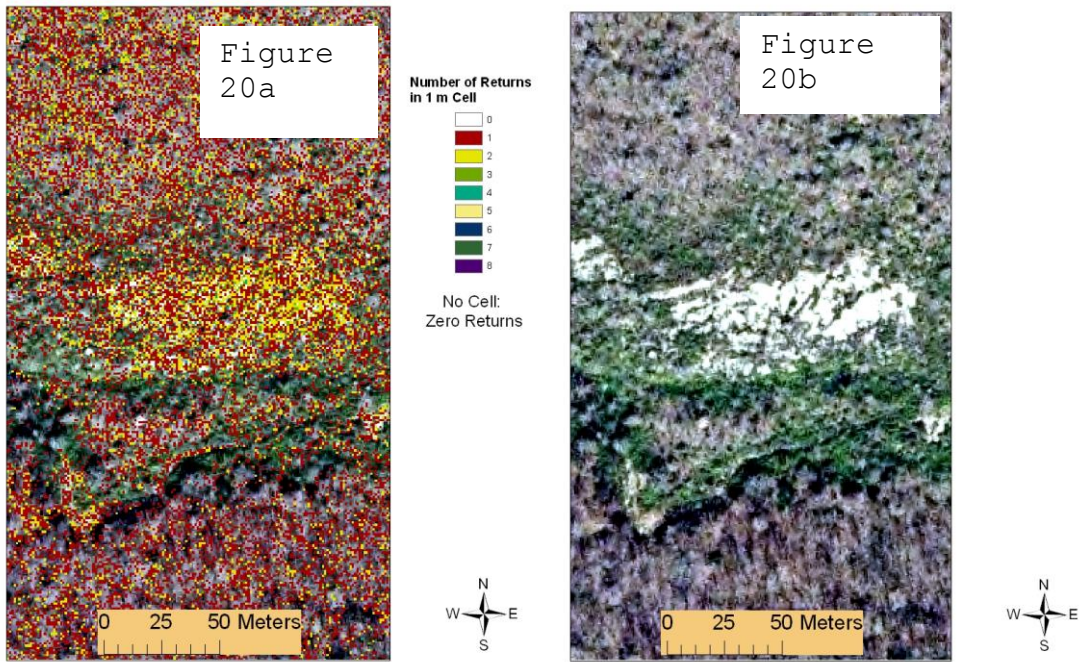


Figure 20: Examples of bouldery landforms included in ground model. Base image is the 2003 SAMB imagery.

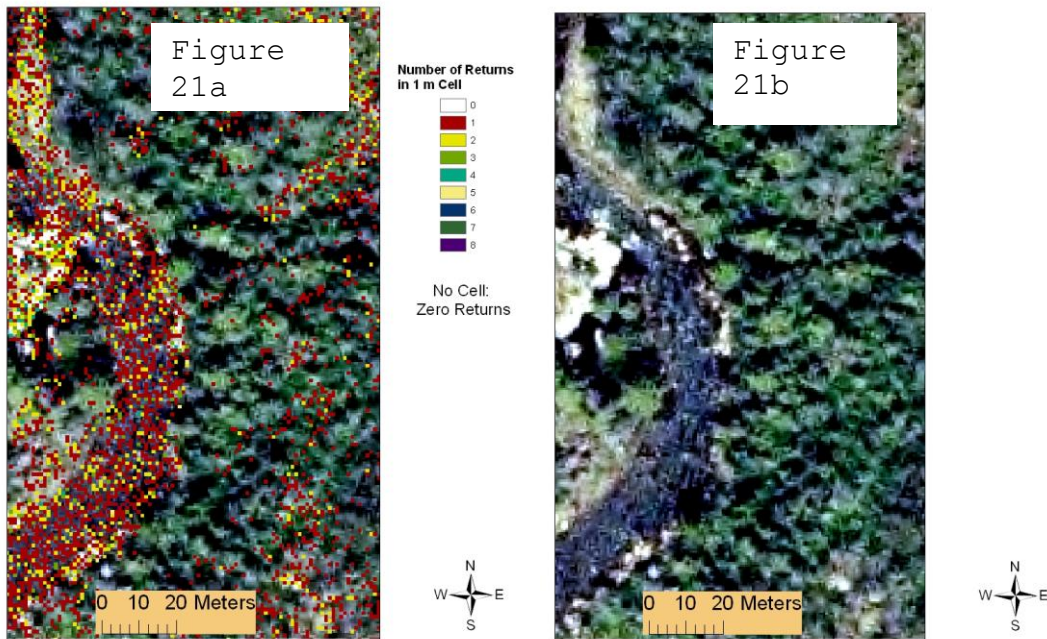


Figure 21: Examples of LiDAR data density reduction in area with coniferous canopy. The base image is the 2003 SAMB imagery.

Figure 22a: Site 1 Number of Returns in Site 1 m Cell

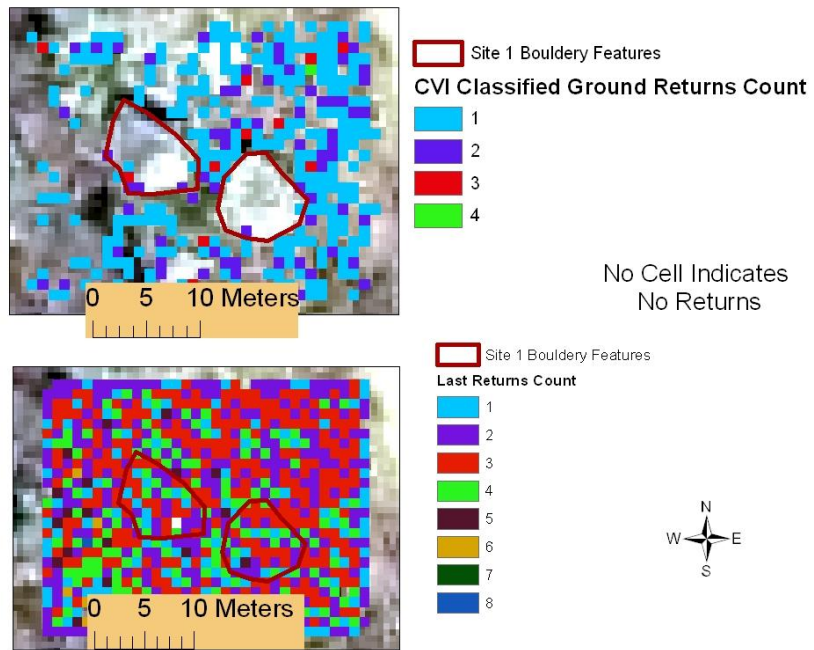


Figure 22b: Site 4 Number of Returns in Site 1 m Cell

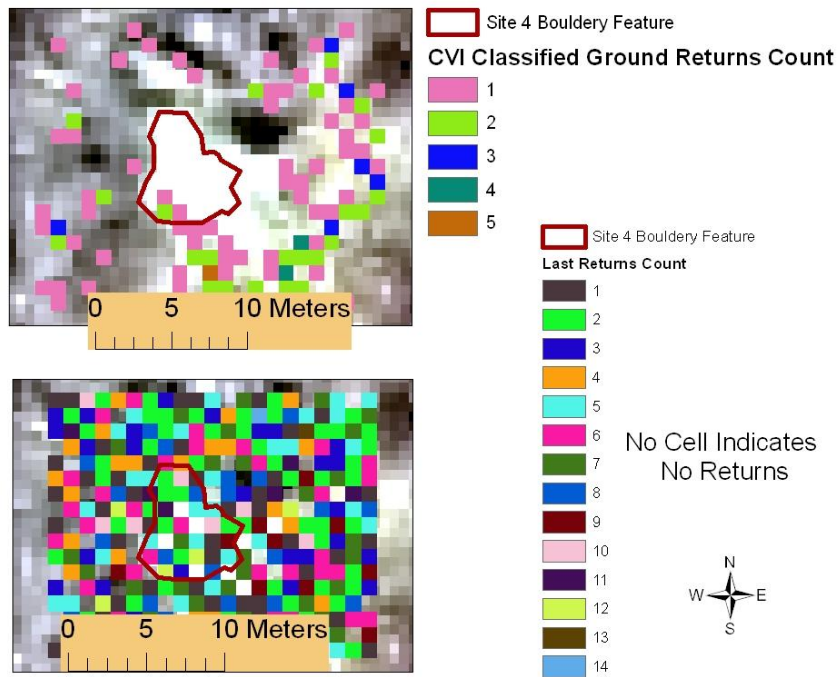


Figure 22: Data density reduction over bouldery features at Sites 1 and 4. The base image is the 2003 SAMB imagery.

Elevation Comparison of LiDAR Last Returns and CVI Classified Ground Returns Data:

Elevation values were compared between elevations raster grids produced from the last returns data and the CVI classified ground returns data. The two raster grids were subtracted to produce an elevation difference raster grid (Figure 23). Local elevation difference between last returns and CVI classified ground returns was used to highlight where last returns points were not included as ground in the CVI model. Figure 24 at Site 1 shows that the two fine blocks were not classified as ground as indicated by the positive elevation difference. In open areas, where bouldery landforms were not classified as ground, this deviation from the ground surface can be used to show where bouldery features may reside.

The elevation difference is more complex under a tree canopy such as Site 4 (Figure 25) and Site 2 (Figure 26). Because not all last returns were reaching the ground surface, vegetation is a problem in this model. Vegetation induced variability is evident at Site 2 where elevation difference values are erratic and the medium block present there cannot be easily outlined based on elevation difference between last returns and CVI classified ground returns. An area of predominantly coarse boulders under a tree canopy at Site 5 (Figure 27) also cannot be mapped using this method.

Elevation Difference (Last Returns 0.69 m Raster Grid - CVI Classified Ground Returns 0.69 m Raster Grid)

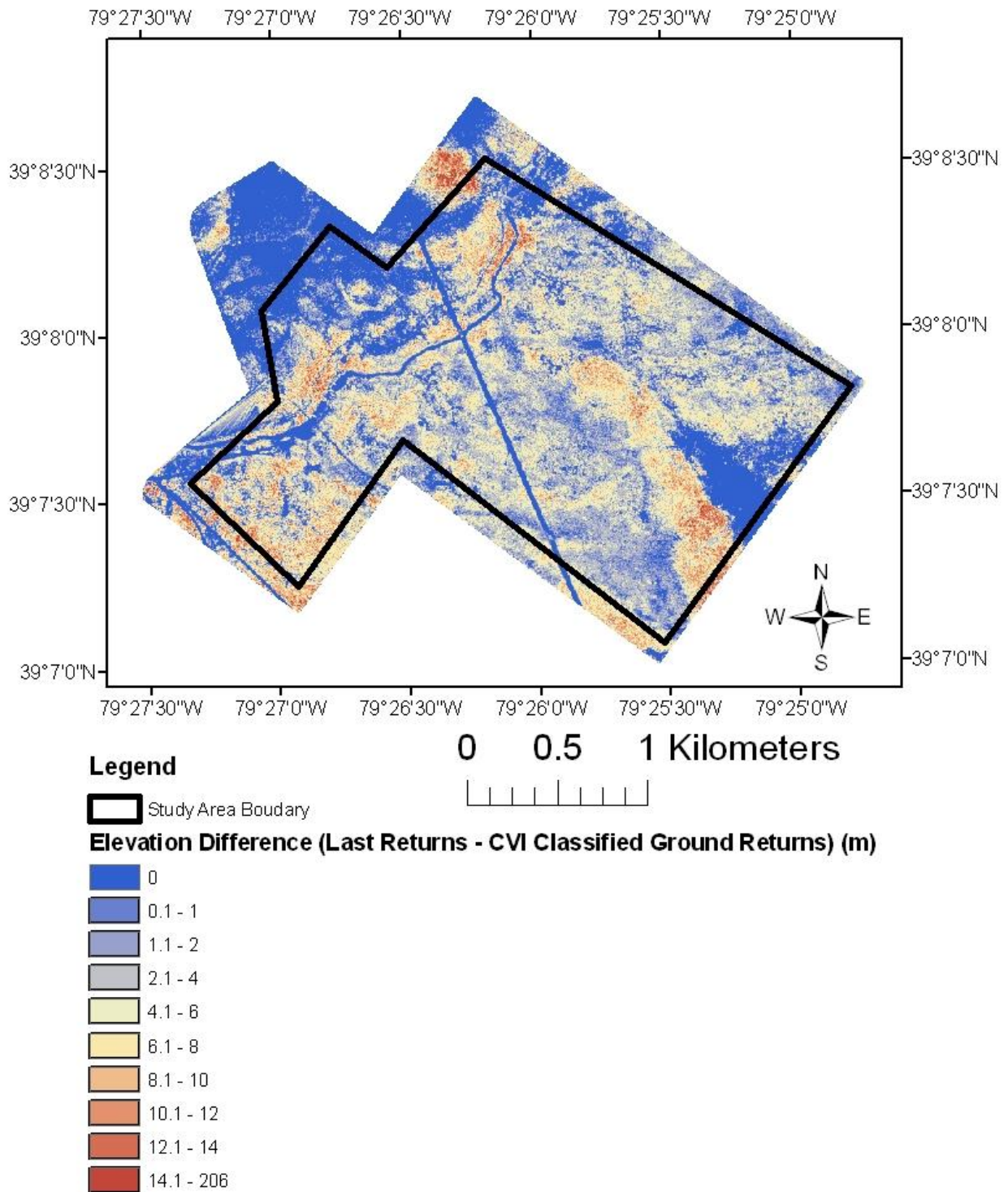


Figure 23: Elevation difference between last returns and CVI classified ground returns raster grid. Raster grid is grouped into quantiles.

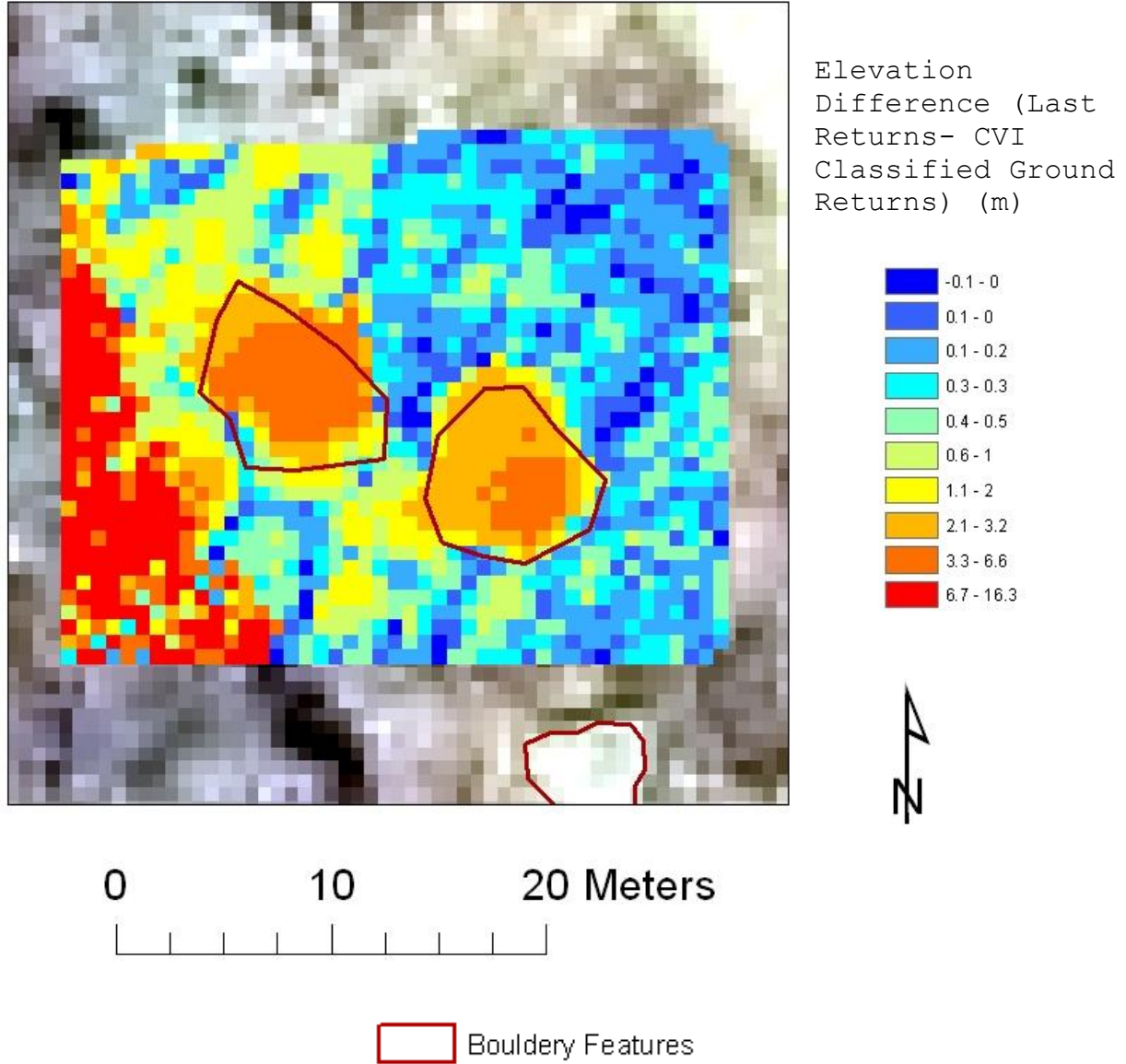


Figure 24: Elevation difference between last returns and CVI classified ground returns at Site 1. Base image is the 2003 SAMB imagery. The elevation difference raster grid is grouped into quantiles. Note that the two fine blocks can be mapped using elevation difference between last returns and CVI classified ground returns data at this location.

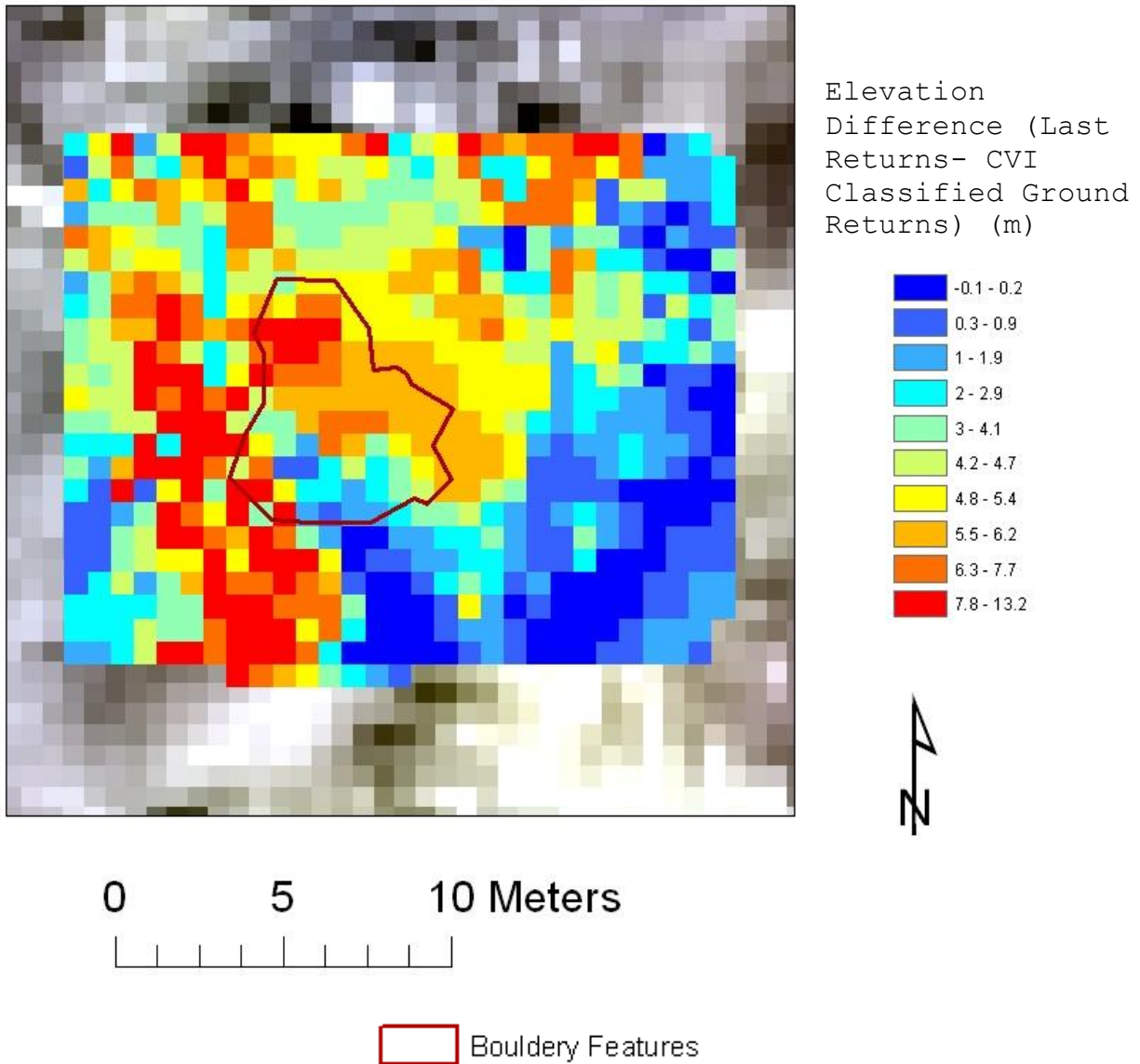


Figure 25: Elevation difference between last returns and CVI classified ground returns at Site 4. Base image is the 2003 SAMB imagery. The elevation difference raster grid is grouped into quantiles. Note that the fine block cannot be mapped using elevation difference between last returns and CVI classified ground returns at this location.

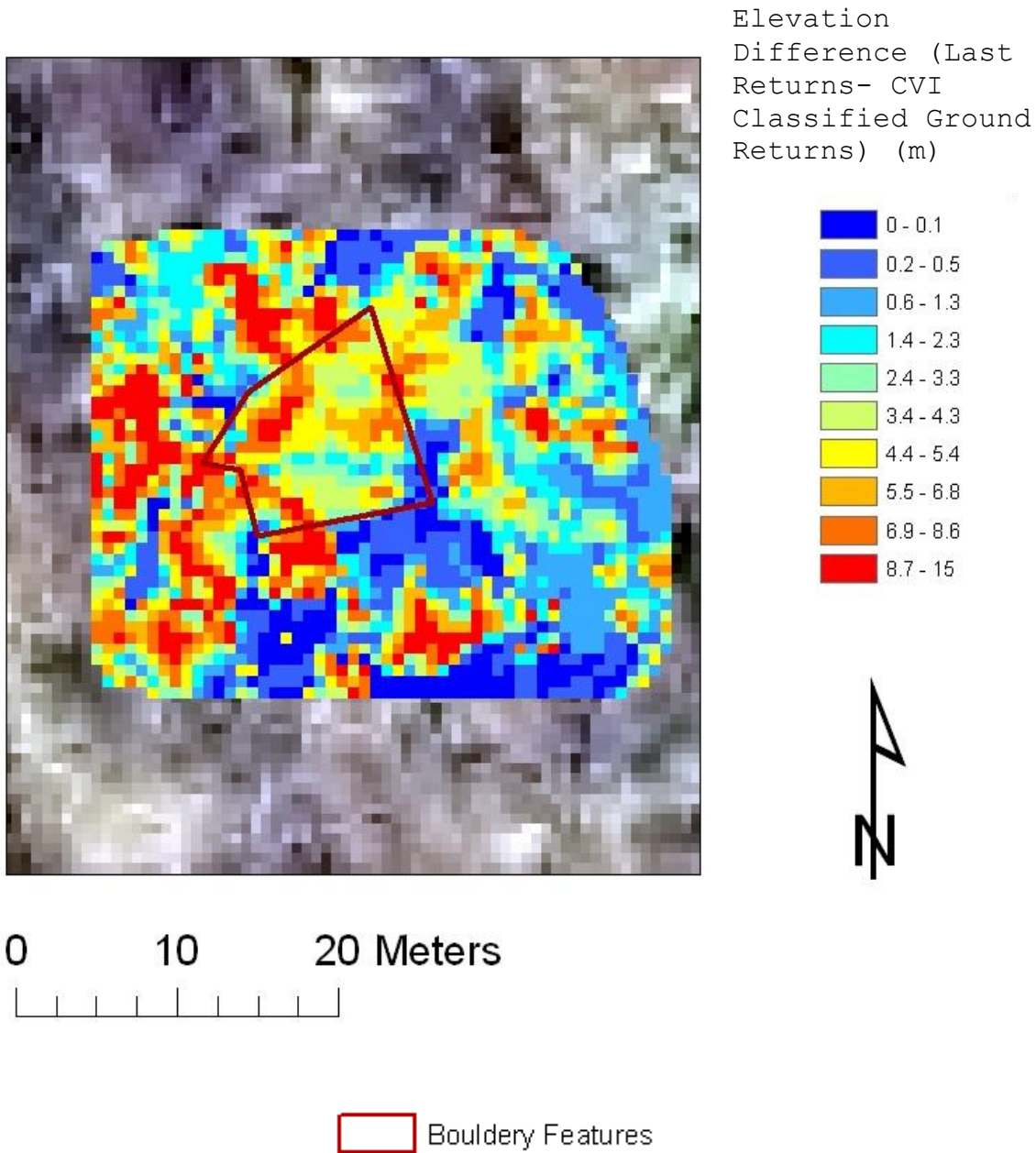


Figure 26: Elevation difference between last returns and CVI classified ground returns at Site 2. Base image is the 2003 SAMB imagery. The elevation difference raster grid is grouped into quantiles. Note that the medium block cannot be mapped using elevation difference between last returns and CVI classified ground returns at this location under a tree canopy.

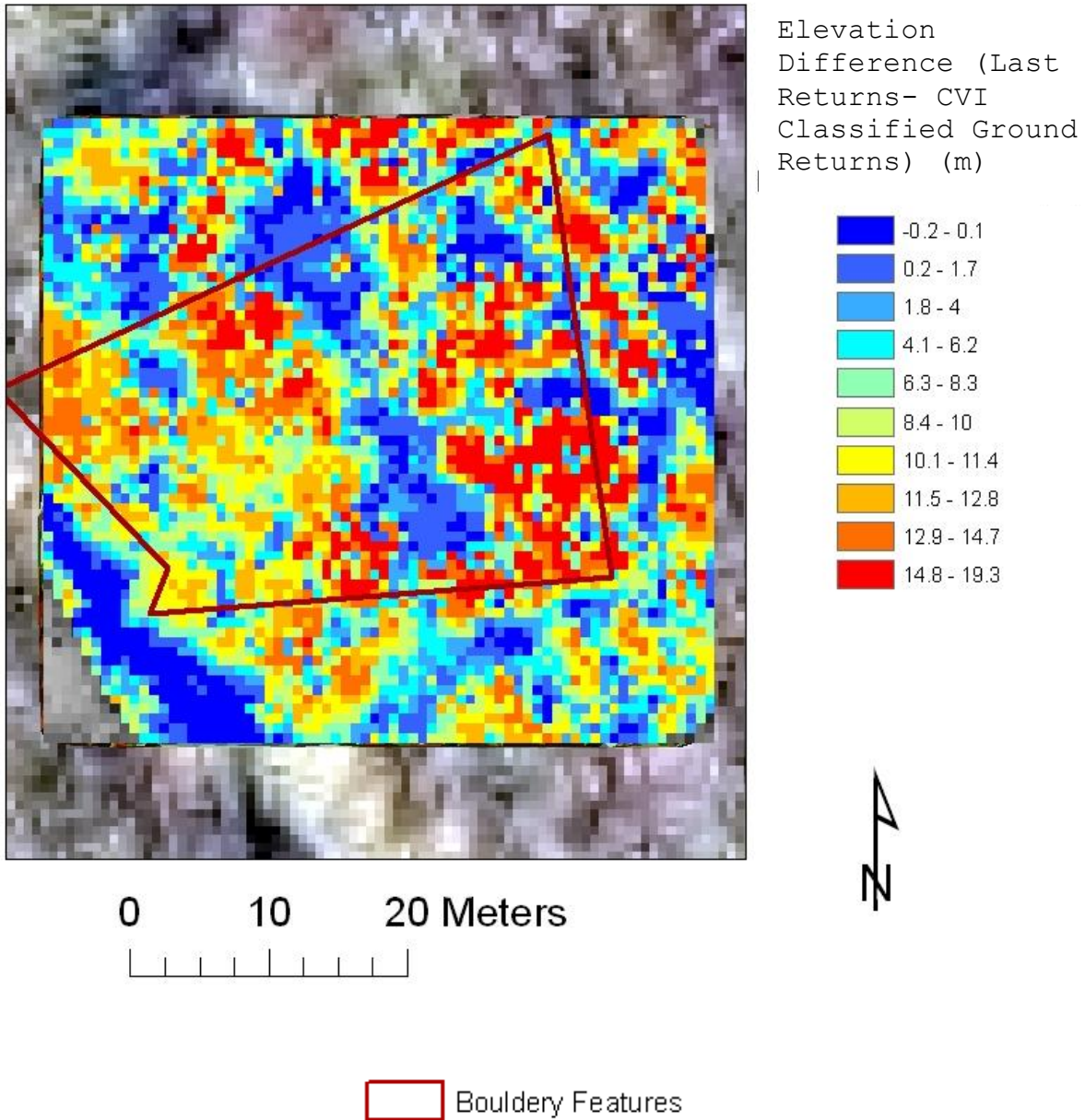


Figure 27: Elevation difference between last returns and CVI classified ground returns at Site 5. Base image is the 2003 SAMB imagery. The raster grid was grouped into quantiles. Note that the boulder field cannot be mapped using elevation difference between last returns and CVI classified ground returns at this location under a tree canopy.

On the CVI property, the influence of slope and vegetation on ground returns classification was explored. Elevation difference between last returns and CVI classified ground returns and ground point density were used as surrogates for ground classification. The box and whisker plot (Figure 28) shows that the median value for areas classified as field in the natural color supervised classification is lower than the median value for other classifications. In other words, open areas were more likely classified as ground, and vegetation influences ground classification. Grid cells classified as water had a large range of values because many cells were misclassified into that group due to shadows.

The ordinary least squares regression results (Table 15) show that elevation difference and CVI classified ground point density are not strongly correlated with slope, ground returns intensity, and normalized difference vegetation index (NDVI). Ground intensity and NDVI were used as surrogates for vegetation. The AIC value shows that elevation difference between last returns and CVI classified ground returns and CVI classified ground point density are more correlated with NDVI and ground returns intensity than slope. This value shows that ground returns classification was more influenced by vegetation than slope. All of the adjusted R^2 values are less than 0.3, but T-tests, F-tests, and Wald-tests calculated in ArcMap show that

the adjusted R^2 values are statistically significant. Ordinary least squares regression was used and not geographically weighted regression because the global pattern is of interest. Sithole and Vosselman (2004) found that slopes, discontinuities, vegetation, low ground return density, and terrain complexity can induce error in classification of ground points.

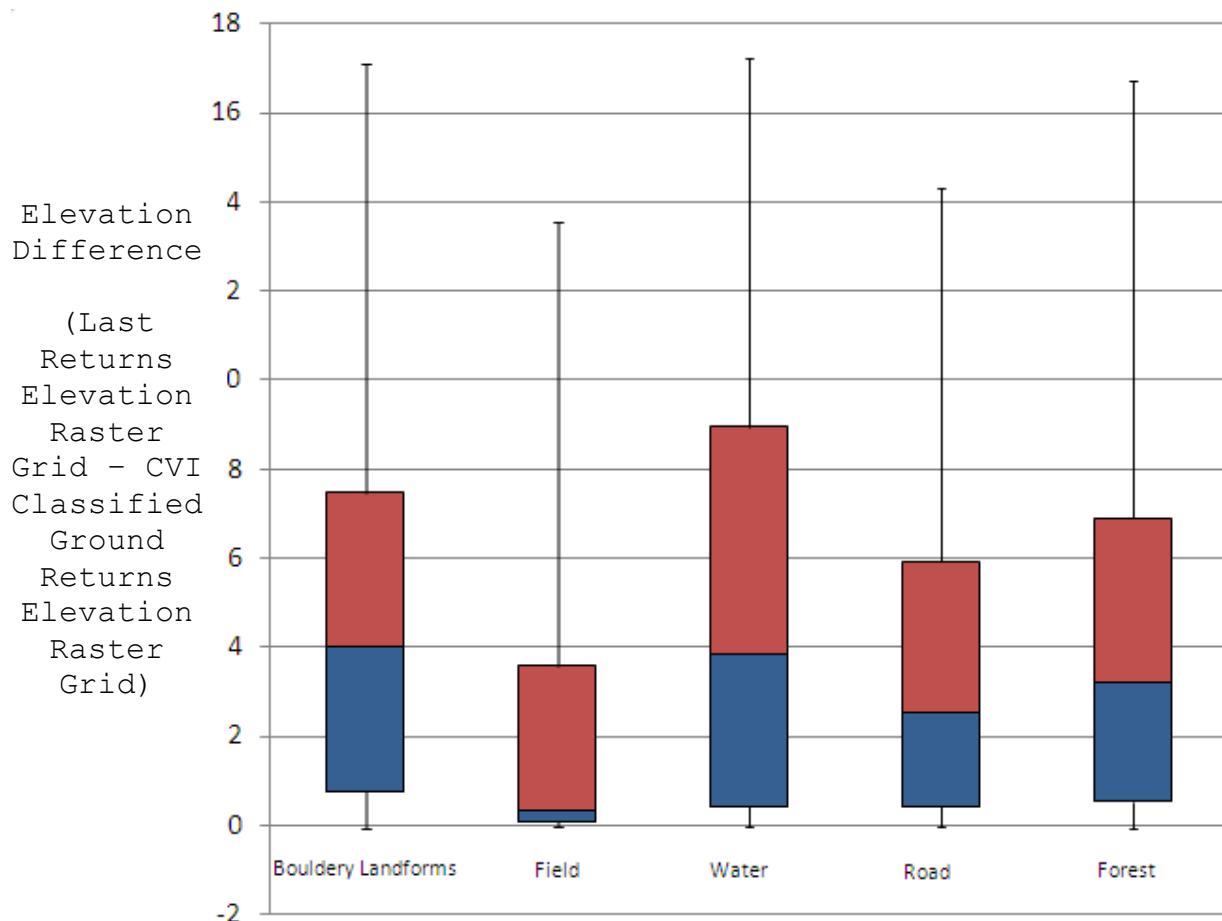


Figure 28: Elevation difference between last returns and CVI classified ground returns and natural color supervised classification comparison. Note that the median value is lower for fields (open areas) than the other classifications; therefore, vegetation has an influence on ground return classification.

CVI Classified Ground Return Density			
	Slope	CVI Ground Intensity	NDVI
R^2	0.0098	0.0417	0.0121
R^2 Adjusted	0.0091	0.0410	0.0117
AIC	3389.1	3342.6	3385.3
T-Test	-3.74	7.85	-4.22
T-Test Statistical Probability (p-value)	0.000202	0	0.000031
F-Test	14	61.7	17.8
F-Test Statistical Probability (p-value)	0.00019	0	0.000026
Wald-Test	12.9	48.5	14.82
Wald-Test Statistical Probability (p-value)	0.000328	0	0.000118
Elevation Difference (Last Returns - CVI Classified Ground Returns)			
	Slope	CVI Ground Intensity	NDVI
R^2	0.0120	0.2596	0.0911
R^2 Adjusted	0.0011	0.2590	0.0904
AIC	8000.9	7591.3	7882.4
T-Test	4.15	-22.3	11.9
T-Test Statistical Probability (p-value)	0.00004	0	0
F-Test	17.2	497.1	188.2
F-Test Statistical Probability (p-value)	0.000035	0	0
Wald-Test	15.2	763.5	188.2
Wald-Test Statistical Probability (p-value)	0.000097	0	0
NDVI	Normalized Difference Vegetation Index		
Statistical Probability (p-value)	If p-value is less than 0.05 the variable is statistically significant.		
R^2	Coefficient of Determination: The proportion of variation in the dependent variable that is explained by the model		
R^2 Adjusted	R-Squared adjusted for model complexity (number of variables) as it relates to the data		
AICc	Akaike's Information Criterion: A relative measure of performance to compare models; smaller AIC indicates the superior model		

Table 15: Ordinary least squares regression results. Note that vegetation and slope are not strongly correlated with elevation difference between last returns and CVI classified ground data.

Local topographic change and variability were described using the profiling tool within the 3D Analyst Extension. Last returns data and CVI classified ground returns data, as TINs and 0.69 m raster grids, were compared (Figures 29-32). At Site 1 (Figure 29) the two fine blocks are characterized well using the raster grid and TIN last returns data. The height and orientation of the feature can be determined; however, the CVI classified ground data do not portray the features because the returns striking the objects were not included in the ground classification. As a result, the CVI classified ground data analyzed here cannot be used to study local topographic variation because of the smoothing that occurred due to ground returns classification; raster grid cells or TIN surfaces at the boulder locations were interpolated from neighboring data points that were included in the ground surface. This conclusion is further supported in Figure 30 where a fine block at Site 1 is not completely portrayed in the ground data. A fine block under a partial tree canopy, Site 4 (Figure 31), is also not portrayed in the CVI ground classified points. The last returns show this topographic feature; however, some vegetation is also included as part of the texture. Figure 32 is a topographic profile over a medium block under a tree canopy at Site 2. Because not all last returns reflected from the ground surface, vegetation is a problem in mapping bouldery landforms using last returns data.

Modeling bouldery landforms in open areas can be accomplished using the last returns data: the features at Site 1 exist in the last returns data. Modeling bouldery landforms under a tree canopy requires ground classifications: vegetation returns are a problem at Site 2.

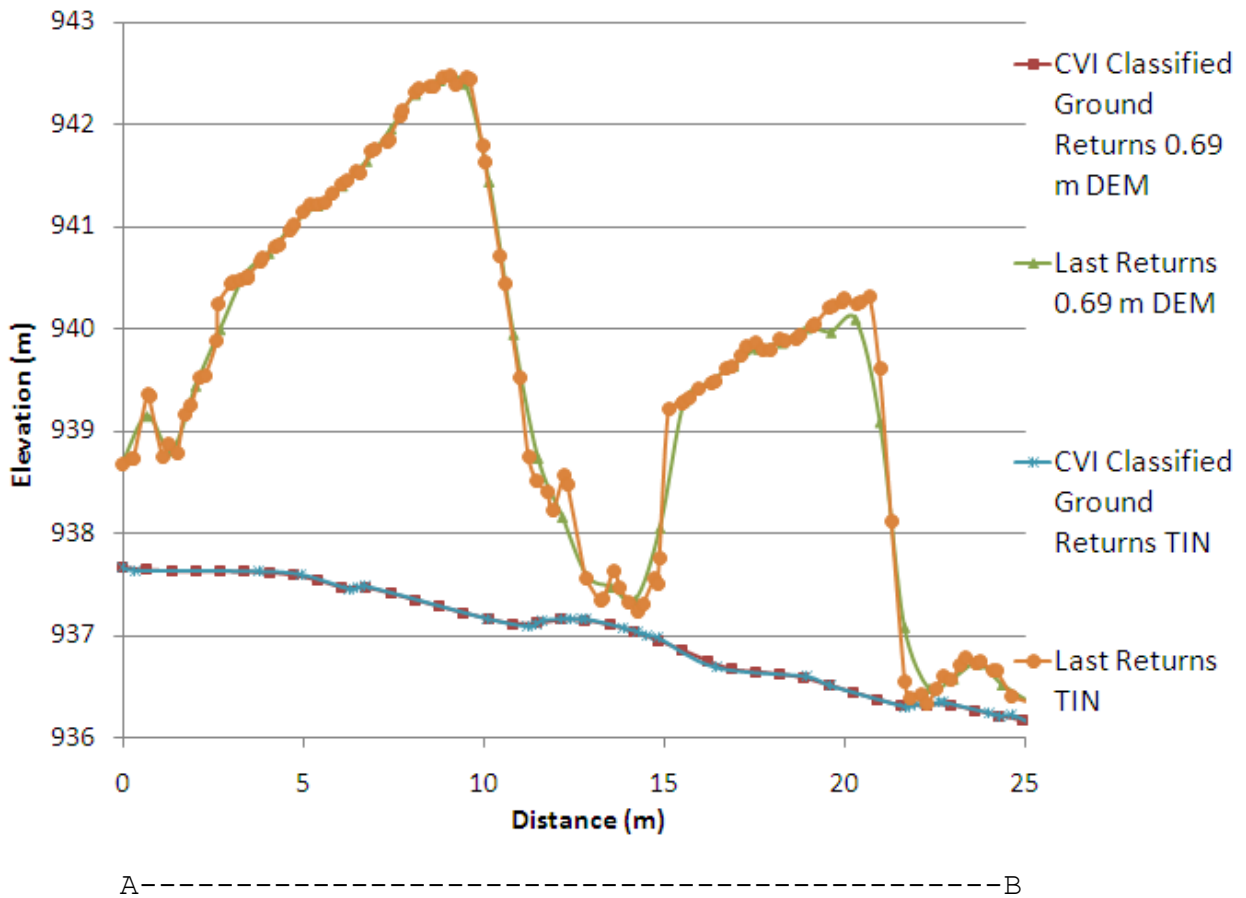
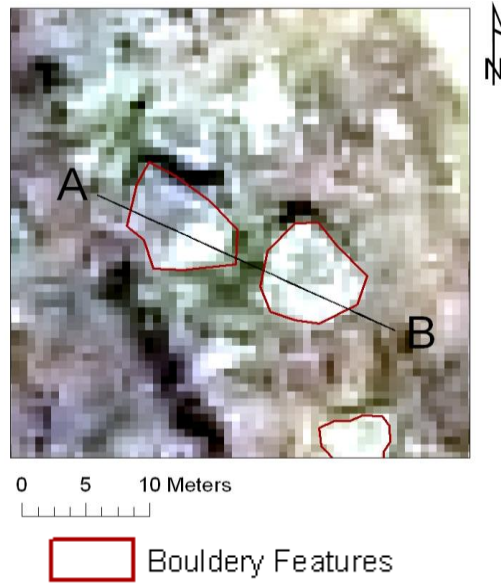


Figure 29: Topographic profile at Site 1a. Base image is the 2003 SAMB imagery. Note that processing removed bouldery landforms from the CVI classified ground data.

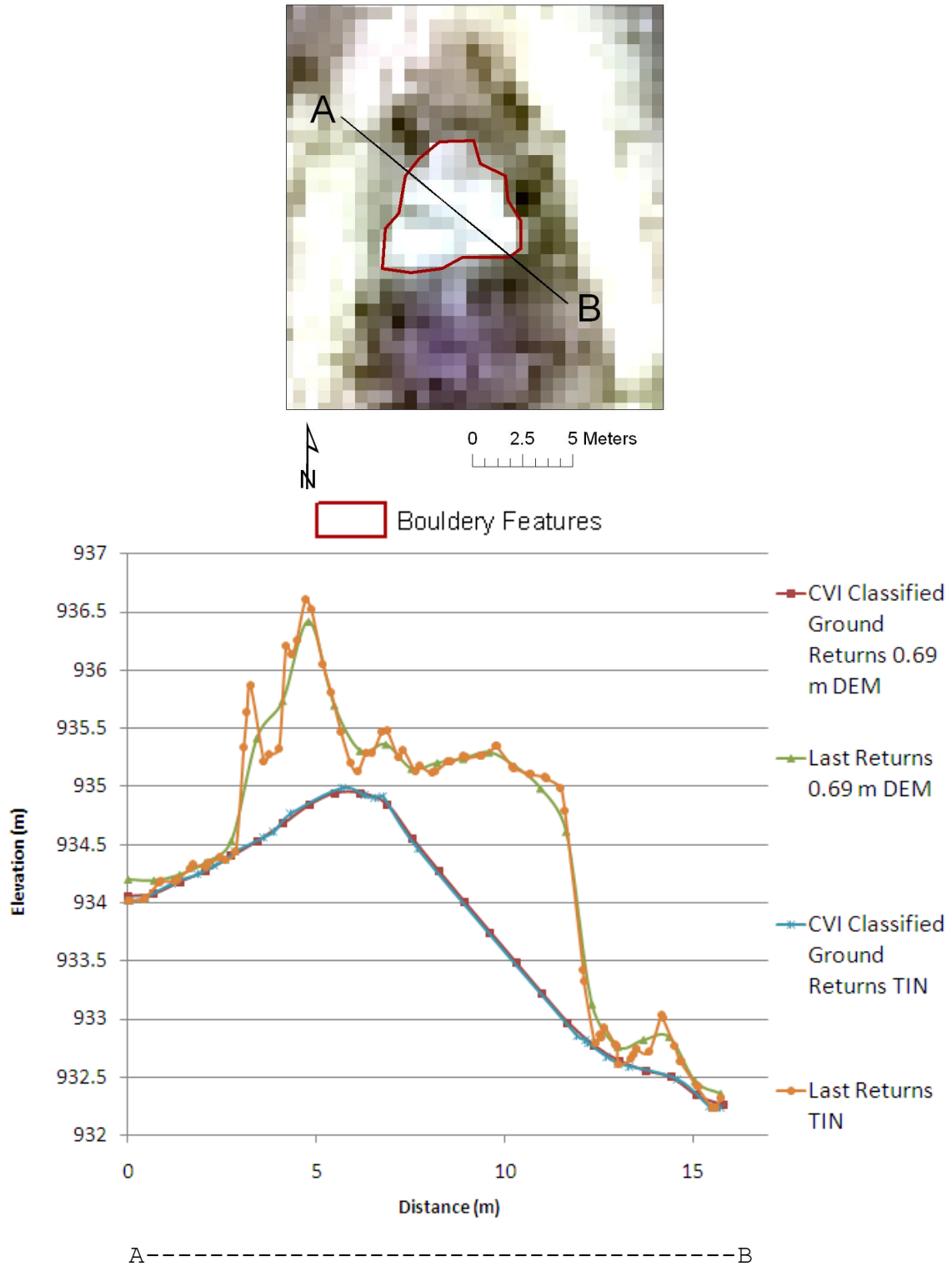


Figure 30: Topographic profile at Site 1b. Base image is the 2003 SAMB imagery. Note that processing resulted in a partial representation of the bouldery landforms in the CVI classified ground data.

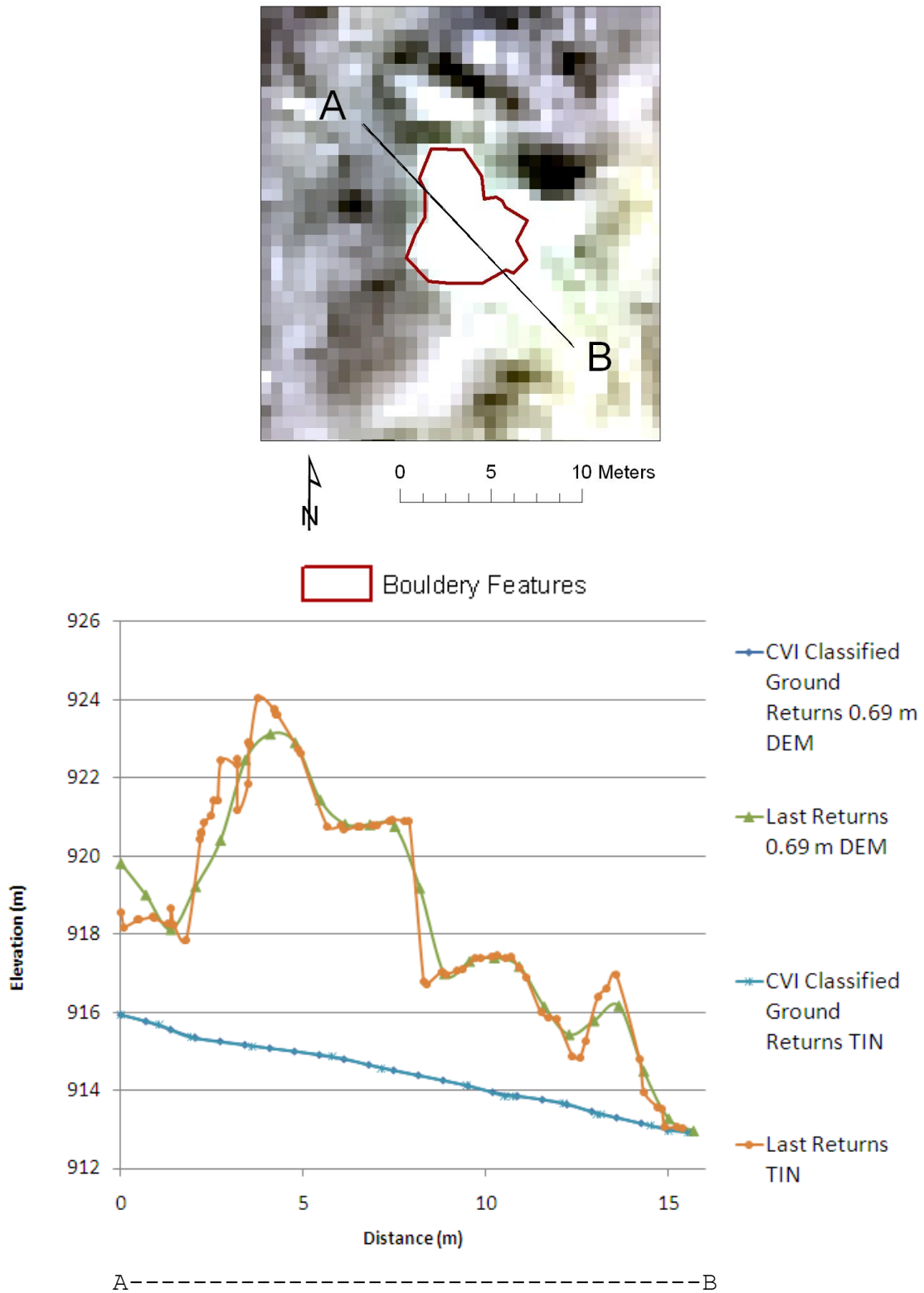


Figure 31: Topographic profile at Site 4. Base image is the 2003 SAMB imagery. Note that processing removed bouldery landforms from the CVI classified ground data.

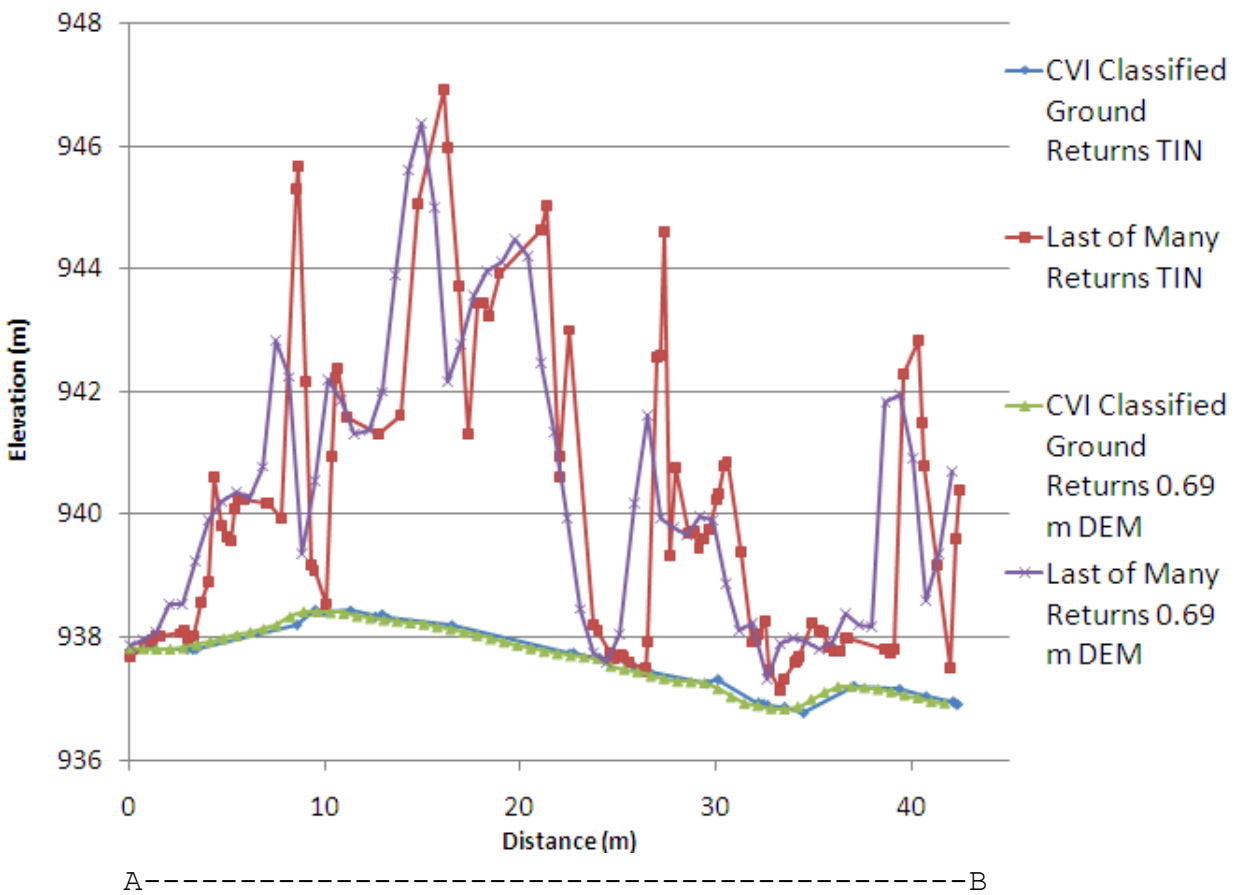
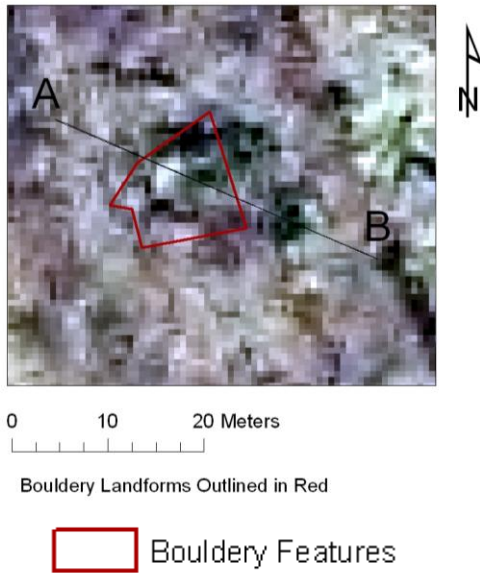


Figure 32: Topographic Profile at Site 2. Base image is the 2003 SAMB imagery. Note that not all last returns reached the ground surface. The LiDAR energy may be dissipated in the tree canopy.

Intensity of LiDAR Last Returns Data:

Intensity of LiDAR last returns was used to create images from LiDAR data (Figure 33). Return intensity is lower for bouldery features than the surrounding vegetation in open areas. This relationship is described in Table 6 and shown in Figure 34. Bouldery features can be identified in open areas, such as Site 1, using LiDAR last returns intensity. However, this approach under a tree canopy is not adequate; it is not possible to map bouldery features at Sites 2 and 4 using this method. Intensity values in forested areas vary greatly, highlighting the problem induced by vegetation. Furthermore, vegetation growing on top of bouldery features increases the return intensity values; as a result, intensity measurements are not reliable under such circumstances.

Figure 35 compares the intensity of last returns data to CVI classified ground returns data. Because returns over bouldery landforms were generally not classified as ground by CVI's processing, the bouldery features cannot be mapped based on intensity using the classified ground data. The point data that provided the lower intensities were generally removed from the CVI ground classified data.

Prior research by Lin and Mills (2010) has shown that last returns intensity is influenced by many variables including footprint size, scan angle, return number, and range distance.

It is difficult to use the intensity variable quantitatively (Lin and Mills, 2010). As a result, it is difficult to compare intensity values over large areas or between data sets. Also, it is necessary to take return number into account when using this data (Lin and Mills, 2010). This research supports these previous findings.

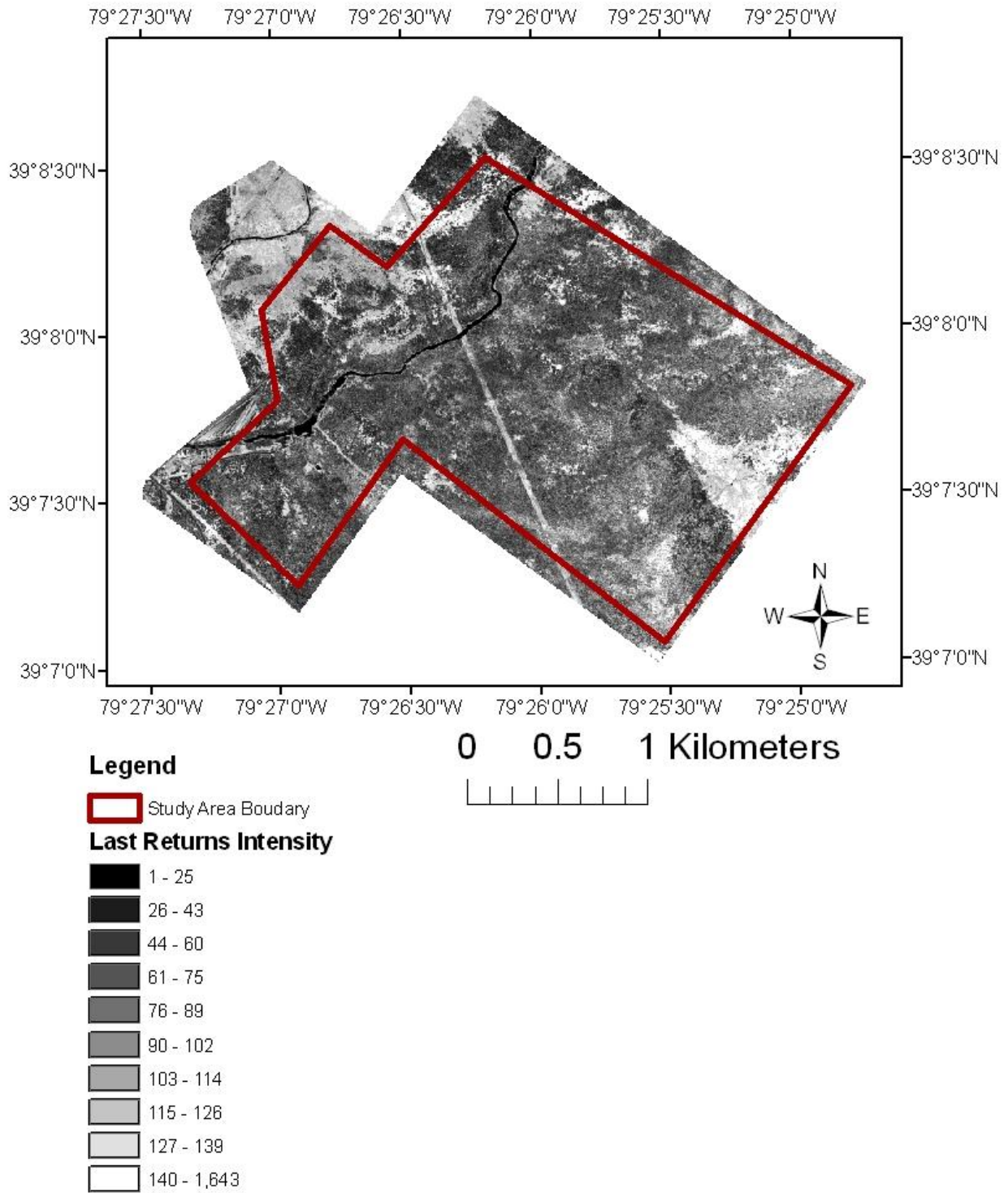


Figure 33: Last returns intensity raster grid. Raster grid is grouped into quantiles.

Figure 34a:
Intensity Raster at Site 1a

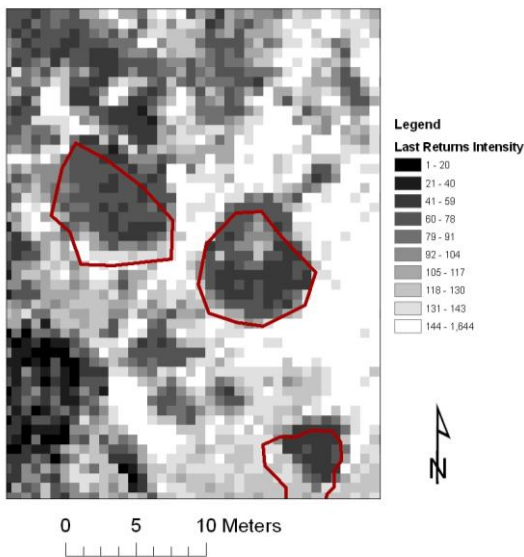


Figure 34b
Intensity Raster at Site 1b

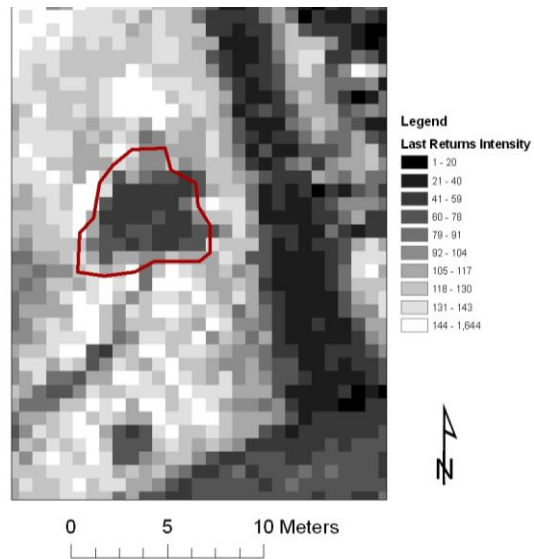


Figure 34c
Intensity Raster at Site 4

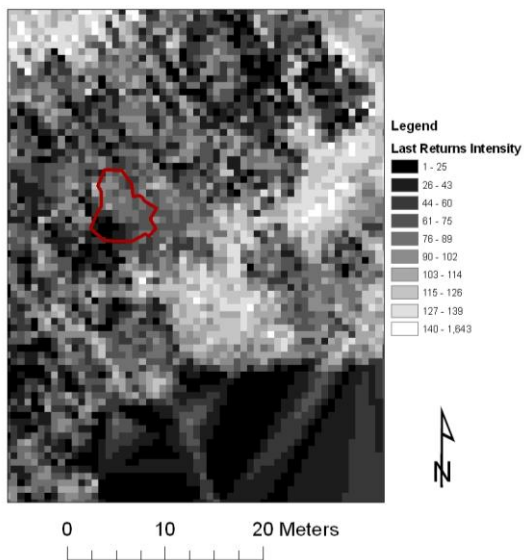
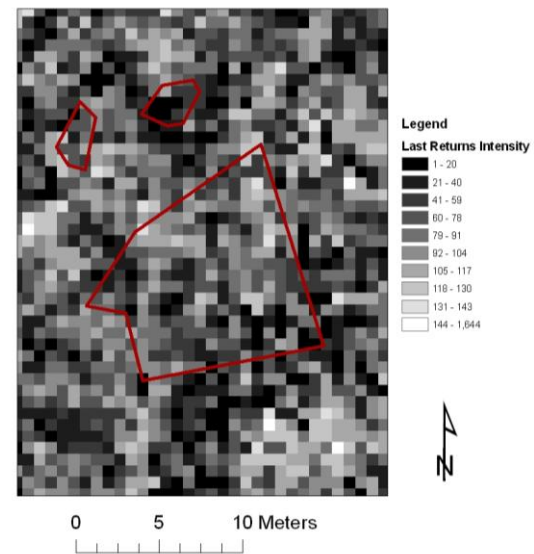


Figure 34d
Intensity Raster at Site 2




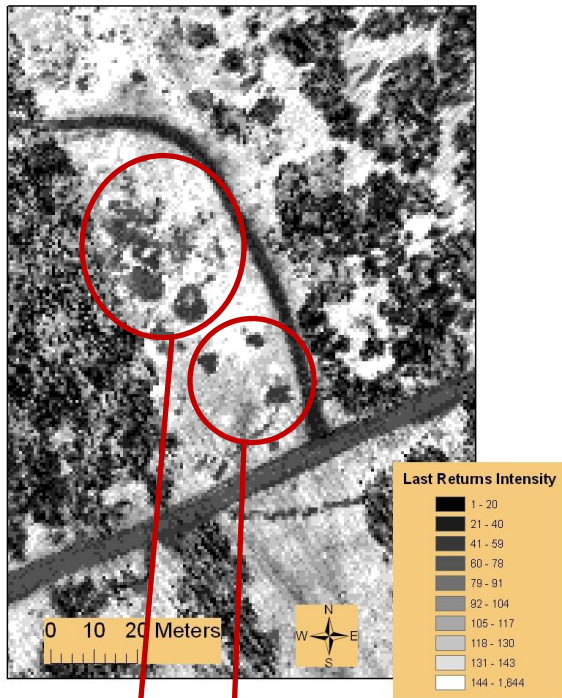
 Bouldery Features

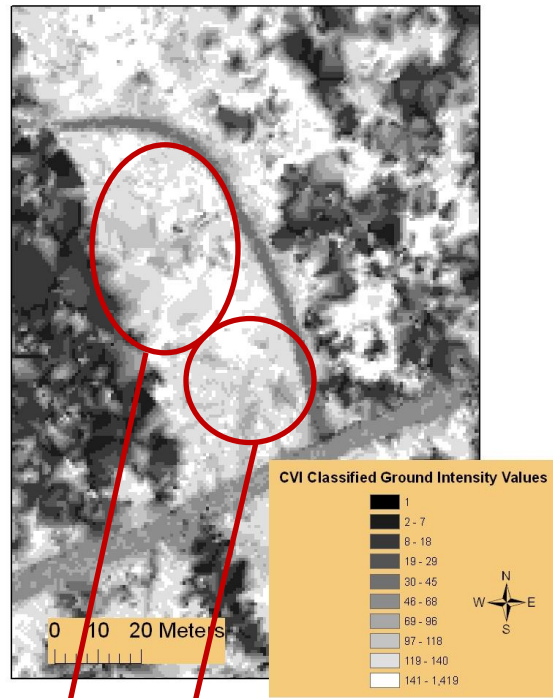
Figure 34: Intensity value within 0.69 m raster grids at selected study sites. Raster grids are grouped into quantiles. Note that intensity is a useful variable in open areas; mapping bouldery landforms in forested areas using this variable is not effective.

Figure 35a: Last Returns Intensity in Power Line Clearing



Bouldery landforms portrayed in last returns data

Figure 35b: CVI Classified Ground Returns Intensity in Power Line Clearing



Bouldery landforms not portrayed in CVI classified ground data

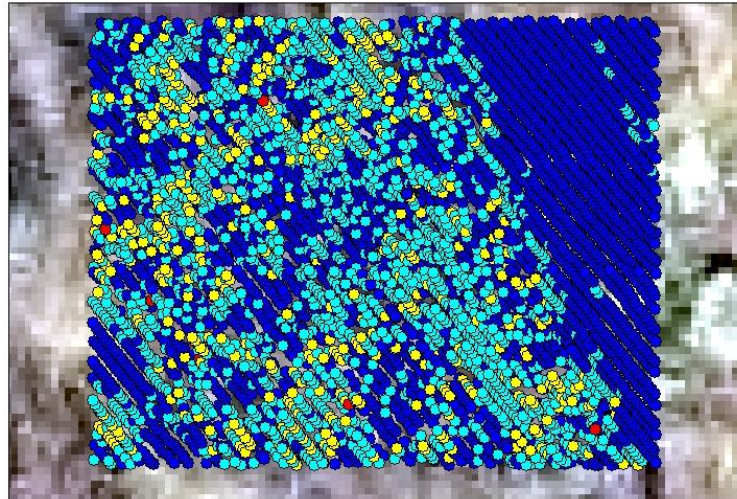
Figure 35: Intensity comparison in power line clearing. Raster grids grouped into quantiles. Note that dark grid cells within the highlighted areas, or relatively low LiDAR returns intensity, in the power line clearing indicate bouldery features. These intensity data are not portrayed in the CVI classified ground model.

Return Number of LiDAR Last Returns Data:

The ALTM 3100 LiDAR sensor is capable of recording up to four returns for each transmitted laser pulse. Return number for the last returns tends to be higher under a tree canopy (Figure 36) than in open areas because canopy cover causes multiple returns, and each subsequent return by definition has less illuminating radiation. Reflection of multiple returns has an influence on return intensity; the last returns intensities are generally lower under a tree canopy than returns in open areas. The recording of multiple returns for each laser pulse hinders the usefulness of last returns intensity to be used quantitatively.

Return intensity of last returns generally decreases with increasing return number; however, there is a wide intensity range as shown by the box and whisker plots, created at two sample locations under the tree canopy (Figure 37). As a result, correcting intensity values with respect to return number is necessary. Although last return intensity values are correlated with the surface material, such as bouldery landforms, intensity values are also correlated with return number. Corrections with respect to return number cannot be applied because methods of doing so are not available, making return intensity values difficult to use quantitatively (Lin and Mills, 2010).

Figure 36a



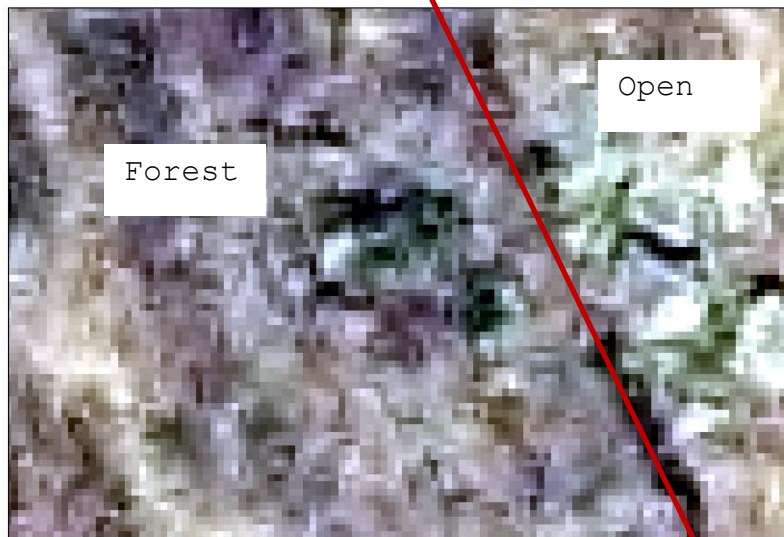
0 10 20 Meters



Legend

- 1st Return
- 2nd Return
- 3rd Return
- 4th Return

Figure 36b



0 10 20 Meters



Figure 36: Return number of last returns. Note that return number of last returns generally increases in forested areas.

Last Returns Intensity Box and Whisker Plots

Figure 37a: Forest Sample 1

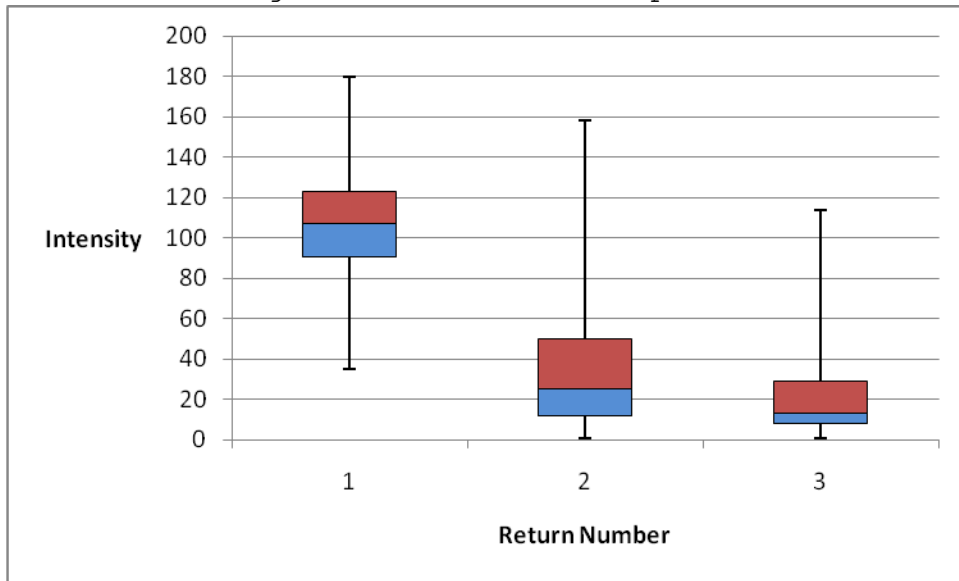


Figure 37b: Forest Sample 2

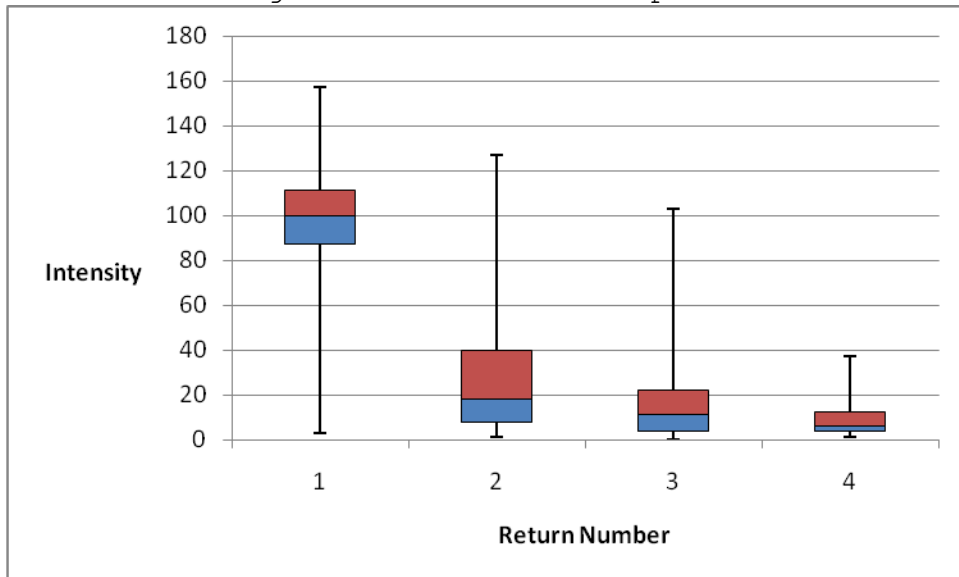


Figure 37: Last returns intensity box and whisker plots. Samples were collected in two forested locations in the study area, and no 4th returns were recorded at the first location. Note that last returns intensity values are correlated with return number.

Prologic LiDAR Explorer Ground Classifications:

Ground classifications were conducted for this research within Prologic LiDAR Explorer using different parameters for kernel size and elevation (Z) tolerance. These classifications were compared to the last returns and CVI classified ground returns data. In open areas, such as Site 1 (Figures 38 through 43), last returns portray the two fine blocks better than Prologic LiDAR Explorer ground classifications. Prologic LiDAR Explorer classifications reduce the horizontal extent of the feature and change either bouldery shape or morphology. Figure 44 shows similar results to Figures 38 through 43: last returns portray the fine block better than Prologic LiDAR Explorer ground classifications in open areas. Some classifications are effective in open areas; for example, classifications using Kernel Size = 5x5 and Z Tolerance = 1 remove vegetation returns while portraying the bouldery landforms at Site 1.

Under a canopy, Prologic LiDAR Explorer ground classifications are more effective at portraying bouldery landforms than last returns because not all last returns reached the ground. The laser energy may be dissipated in the canopy. At Site 4 (Figures 45 through 50) Prologic LiDAR Explorer ground classifications remove canopy returns but maintain the fine block. At Site 2 (Figure 51 through 56) and Site 3 (Figure 57) the bouldery features under a tree canopy are maintained;

however, not all vegetation returns are removed. The boulders are represented as a positive topographic feature, but detailed morphology is not maintained. Perhaps fewer returns reflecting from the boulder and decreased return density due to vegetation will not allow complete characterization of the landform under a tree canopy. Accurately mapping and characterizing bouldery landforms under a tree canopy on the CVI property requires a ground classification process using this LiDAR data. Last returns are not effective at portraying rugged topography and representing bouldery landforms under the tree canopy because some last returns did not reach the ground. The best classifications for maintaining topographic variability under a tree canopy used Kernel Size = 5x5/Z Tolerance = 2 and Kernel Size = 5x5/Z Tolerance = 5 based on visual and graphic comparison.

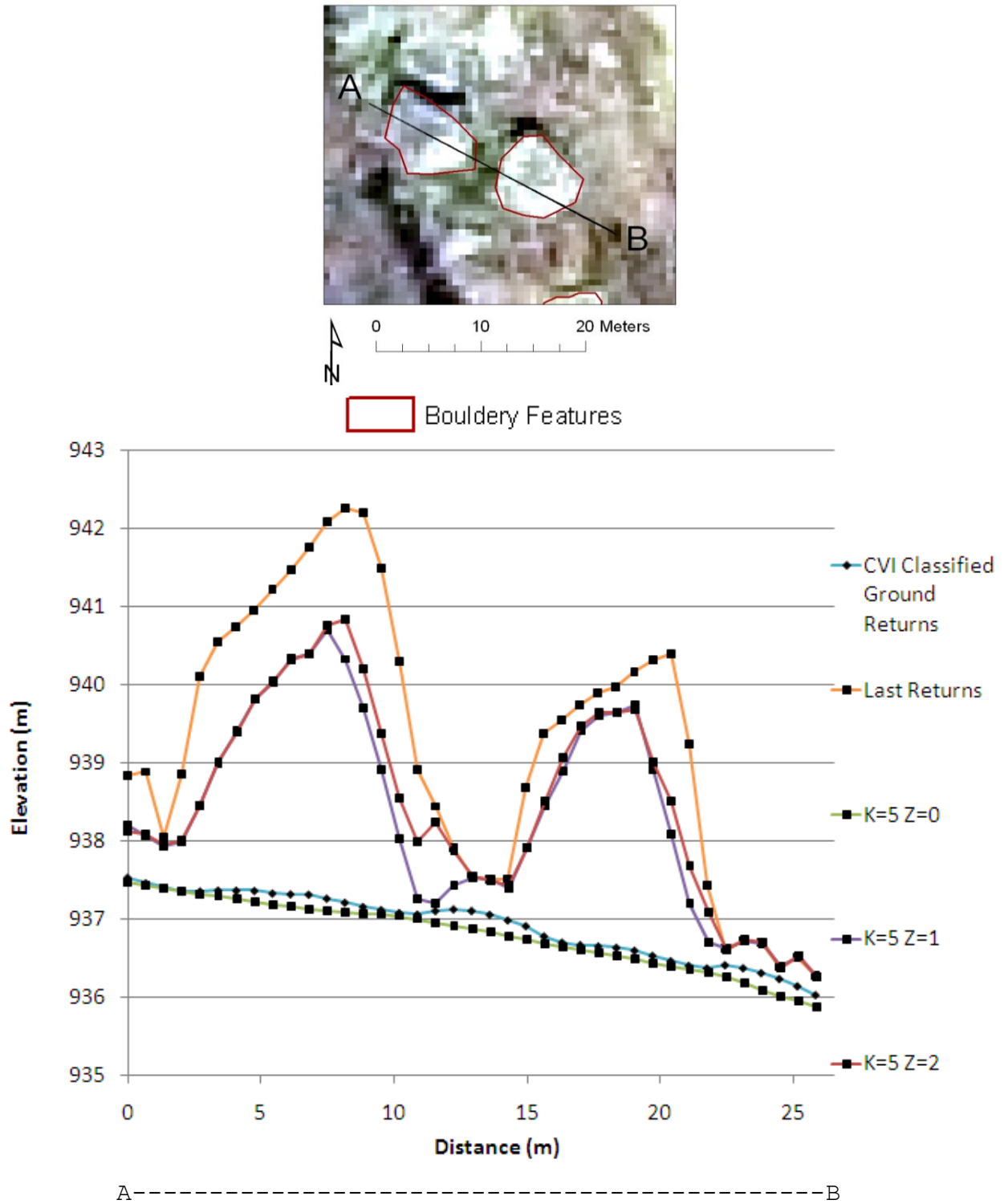


Figure 38: Prologic LiDAR Explorer ground classifications at Site 1a. Note that the height and horizontal extent of the two fine blocks are reduced when Prologic LiDAR Explorer ground classifications are performed. Last Returns are best at portraying topographic variability in open area.

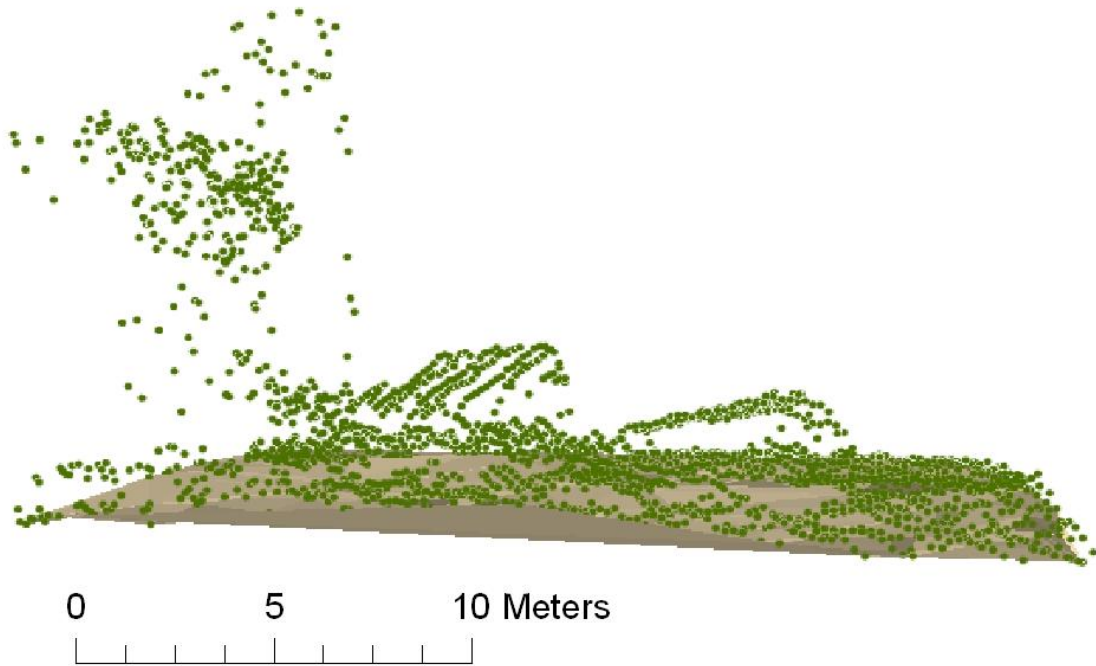


Figure 39: 3D point distribution of last returns at Site 1a. Note that the two fine blocks remain in the classification, but vegetation is also included.

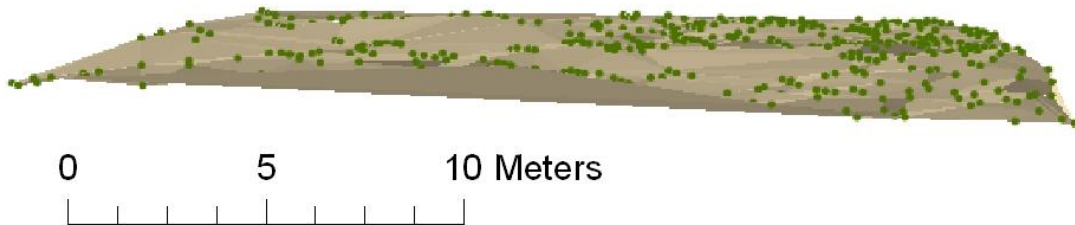


Figure 40: 3D point distribution of CVI classified ground returns at Site 1a. Note that the two fine blocks are not included in this classification.

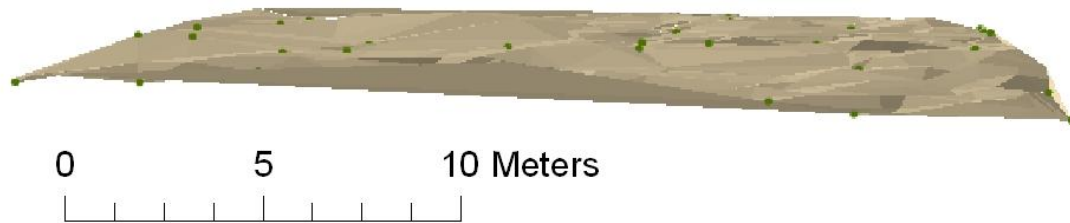


Figure 41: 3D point distribution of Prologic LiDAR Explorer classification Kernel Size = 5 and Z Tolerance = 0 at Site 1a. Note that the two fine blocks are not included in this classification.

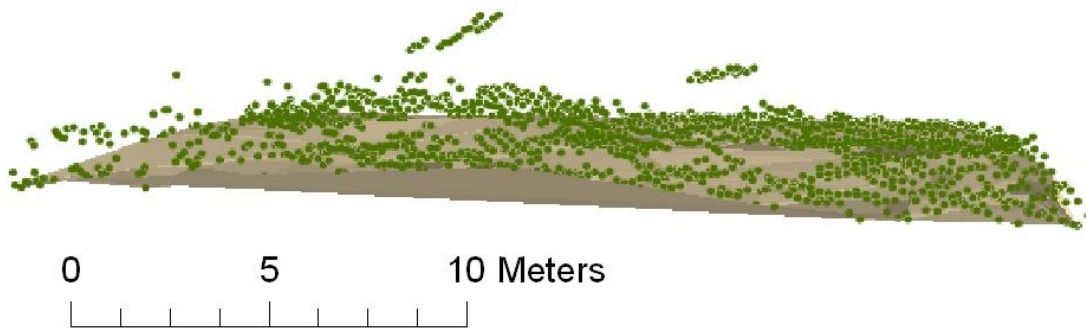


Figure 42: 3D point distribution of Prologic LiDAR Explorer classification Kernel Size = 5 and Z Tolerance = 1 at Site 1a. Note that the two fine blocks are portrayed, but the morphology is altered.

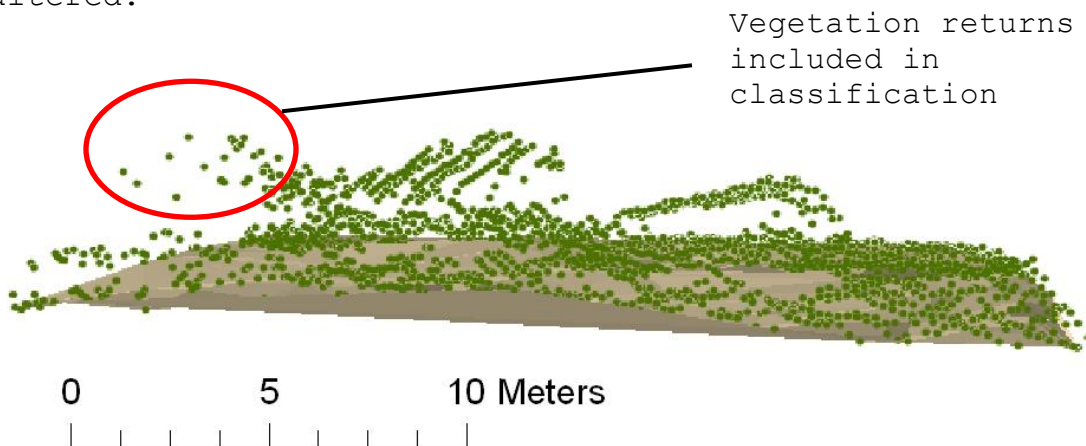


Figure 43: 3D point distribution of Prologic LiDAR Explorer classification Kernel Size = 5 and Z Tolerance = 2 at Site 1a. Note that the two fine blocks are portrayed, but vegetation is maintained in the classification.

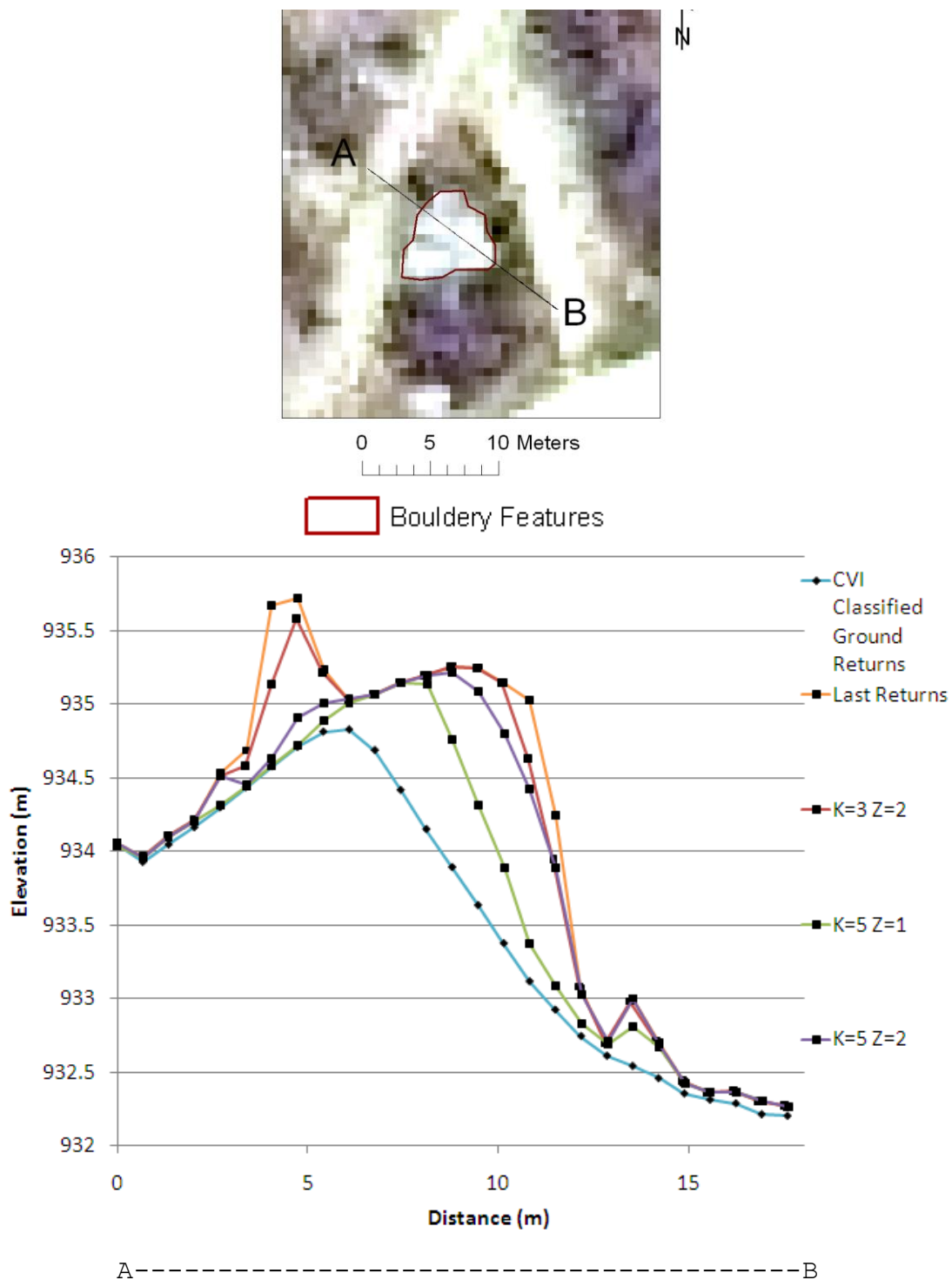


Figure 44: Prologic LiDAR Explorer ground classifications at Site 1b. Note that the height and horizontal extent of the fine block are reduced when Prologic LiDAR Explorer classifications are performed. Last returns are best at portraying topographic variability in open areas.

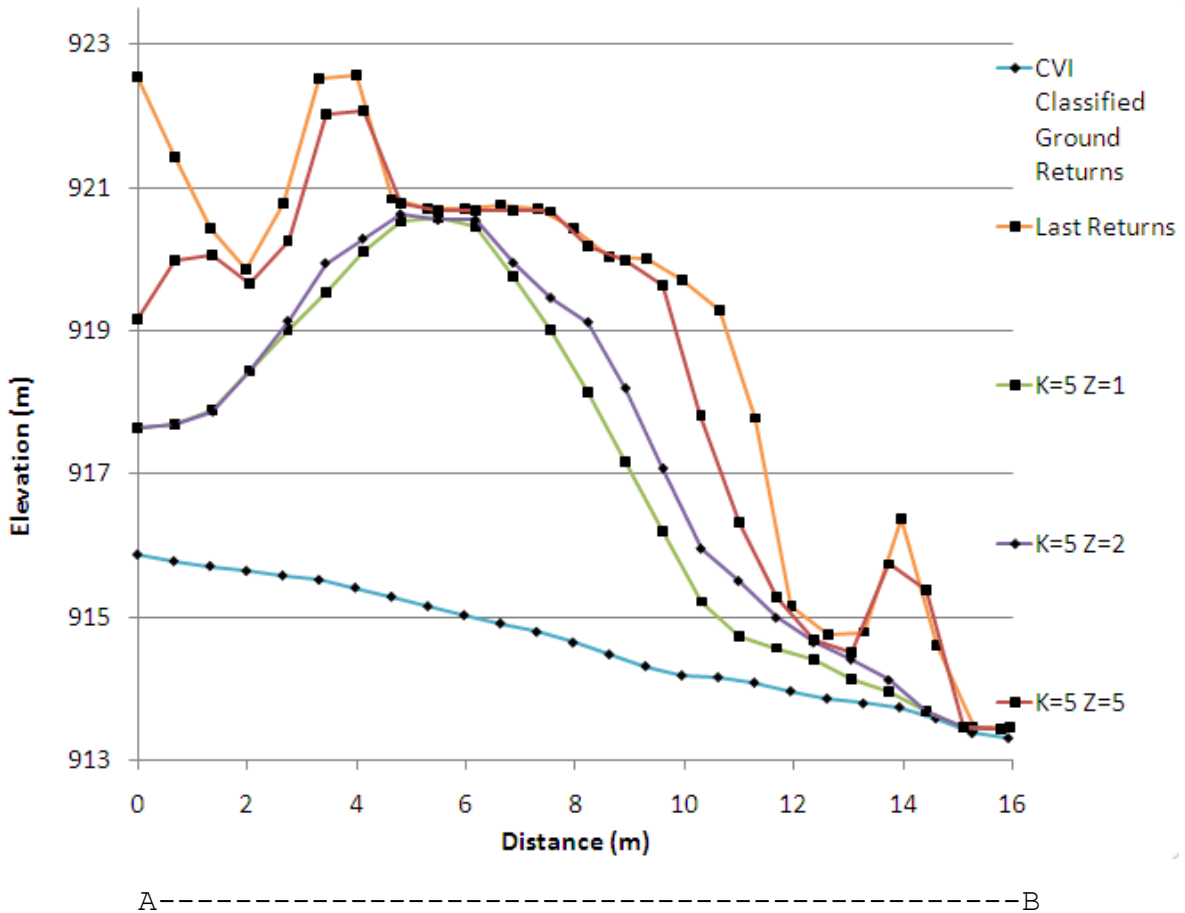
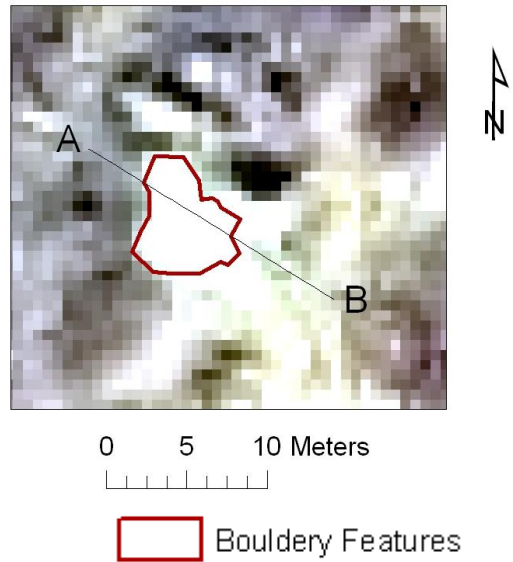


Figure 45: Prologic LiDAR Explorer ground classifications at Site 4. Note that Prologic LiDAR Explorer classifications generally remove vegetation while portraying the fine block.

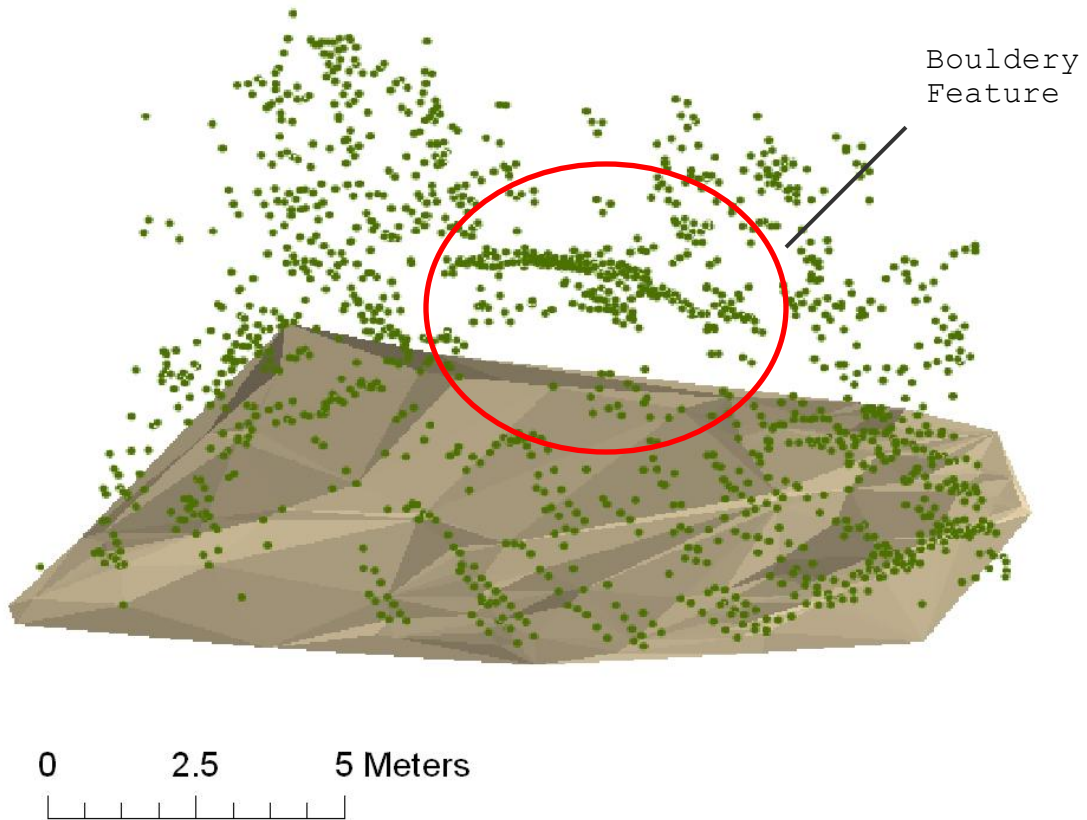


Figure 46: 3D point distribution of last returns at Site 4. Note that the fine block is portrayed, but vegetation is also included.

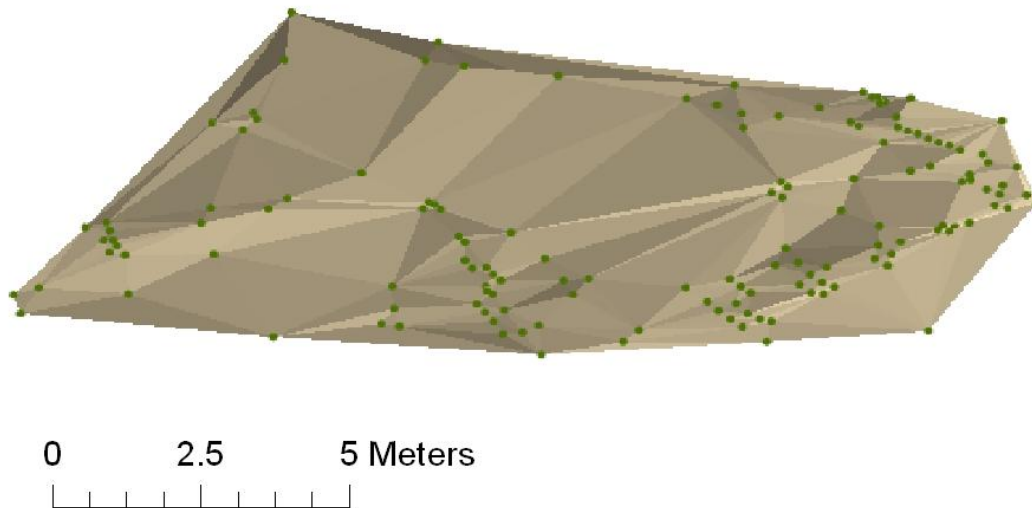


Figure 47: 3D point distribution of CVI classified ground returns at Site 4. Note that the fine block is not represented.

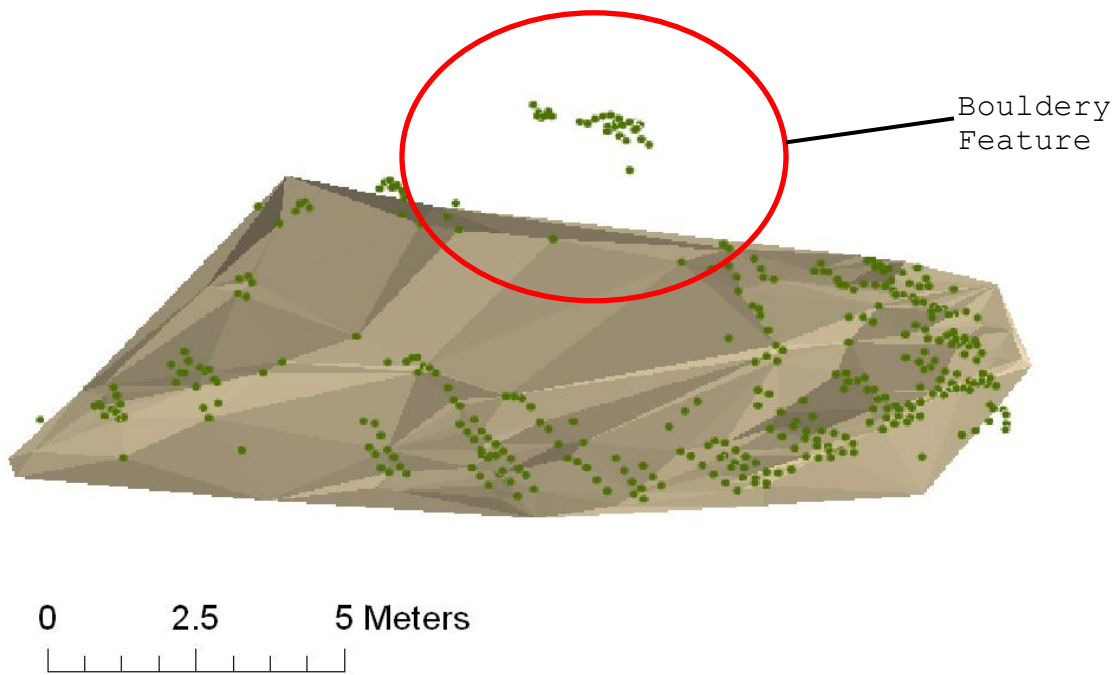


Figure 48: 3D point distribution of Prologic LiDAR Explorer classification Kernel Size = 5 and Z Tolerance = 1 at Site 4. Note that the fine block is portrayed, but the morphology is altered.

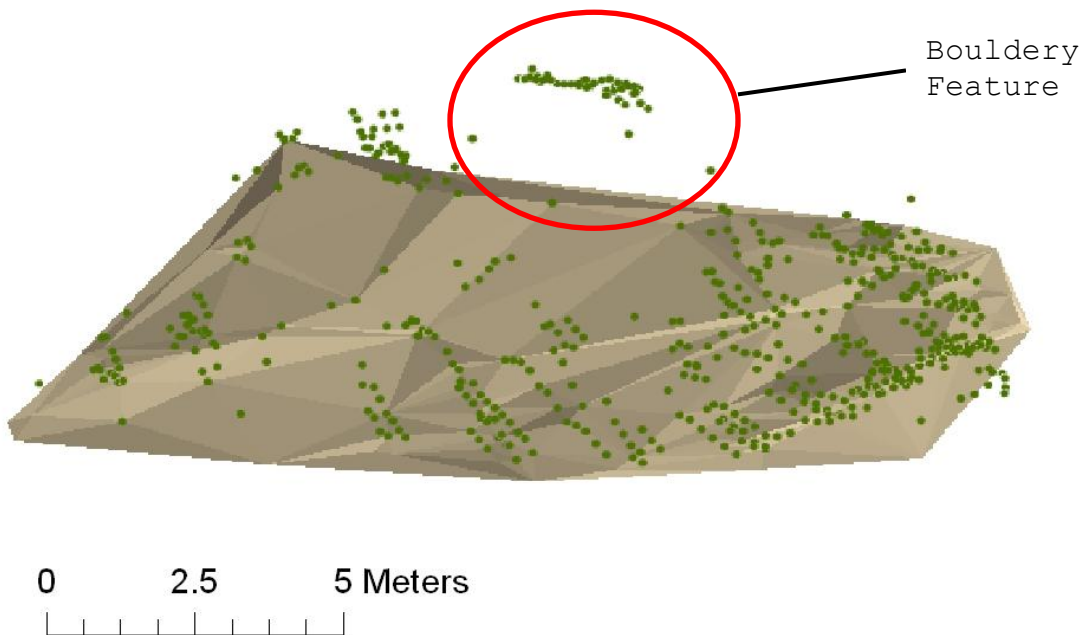


Figure 49: 3D point distribution of Prologic LiDAR Explorer classification Kernel Size = 5 and Z Tolerance = 2 at Site 4. Note that the spatial extent of the fine block is portrayed in the classification.

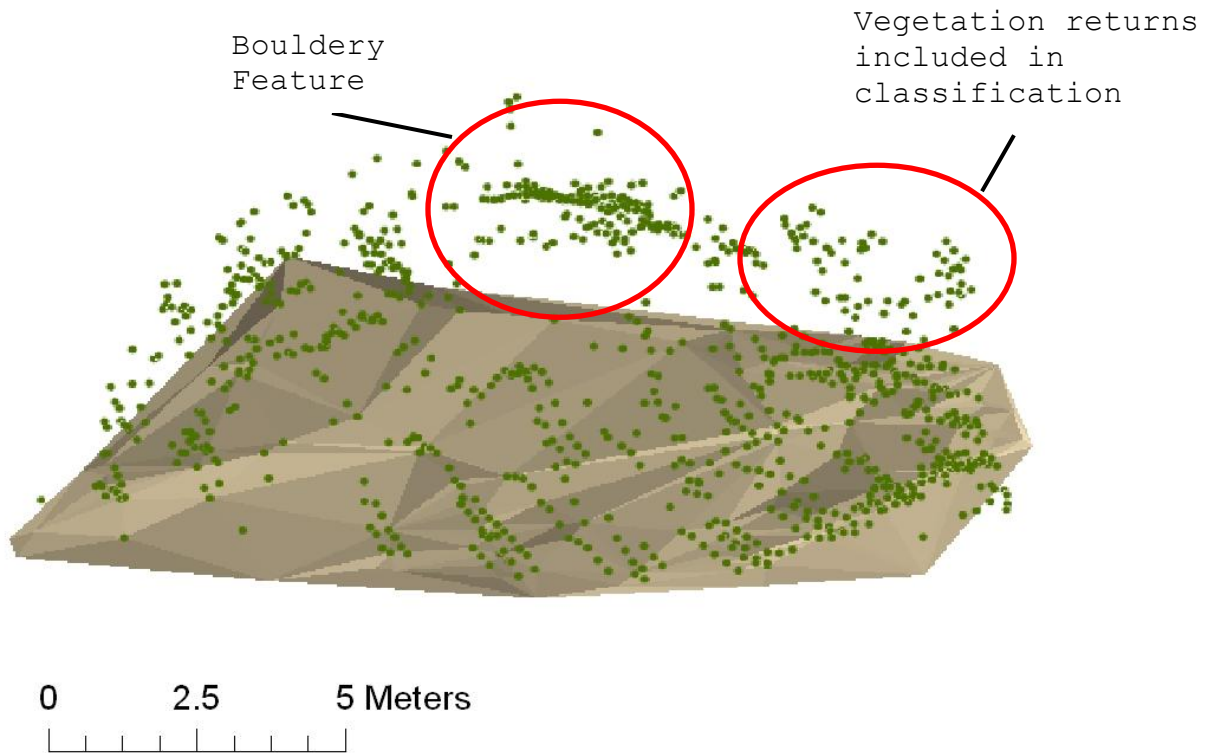


Figure 50: 3D point distribution of Prologic LiDAR Explorer classification Kernel Size = 5 and Z Tolerance = 5 at Site 4. Note that the spatial extent of the fine block is portrayed, but vegetation is also included.

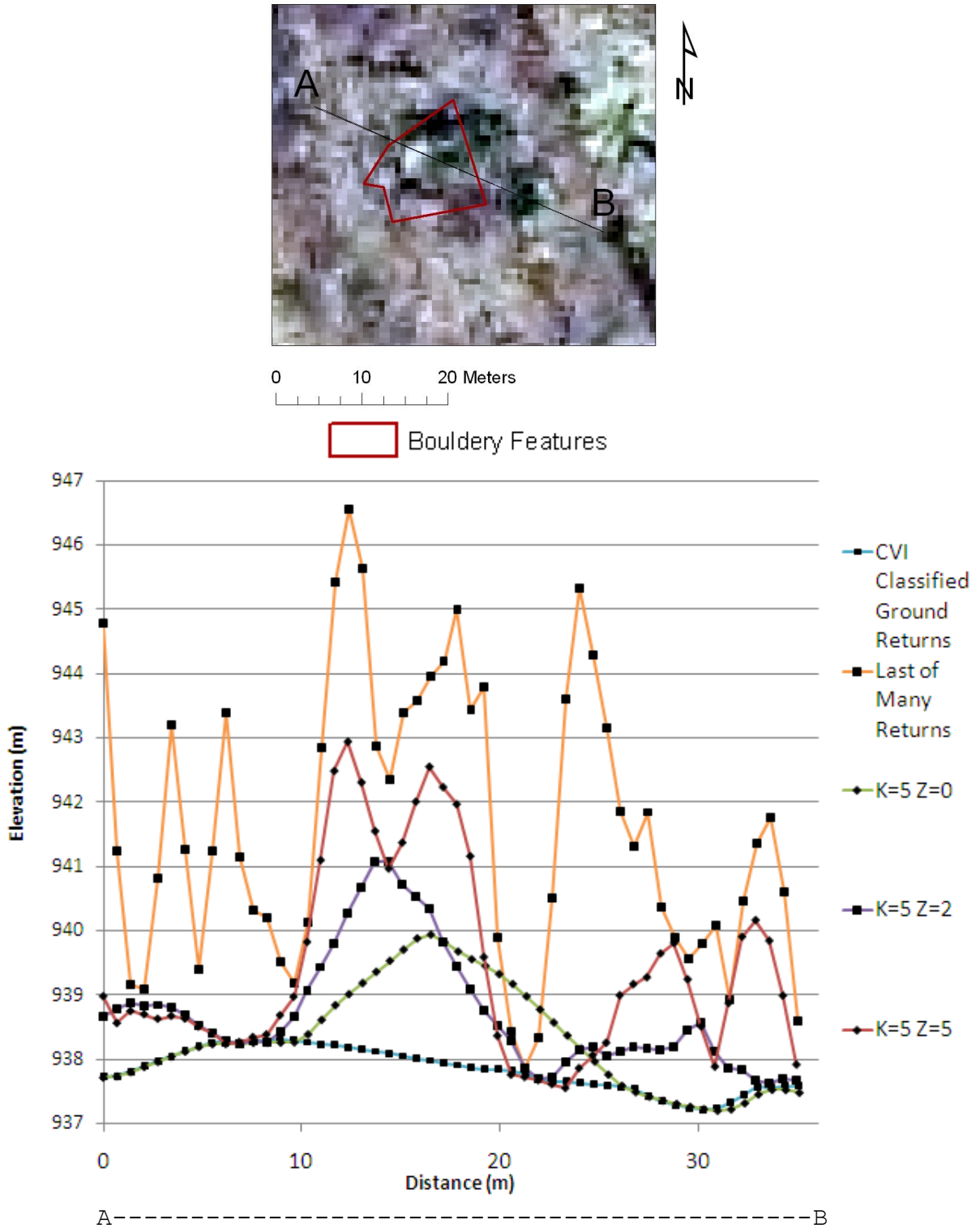


Figure 51: Prologic LiDAR Explorer ground classifications at Site 2. Note that identifying bouldery landforms under a tree canopy at this location using this data requires ground classification.

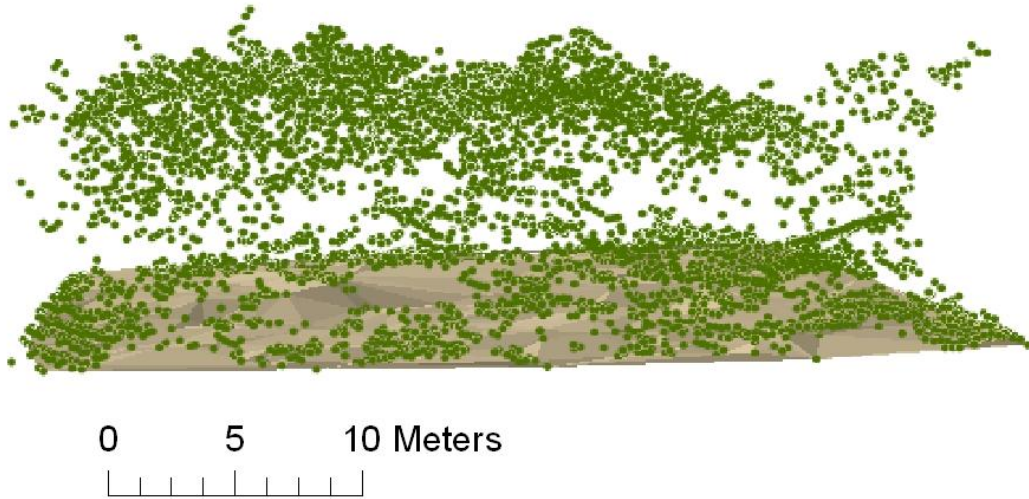


Figure 52: 3D point distribution of last returns at Site 2. Vegetation was not removed. Note that last returns include vegetation because the energy was dissipated in the tree canopy.



Figure 53: 3D point distribution of CVI classified ground returns at Site 2. Note that bouldery landforms are not included in the classification.

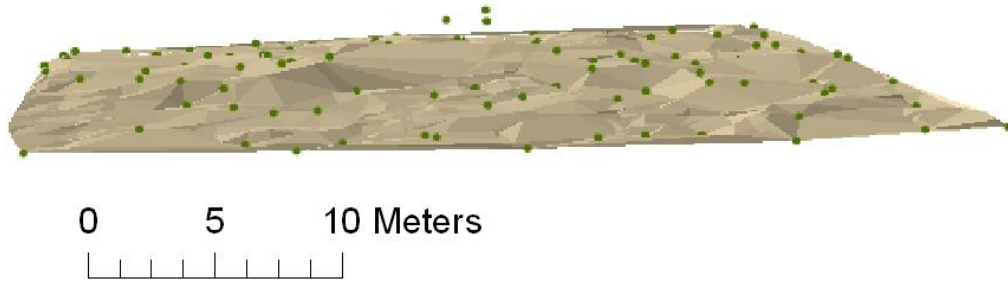


Figure 54: 3D point distribution of Prologic LiDAR Explorer classification Kernel Size = 5 and Z Tolerance = 0 at Site 2. Note that bouldery landforms are generally not included in the classification.

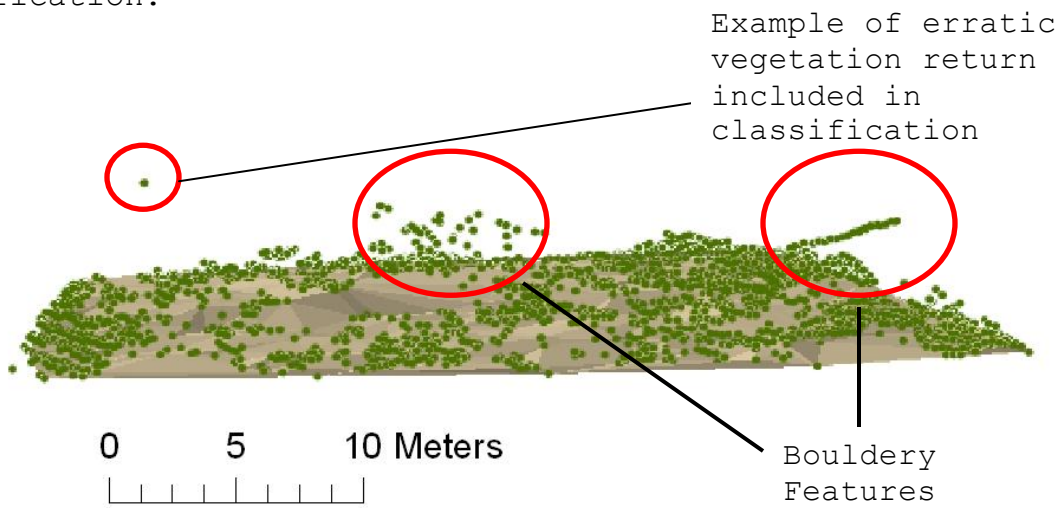


Figure 55: 3D point distribution of Prologic LiDAR Explorer classification Kernel Size = 5 and Z Tolerance = 2 at Site 2. Note that bouldery landforms are generally portrayed, but vegetation is also included in the classification.

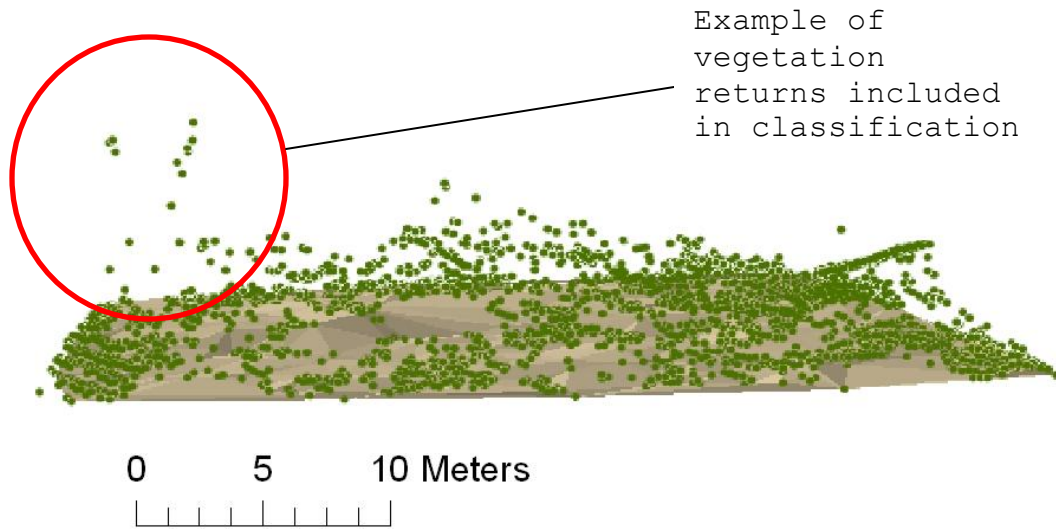


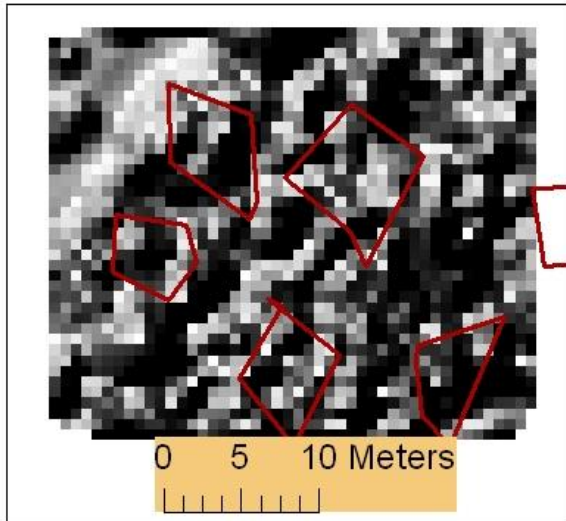
Figure 56: 3D point distribution of Prologic LiDAR Explorer classification Kernel Size = 5 and Z Tolerance = 5 at Site 2. Note that bouldery landforms are generally portrayed, but vegetation is not completely removed.

Figures 58 (Site 3) and Figure 59 (Site 2) illustrate how different point classification parameters portray rugged topography in forested areas using hillshade imagery. Last returns data (Figures 58a and 59a) provide more variability because many last returns did not reach the ground surface, and vegetation returns remain in the data. The CVI classified ground data (Figures 58b and 59b) provide a smoothed surface model in which bouldery landforms are not represented. Under a tree canopy, the Prologic LiDAR Explorer ground classification tool creates a better representation of rugged topography for mapping bouldery landforms (Figures 58c and d and Figures 59c and d). Rough topography is portrayed, but it is difficult to determine if the positive topographic features are bouldery landforms or if vegetation is inducing noise. The shapes of boulders are not maintained. The ground classification operation within Prologic is meant for crude ground return classification (Prologic, 2008). For example, elevation (Z) tolerance values have to be integer. More sophisticated tools are available for ground return classification, such as the more robust TerraScan software, but could not be obtained for this research.

Figure 60 shows a large bouldery outcrop in a power line clearing. This large bouldery feature is modeled well in the last returns data; although last returns data are useful for mapping bouldery features in open areas such as the power line

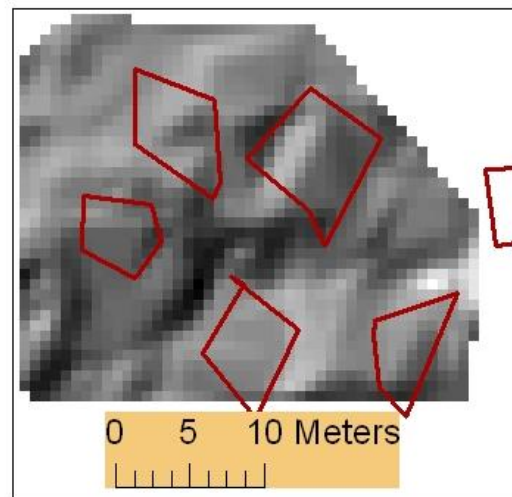
clearing shown in Figure 60, last returns are not as effective at portraying topography under a tree canopy also shown in this figure. Some ground classification process is required to represent rugged topography. Although precise characterization of individual features is not possible, adequate terrain surface information is provided in order to map generalized rugged topography.

Figure 58a

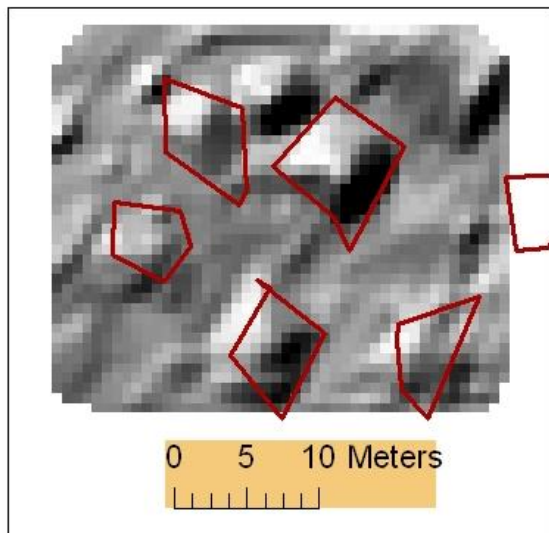


Last Returns
Figure 58c

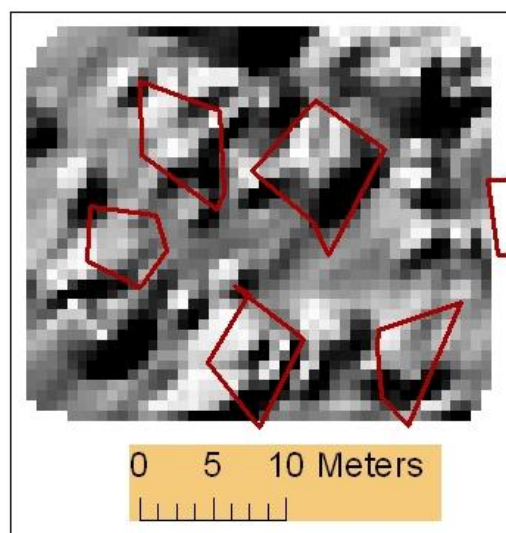
Figure 58b



CVI Classified Ground Returns
Figure 58d



Kernel Size = 5x5 and Z
Tolerance = 2



Kernel Size = 5x5 and Z
Tolerance = 2




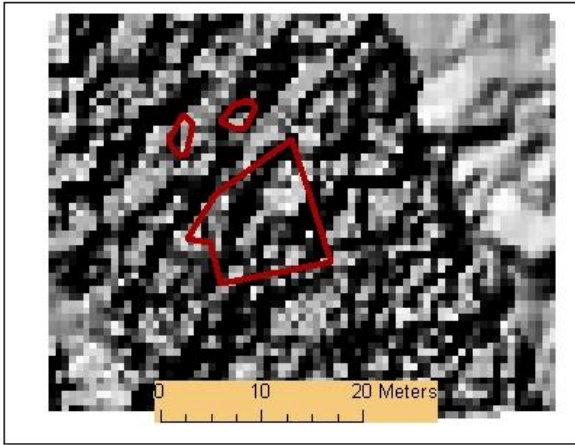
 Bouldery Features

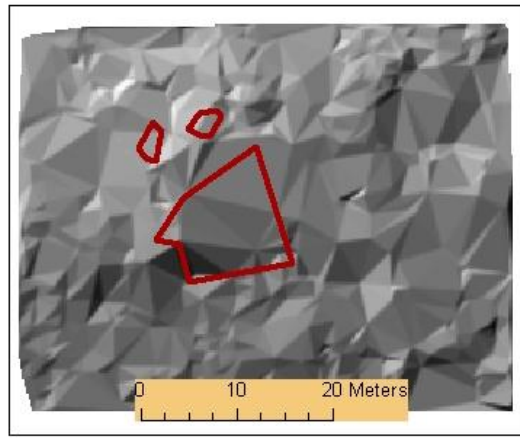
Figure 58: Prologic LiDAR Explorer ground classifications hillshade comparison at Site 3. Note that Kernel Size = 5x5 and Z Tolerance = 2 provide the best classification for mapping bouldery landforms.

Figure 59a



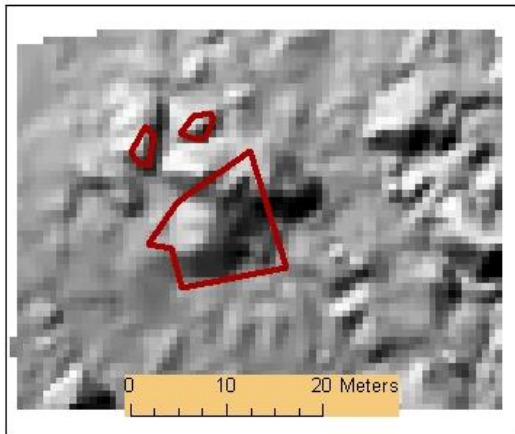
Last Returns

Figure 59b



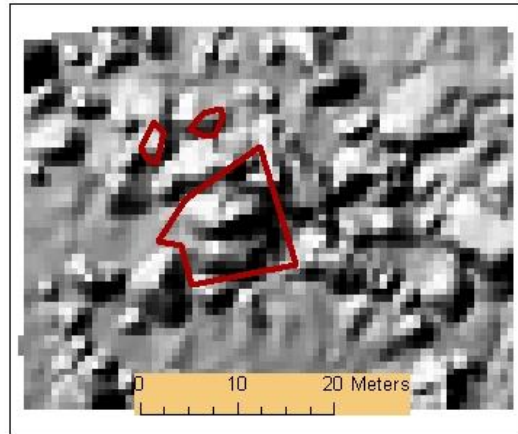
CVI Classified Ground Returns

Figure 59c



Kernel Size: 5x5 and Z Tolerance: 2
 Kernel Size = 5x5 and Z
 Tolerance = 2

Figure 59d



Kernel Size: 5x5 and Z Tolerance: 5
 Kernel Size = 5x5 and Z
 Tolerance = 2



Bouldery Features

Figure 59: Prologic LiDAR Explorer ground classifications hillshade comparison at Site 2. Note that Kernel Size = 5x5 and Z Tolerance = 2 provide the best classification for this for mapping bouldery landforms.

Figure 60b: Last
Returns Hillshade

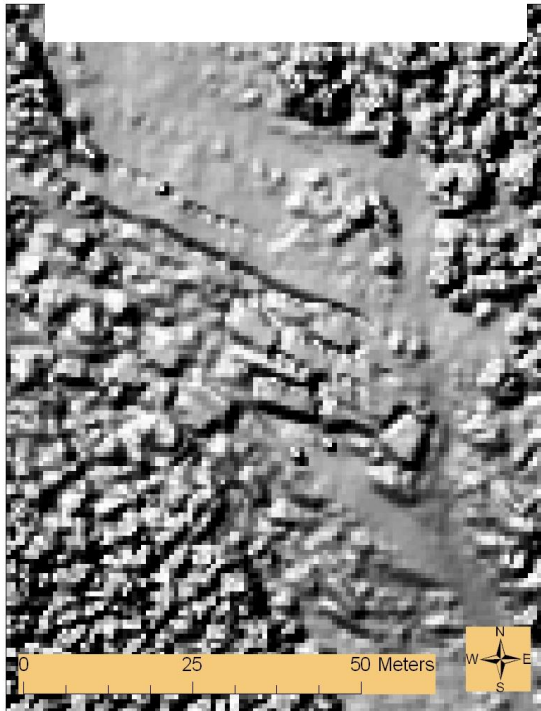


Figure 60a: CVI
Classified Ground
Returns Hillshade

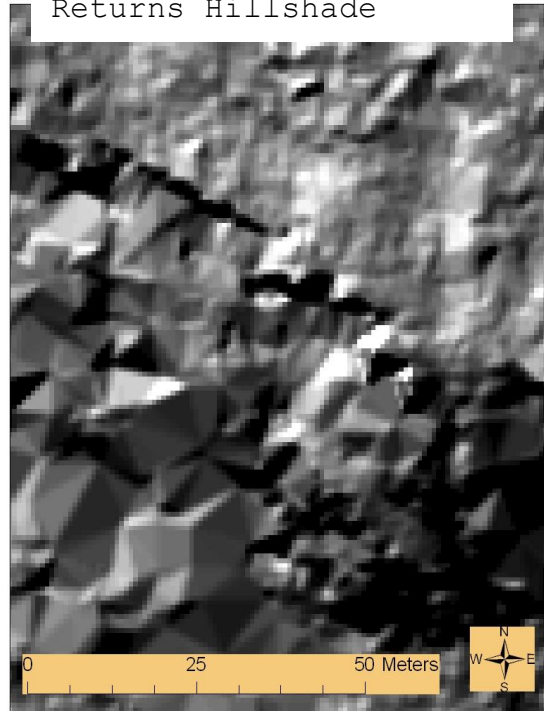


Figure 60a:
Natural Color
Imagery

Figure 60: Hillshade comparison of last returns and CVI classified ground returns at large bouldery feature in power line clearing. Note that the last returns data (Figure 60a) in this open area characterize the features well, whereas CVI classified ground return data (Figure 60b) are inadequate for mapping bouldery landforms. The natural color SAMB image (Figure 60c) shows the extent of the bouldery feature.

Index Overlay for Likelihood of Presence of Bouldery Landforms Analysis:

Fusing LiDAR data with other remotely sensed data is becoming common (Luccio, 2010). Natural color, color infrared, and hyperspectral imagery are being collected along with LiDAR to accompany the intensity and elevation data for increased functionality. Methods are being developed to append image DN values to each LiDAR data point (Luccio, 2010). This research attempted to combine natural color imagery and LiDAR-derived information in a raster environment. An attempt was made to detect bouldery landforms using an index overlay for likelihood of presence of bouldery landforms analysis. Prior research results were used to produce these raster models. This analysis was explored as an alternative method to detect bouldery landforms using natural color imagery and LiDAR-derived parameters because hillshade models produced from the CVI classified ground data are not adequate for accurate mapping of bouldery landforms. Based on the data collected in prior objectives, user-based index overlay for likelihood of presence of bouldery landforms models were performed within the 5.4 km² study area. The assumptions in these models are as follows:

1. Bouldery landforms were not classified as ground by CVI and had positive elevation difference values between the last returns elevation raster grid and CVI classified

- ground returns elevation raster grid predominantly between 0.5 m and 6.0 m (medium boulder to medium block).
2. Bouldery landforms produced last returns intensities that were lower than surrounding vegetation in open areas based on the statistics provided in Table 6. Return intensity is less useful under the tree canopy. Because it was not possible to normalize intensity values with respect to the return number, only high intensity values were removed. Low values were maintained.
 3. Bouldery landforms exist in areas of low CVI classified ground return density as portrayed by the CVI classified ground point count raster.
 4. Bouldery landforms occur in areas classified as boulder in the natural color imagery; however, such features were commonly misclassified as road or water due to similar natural color DN values or shadows, respectively.

Table 16 and Figure 61 show the likelihood of presence of bouldery landforms model results produced by averaging the three models. Increased likelihood indicates a better fit using the model criteria. These grid cells are areas predicted to contain bouldery landforms. Within the study area boundaries the results are as follows:

Classification	Score Ranges	Percentage of Study Area
Does Not Meet Criteria for Bouldery Landforms	0-48	55.60%
Least Likely for Bouldery Landforms	48-138	21.80%
Moderately Likely for Bouldery Landforms	138-318	16.60%
Most Likely For Bouldery Landforms	318-625	5.90%

Table 16: Percentage of study area classified as likely to be bouldery landforms. Ranges were determined based on natural breaks in the data set.

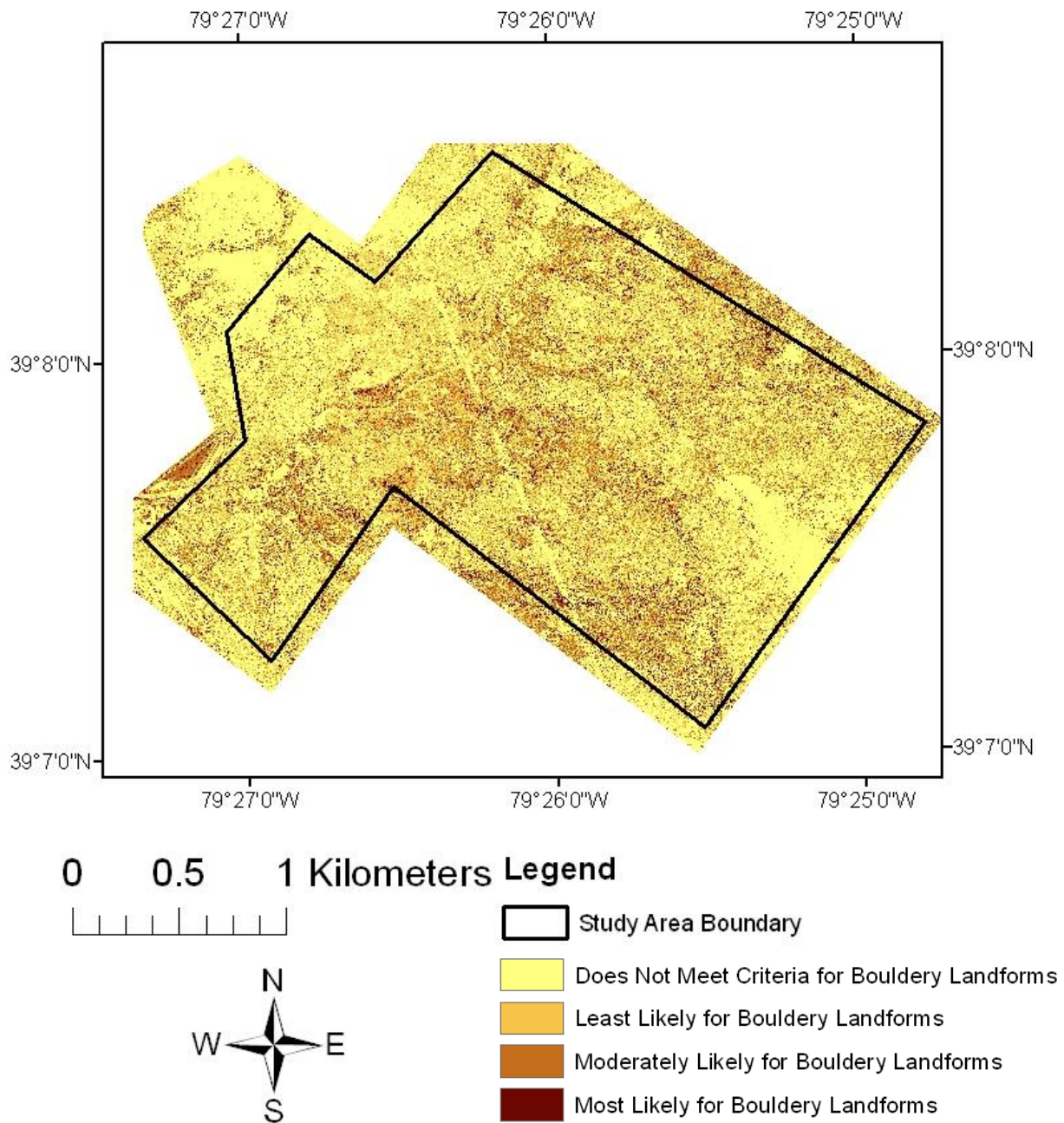


Figure 61: Averaged index overlay for likelihood of presence of bouldery landforms.

Figure 62 shows the likelihood of presence for bouldery landforms in the power line area (Site 1). The very coarse boulders to fine blocks outlined in this area are classified as likely for bouldery landforms. Figures 63 and 64 show two additional locations for discussion. The large outcrops at these locations are classified as likely for bouldery landforms. At these three open locations, this model maps bouldery features successfully.

Figure 65 shows a large, bouldery area, also shown in Figure 16, that is not classified as likely for bouldery landforms. Classification is hindered because the CVI ground classification did not remove bouldery landforms consistently or completely. Because the assumptions used to create this model are not accurate at this site, it is not considered likely for bouldery landforms in this model.

As shown in Figure 66, forested areas are a problem in this classification; the very coarse boulders to fine blocks at Site 3 are not completely classified as likely for bouldery landforms, offering further support for the conclusion that ground classification algorithms that maintain boulders are necessary for mapping such features under a tree canopy. Because of the complexity of last returns intensities under a tree canopy, this criterion is not reliable in forested areas, such as Site 3. Intensity was used to remove high return values and

not low values. Last returns intensity was useful only in open areas and had little predictive power in forested areas.

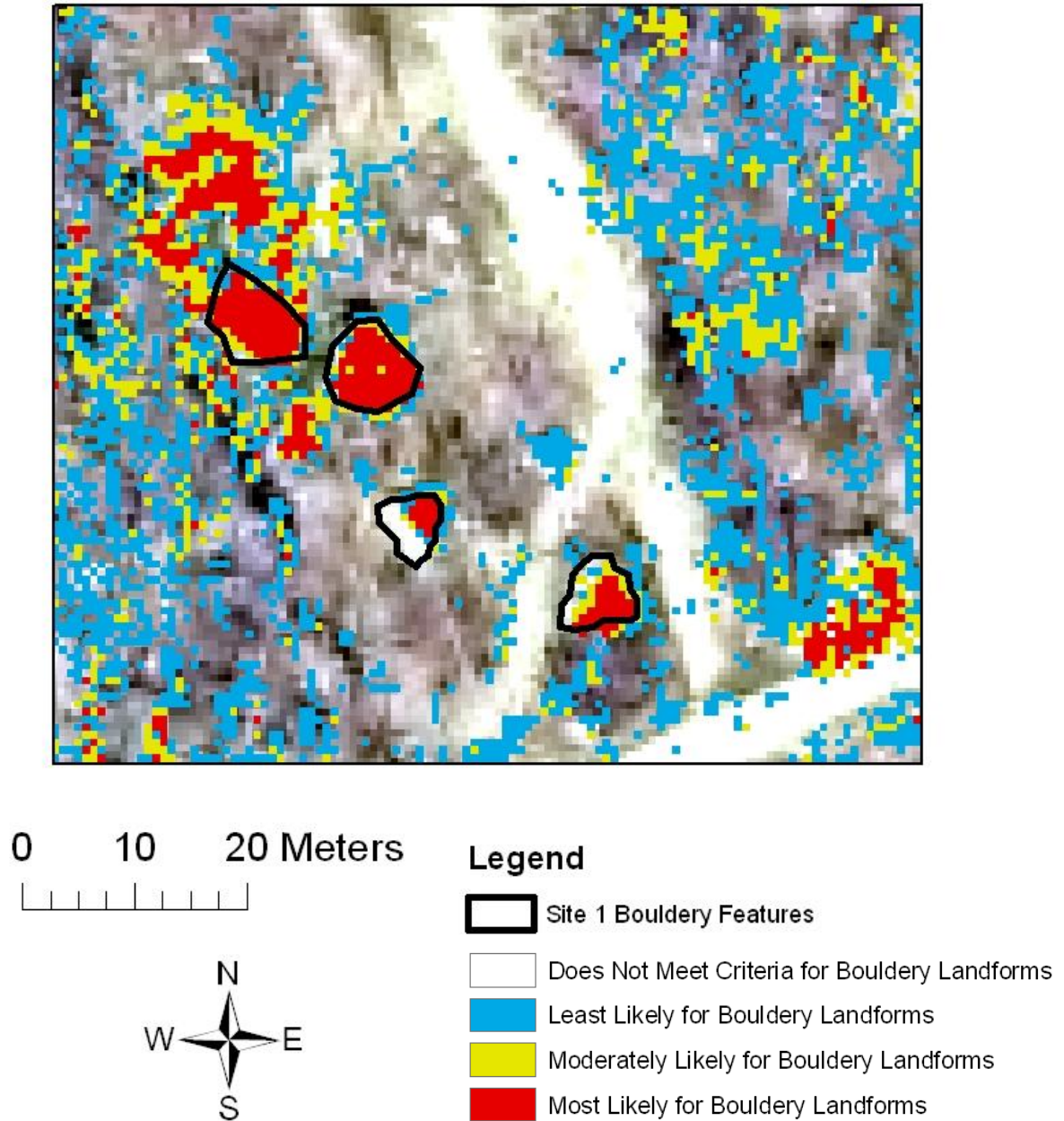
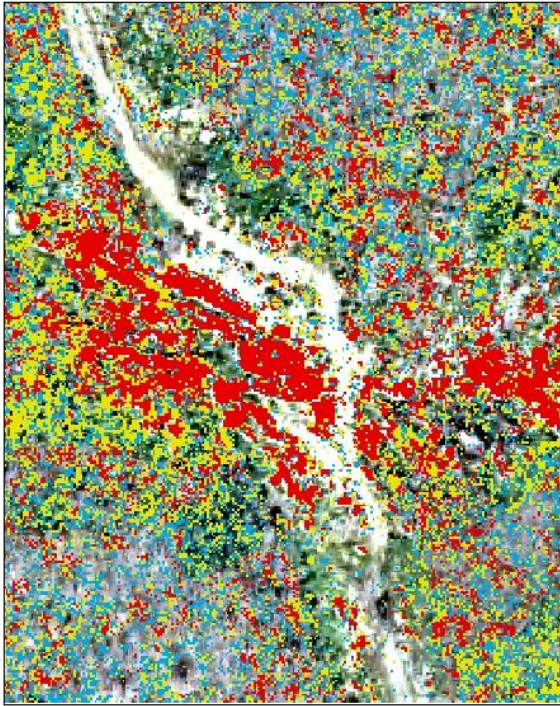


Figure 62: Index overlay for likelihood of presence of bouldery landforms at power line clearing (Site 1). Note that very coarse boulders to fine blocks outlined within this open area are mapped successfully using this model.

Figure 63a



0 25 50 Meters
| | | | | | | |



Figure 63b



0 25 50 Meters
| | | | | | | |



Legend





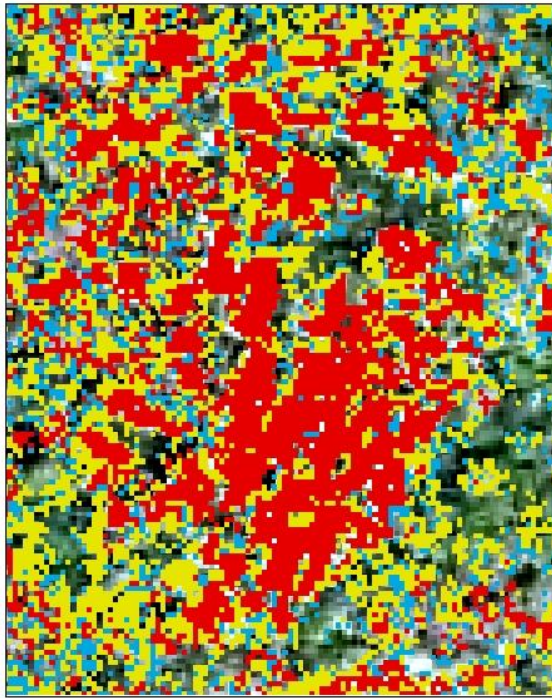
-  Does Not Meet Criteria for Bouldery Landforms
-  Least Likely for Bouldery Landforms
-  Moderately Likely for Bouldery Landforms
-  Most Likely for Bouldery Landforms

Figure 63: Index overlay for likelihood of presence of bouldery landforms at boulder feature in power line clearing. Note that bouldery landforms within this open area are mapped successfully using this model.

Figure 64a



0 10 20 Meters
| | | | |



Legend

- Does Not Meet Criteria for Bouldery Landforms
- Least Likely for Bouldery Landforms
- Moderately Likely for Bouldery Landforms
- Most Likely for Bouldery Landforms

Figure 64b



0 10 20 Meters
| | | | |



Figure 64: Index overlay for likelihood of presence of bouldery landforms at bouldery feature in forest. Note that large, bouldery landforms within this rock city are mapped successfully using this model.

Figure 65a

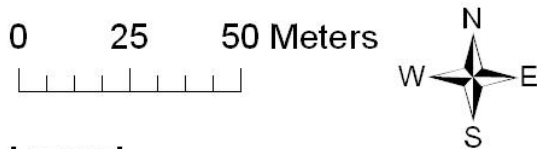
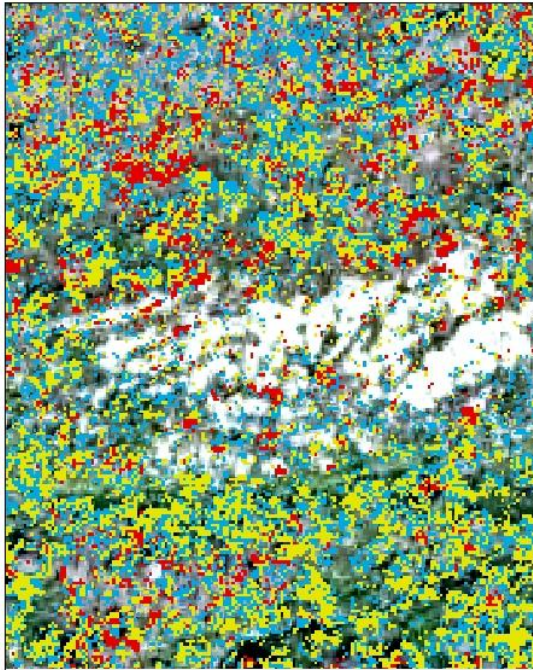
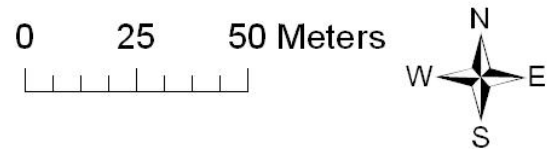


Figure 65b



Legend





-  Does Not Meet Criteria for Bouldery Landforms
-  Least Likely for Bouldery Landforms
-  Moderately Likely for Bouldery Landforms
-  Most Likely for Bouldery Landforms

Figure 65: Index overlay for likelihood of presence of bouldery landforms at bouldery feature included in CVI classified ground surface. Note that the intact block and boulder field included in CVI's classified ground surface is not mapped successfully using this model.

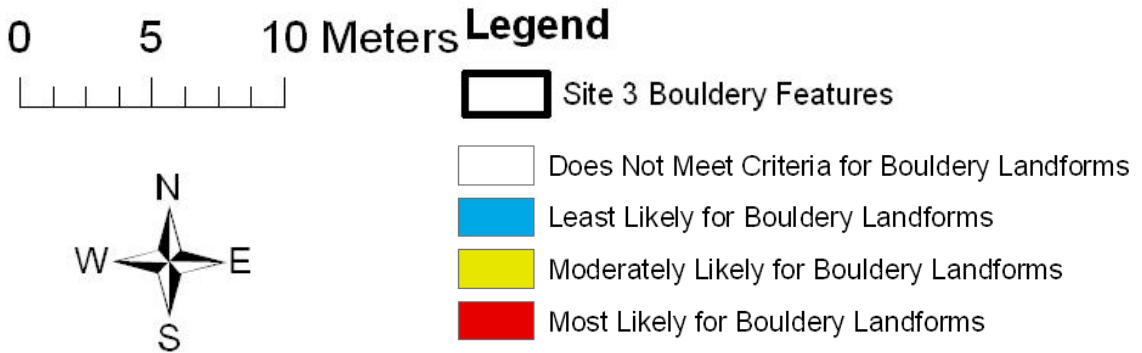


Figure 66: Index overlay for likelihood of presence of bouldery landforms in forest (Site 3). Note that very coarse boulders to fine blocks under a forest canopy are not detected as well as open areas in this model.

The results of the index overlay for likelihood of presence of bouldery landforms models were evaluated using a spatial compromise programming technique in which 35 test areas, as polygons, were ranked based on how well they meet the user defined parameters for natural color supervised classification, elevation difference between last returns and CVI classified ground returns raster grids, last returns LiDAR intensity, and CVI classified ground returns density described in Table 7. Test areas were digitized at known bouldery locations, non-bouldery forest, and non-bouldery open areas for comparison using differential GPS and aerial imagery interpretation. The following numbers of sites were ranked using spatial compromise programming: bouldery landforms in open areas (9), boulder landforms under forest canopy (6), non-bouldery forest areas (10), and non-bouldery field areas (10).

The results are summarized in Table 17. Boulders in open areas generally fit the model criteria for detecting bouldery landforms best. Some non-bouldery forest locations have a higher rank as likely bouldery landforms than did bouldery landform locations under a forest canopy. Test areas in non-bouldery field areas generally have the lowest ranking. This model is effective in open areas. Bouldery features under a tree canopy are difficult to detect due to variability of elevation difference between last returns and CVI classified ground

returns and last returns intensity. Last returns intensity is difficult to use under the tree canopy. This further supports the conclusion that modeling such features under a tree canopy requires ground classification algorithms that maintain topographic variability. This test area comparison technique supports the index overlay models produced.

Rank	Model 1	Model 2	Model 3		
1	D	D	D		Boulder in Open (A-I)
2	E	E	E		Boulder in Forest (J-O)
3	I	I	I		Non-bouldery Forest (P-Y)
4	H	H	H		Non-Bouldery Field (Z-II)
5	G	G	G		
6	B	B	B		
7	A	A	A		
8	M	M	M		
9	F	F	F		
10	C	C	C		
11	L	J	J		
12	J	L	L		
13	N	N	N		
14	O	S	S		
15	S	O	O		
16	P	K	K		
17	K	P	P		
18	T	V	V		
19	V	T	T		
20	W	W	Q		
21	X	Q	X		
22	Y	X	W		
23	Q	R	R		
24	HH	Y	Y		
25	R	HH	HH		
26	AA	U	AA		
27	II	AA	U		
28	U	Z	Z		
29	Z	II	II		
30	CC	CC	CC		
31	EE	BB	BB		
32	BB	EE	EE		
33	GG	GG	GG		
34	FF	FF	FF		
35	DD	DD	DD		

Table 17: Index overlay for likelihood of presence of bouldery landforms polygon ranking using spatial compromise programming results. Higher ranking means site agrees with the model criteria for detection more completely.

The index overlay for likelihood of presence of bouldery landform model was compared to the natural color supervised classification previously performed. Only moderate and most likely raster grid cells were considered due to the large number of least suitable cells. Moderate and most likely cells were grouped into one class. Table 18 describes the results.

Positive for Both	4.6%
Positive for Index Overlay Only	17.9%
Positive for Supervised Classification Only	6.2%
Negative for Both	71.3%
Positive for Index Overlay	22.5%
Positive for Supervised Classification	10.8%

Table 18: Comparison of index overlay and supervised classification results. These data provides a description of how well the supervised classification and averaged index overlay model agreed. Note that the models do not overlap completely.

The results show that the models do not overlap completely; not all areas included in the supervised classification are included in the index overlay model. Natural color classification was used as a variable in this model, and this comparison shows that the LiDAR-derived criteria are also important. One source of disagreement is that the natural color supervised classification includes road surfaces as well as boulders while the index overlay model does not include such features. Bouldery surfaces cannot be separated from other surfaces based on natural color DN values alone due to similar brightness values compared with other surfaces, such as roads.

Vegetation is a problem in both models. Combining LiDAR-derived data with other data sources, such as natural color imagery, aids in classification.

An error matrix (Table 19) was created using the same one hundred ground reference points used in the natural color and CIR classification. Least, moderately, and most likely grid cells were grouped into one class. An overall accuracy of 67% (+/- 7.2%) was found. This is a lower accuracy than that calculated for the natural color classification alone. The reasons for this are not certain. The error may have been higher due to an overestimation of bouldery area. Vegetation may have caused higher elevation difference between last returns and CVI classified ground returns raster grids values that caused grid cells to not be classified as likely for bouldery landforms. Many of the bouldery features observed in the field at the one hundred sample that were not considered likely for bouldery landforms in the index overlay model were at locations under a forest canopy. Detection of bouldery landforms under a forest canopy was inadequate.

		Ground Reference Data		User's Accuracy
		Bouldery	Non-Bouldery	
Index Overlay Data	Bouldery	25	14	63 %
	Non-bouldery	9	42	69%
Producer's Accuracy		57%	75%	
Overall Accuracy		67%		

Table 19: Index overlay for likelihood of presence of bouldery landforms error matrix (accuracy estimated as +/- 7.2%).

Conclusions

The purpose of this thesis project was to assess the viability of using LiDAR-derived elevation data in accurately mapping and characterizing bouldery geomorphic features. Bouldery landforms of the Pottsville Group were investigated within a rugged topographic area of the Allegheny Mountains. CVI ground classified data poorly represented bouldery landforms.

The LiDAR ground returns classification process conducted by CVI using the TerraScan software removed local topographic variability, and a smoothed elevation model was created. Bouldery landform representation is not consistent in this data set. LiDAR returns reflecting from bouldery features are commonly not included in the CVI classified ground data; however, some bouldery features are included in this CVI classification. Although this research indicated a mean ground sampling distance of 0.62 m, and CVI reported 0.69 m, the distances between CVI classified ground points are unevenly distributed. Clusters and large gaps exist in the CVI ground data, and bouldery features often exist in the data gaps. The CVI ground classification does not adequately represent the topographic surface for mapping bouldery geomorphic features and rugged topography.

Rough texture in hillshade images is often induced by a lack of data, which can be a result of multiple factors including the following: vegetation, rough topography, slope, and bouldery landforms. Researchers using such models should be aware that rough texture in hillshade imagery cannot be considered a unique result of rough topography. Researchers using hillshade imagery for surficial mapping should interpret such features carefully and seek confirmation through multiple types of data.

In open areas, last returns data can be used to map bouldery landforms. Research in mapping bouldery features can benefit from inclusion of last returns data because of the terrain information offered that may be missing from the ground classified data. Last returns intensity is very useful in open areas because bouldery features tend to yield relatively lower intensity returns than surrounding vegetation; however, this may be seasonally dependent. The last returns intensity from boulders is similar to road or gravel surfaces. It is suggested that LiDAR point classification algorithms consider intensity during the process of creating a ground classification. It should be noted that last returns intensity is variable and difficult to use quantitatively (Lin and Mills, 2010).

Identifying and describing boulders under a tree canopy require LiDAR point classifications. In this LiDAR data set,

collected during leaf-on conditions, many of the last returns do not represent the ground; the LiDAR energy was dissipated through reflection by the tree canopy. Classifications conducted within Prologic LiDAR Explorer provide a better representation of positive topographic features under a tree canopy than last returns; however, bouldery landforms cannot be completely differentiated from vegetation. Noisy DEMs and hillshade images are produced. The morphologies of bouldery features are not well maintained due to a reduction in number of returns reflecting from the surface of interest. Last returns intensity is highly variable under a tree canopy and cannot consistently yield quantitative differentiation of boulders. Although precise characterization of individual features is not possible, adequate terrain surface information is provided in order to map generalized rugged topography.

Index overlay analysis for likelihood of presence of bouldery landforms allows multiple criteria to be utilized to detect bouldery landforms. Fusion of natural color, aerial data with LiDAR data in a raster environment works well in open areas; however, classification under a tree canopy is inadequate to map bouldery landforms. This index overlay technique was supported by spatial compromise programming results and is useful for general representation of rugged topography.

The LiDAR data utilized here provides adequate spatial resolution to map bouldery landforms at this scale; however, ground returns classification processes are necessary to extract the point data of interest. Future research should attempt to determine the potential use of leaf-off ground returns data to map bouldery landforms under a tree canopy and how ground data density changes in comparison to leaf-on data. Fusing LiDAR data with other data sources, such as natural color, CIR, and hyperspectral data, should be explored in a vector environment. Reflectance data may be useful for point classification. Additional ground classification algorithms and processes should be explored in regards to suitability in modeling rough topography and maintaining local topographic changes while removing vegetation.

LiDAR is a useful tool for geomorphologists, but the results of post-processing must be understood in order to properly interpret derived elevation models and hillshade imagery.

References Cited

- Anderson, S., 2008, Surficial geology of the Blackwater Falls Davis 7.7 Quadrangles, West Virginia [Masters Option 2 Project]: Morgantown, West Virginia University, 28 p.
- Anderson, S., and Kite, J.S., 2007, Example of how LiDAR derived hillshade images can be used in surficial mapping: West Virginia Geological and Economic Survey, scale 1:24,000, 1 p., 1 sheet.
- Blair, T., and McPherson, J.G., 1949, Grain-size and textural classification of coarse sedimentary particles: *Journal of Sedimentary Research*, v. 69, p. 6-19.
- Bloom, A.L., 2004, *Geomorphology: A systematic analysis of late cenozoic landforms*, Third Edition: Long Grove, Illinois, Waveland Press, 482 p.
- Cardwell, D.H., Erwin, R.B., and Woodward, H.P., 1968, Geologic map of West Virginia: West Virginia Geological and Economic Survey, scale 1:250,000, 2 sheets.
- Carter, W.E., Shrestha, R.L., and Slatton, K.C, 2007, Geodetic laser scanning: *Physics Today*, v. 60, p. 44-47.
- Downing, J.B., 2008, Application of LiDAR-derived DEMs and there by-products for geomorphic assessment from stream-reach to watershed scale: Horseshoe Run, WV [Masters Thesis]: Morgantown, West Virginia University, 180 p.
- Habib, A.F., Bang, K.I., Shin, S.W., and Mitishita, E., 2008, Tight integration of photogrammetric and LiDAR data for the estimation of LiDAR bore-sighting parameters, 8 p.
- Hinke, J.J., and Wittkop, C.A., 2007, Detailed surficial geologic mapping and terrain analysis of the Blue Hills Felsenmeer Valley, Rusk County, Wisconsin: *Geologic Society of America Abstracts with Programs*, v. 39, p. 1-16.
- Jensen, J.R., 2005, *Digital Image Processing*, Third Edition: Upper Saddle River, NJ, Prentice Hall, 526 pp.
- Kite, J.S., Cenderelli, D.A., Springer, G.S., Behling, R.E., Davis, E.N., and Fedorko, N., 1994, Surficial geology map of the Blackwater Falls 7.5' Quadrangle: West Virginia Geological and Economic Survey Open File Geological Map OF-9405, 4 p., 2 sheets.
- Konsoer, K.M., 2008, LiDAR, GIS, and multivariate statistical analysis to assess landslide risk, Horseshoe Run Watershed [Masters Thesis]: Morgantown, West Virginia University, 129 p.
- Kukko, A., and Hyyppa, J., 2007, Laser scanner simulator for system analysis and algorithm development: A case study with forest measures: *ISPRS Workshope on Laser Scanning 2007*, 7 p.

- Lillesand, T.W., Kiefer, R.W., and Chipman, J.W., 2004, Remote sensing and image interpretation, Fifth Edition: New York, John Wiley and Sons, 756 p.
- Lin, Y., and Mills, J.P., 2010, Factors influencing pulse width of small footprint, full waveform airborne laser scanning data: *Photogrammetric Engineering and Remote Sensing*, v. 76, p. 49-59.
- Liu, X., Zhang, Z., Peterson, J., and Chandra, S., 2007a, LiDAR-derived high quality ground control information and DEM for image orthorectification: *Geoinformatica*, v. 11, p. 37-53.
- Liu, X., Zhang, Z., Peterson, J., and Chandra, S., 2007b, The effect of LiDAR data density on DEM accuracy, *in* MODSIM07 International Congress on Modeling and Simulation: Christchurch, New Zealand, p. 1363-1369.
- Luccio, M., 2010, Beyond terrain models: LiDAR enters the geospatial mainstream: *Imaging Notes*, v. 25, p. 41-46.
- Matchen, D.L., Fedorko, N., and Blake, B.M., Jr., 1999, *Geology of Canaan Valley: West Virginia Geological and Economic Survey Open File Geological Map OF9902*, 1:24,000 scale.
- Prologic, *LiDAR Explorer Version 2.0 for ArcGIS User's Guide Version 2.0 FCE-DME*, 2007: Fairmont, WV, Prologic, 74 p.
- Reusser, L., and Bierman, P., 2007, Accuracy assessment of LiDAR-derived DEMs of bedrock river channels: *Holtwood Gorge, Susquehanna River: Geophysical Research Letters*, v. 34, L23S06.
- Sithole, G., and Vosselman, G., 2004, Experimental comparison of filter algorithms for bare-Earth extraction from airborne laser scanning point clouds: *ISPRS Journal of Photogrammetry & Remote Sensing*, v. 59, p. 85-101.
- Snyder, N.P., 2009, Studying stream morphology with airborne laser elevation data: *EOS Transactions, American Geophysical Union*, v. 5, p. 45-46.
- Terrasolid, *TerraScan User's Guide*, 1998, Terrasolid, 263 p.
- Webster, T.L., 2005, LiDAR validation using GIS: A case study comparison between two LiDAR collection methods: *Geocarto International*, v. 20, p. 11-19.
- Weed, C.A., Crawford, M.A., Neuenschwander A.L., and Guitierrez, R., 2002, Classification of LiDAR data using a lower envelope follower and gradient-based operator, *in* *Proceedings to the IEEE IGARSS Conference: Toronto, Canada*, p. 1384-1386.

Appendix

Field Data:

The following images and measurements collected on March 10, 2010 show the bouldery features used as reference and ground data during this study. These features are present within the five study areas referenced above. Physical measurements were collected using a tape measure and measuring rod to the best of the researcher's ability. These features were outlined in the imagery by aerial photograph interpretation. If this was not possible due to canopy cover, features were outlined using a Magellan Mobilemapper 6 GPS unit with differential post-processing. This research explored how such bouldery features can be mapped using the LiDAR data provided by CVI.

Site 1

The following photographs depict bouldery features in a power line clearing on the CVI property. This site was selected to explore features not under a tree canopy.

Site 1a



Long Axis: 9.4 m
Short Axis: 5.3 m
Intermediate Axis: 6.3 m
Height: 5.35 m
Classification: Fine Block

Site 1a



Long Axis: 7.5 m
Short Axis: 3.8 m
Intermediate Axis: 6.9 m
Height: 3.8 m
Classification: Fine Block

Site 1b



Long Axis: 5.6 m
Short Axis: 2.5 m
Intermediate Axis: 5.5 m
Height: 2.5 m
Classification: Fine Block

Site 1c



Long Axis: 5.0 m
Short Axis: 2.05 m
Intermediate Axis: 3.8
m
Height: 2.05 m
Classification: Very
Coarse Boulder

Site 2

The following photographs depict boulder features under a forest canopy. This site was selected to explore how sub canopy bouldery features were portrayed in the CVI LiDAR data.

Site 2a



Long Axis: 9.5 m
Short Axis: 4.3 m
Intermediate Axis: 9.3 m
Height: 4.3 m
Classification: Medium
Block

Site 2b



Long Axis: 5.2 m
Short Axis: 1.9 m
Intermediate Axis: 3.0 m
Height: 1.9 m
Classification: Very
Coarse Boulder

Site 2c



Long Axis: 4.45 m
Short Axis: 1.05 m
Intermediate Axis: 2.6 m
Height: 1.05 m
Classification: Very
Coarse Boulder

Site 2d



Long Axis: 6.0 m
Short Axis: 2.2 m
Intermediate Axis: 4.4 m
Height: 2.2 m
Classification: Fine
Block

Site 2f



Long Axis: 8.4 m
Short Axis: 1.7 m
Intermediate Axis: 3.9 m
Height: 1.7 m
Classification: Very
Coarse Boulder

Site 3

The following photographs depict bouldery features under a forest canopy. This site was selected to explore how sub canopy bouldery features were portrayed in the CVI LiDAR data.

Site 3a



Long Axis: 7.2 m
Short Axis: 3.9 m
Intermediate Axis: 4.4 m
Height: 3.9 m
Classification: Fine
Block

Site 3b



Long Axis: 6.0 m
Short Axis: 2.6 m
Intermediate Axis: 5.2 m
Height: 2.6 m
Classification: Fine
Block

Site 3c



Long Axis: 5.2 m
Short Axis: 1.8 m
Intermediate Axis: 5.1 m
Height: 1.8 m
Classification: Fine
Block

Site 3d



Long Axis: 4.4 m
Short Axis: 2.6 m
Intermediate Axis: 3.2 m
Height: 2.6 m
Classification: Very
Coarse Boulder

Site 3e



Long Axis: 4.8 m
Short Axis: 2.1 m
Intermediate Axis: 3.1 m
Height: 2.1 m
Classification: Very
Coarse Boulder

Site3f



Long Axis: 4.3 m
Short Axis: 2.4 m
Intermediate Axis: 4.1 m
Height: 2.4 m
Classification: Fine
Block

Site 4

The following photograph depicts a bouldery feature under a partial forest canopy. This site was selected to explore how bouldery features under a partial canopy were portrayed in the CVI LiDAR data.

Site 4a



Long Axis: 7.5 m
Short Axis: 5.2 m
Intermediate Axis: 5.5 m
Height: 5.5 m
Classification: Fine
Block

Site 5:

The following photographs depict bouldery features under a forest canopy. This site was selected to explore how smaller sub canopy bouldery landforms were portrayed in the CVI LiDAR data. These features were generally smaller based on height in relation to the feature at the other study sites.

Site 5a



Long Axis: 8.3 m
Short Axis: 1.7 m
Intermediate Axis: 3.1 m
Height: 1.7 m
Classification: Very
Coarse Boulder

Site 5b



Long Axis: 3.0 m
Short Axis: 1.6 m
Intermediate Axis: 2.6 m
Height: 1.6 m
Classification: Very
Coarse Boulder

Site 5c



Long Axis: 2.4 m
Short Axis: 0.6 m
Intermediate Axis: 1.45 m
Height: 0.6 m
Classification: Coarse
Boulder

Site 5d



Long Axis: 3.5 m
Short Axis: 1.1 m
Intermediate Axis: 2.5 m
Height: 1.1 m
Classification: Very
Coarse Boulder

Site 5f



Long Axis: 4.5 m
Short Axis: 1.05 m
Intermediate Axis: 2.7m
Height: 1.05 m
Classification: Very
Coarse Boulder

Site 5g



Long Axis: 2.3 m
Short Axis: 0.8 m
Intermediate Axis: 1.6 m
Height: 0.8 m
Classification: Coarse
Boulder